(12)

ARPA Order 4669
Program Code 3D60
Name of Contractor: University of Colorado
Effective Date of Contract: 1 October 1982
Grant Expiration Date: 30 September 1984
Amount: $285,000
Contact No.: F49620-83-C-0009
Principal Investigator: C. B. Archambeau (303) 492-8028
Program Manager: William J. Best (202)-767-5011
Title of Work: Deterministic Methods of Seismic Source Identification

Annual Technical Report

October 1, 1982 - September 30, 1983

Sponsored by
Advanced Research Projects Agency (DOD)
ARPA Order No. 4669
Monitored by AFOSR Under Contract No. F49620-83-C-0009

The views and conclusions contained in this document are those of the authors and should not be interpreted as necessarily representing the official policies, either expressed or implied, of the Defense Advanced Research Projects Agency or the U. S. Government

Table of Contents

UNCLASSIFIED

SECURITY CLASSIFICATION OF THIS PAGE (When Data Entered)

REPORT DOCUMENTATION PAGE	READ INSTRUCTIONS BEFORE COMPLETING FORM
1. REPORT NUMBER: AFOSR-TR- 84-0229	2. GOVT ACCESSION NO.: AD-A135 675
	3. RECIPIENT'S CATALOG NUMBER:
4. TITLE (and Subtitle): Deterministic Methods of Seismic Source Identification	5. TYPE OF REPORT & PERIOD COVERED: 10/1/82 - 9/30/83, Annual
	6. PERFORMING ORG. REPORT NUMBER:
7. AUTHOR(s): Charles B. Archambeau	8. CONTRACT OR GRANT NUMBER(s): F49620-83-C-0009
9. PERFORMING ORGANIZATION NAME AND ADDRESS: CIRES, University of Colorado, Boulder, CO 803039	10. PROGRAM ELEMENT, PROJECT, TASK AREA & WORK UNIT NUMBERS: 2309/A1 61102F
11. CONTROLLING OFFICE NAME AND ADDRESS: Defense Advanced Research Projects Agency, 1400 Wilson Blvd., Arlington, VA 22209	12. REPORT DATE: Sept. 30, 1983
	13. NUMBER OF PAGES: 76
14. MONITORING AGENCY NAME & ADDRESS (if different from Controlling Office): AFOSR/NP, Bolling AFB, DC 20332	15. SECURITY CLASS. (of this report): unclassified
	15a. DECLASSIFICATION/DOWNGRADING SCHEDULE:

16. DISTRIBUTION STATEMENT (of this Report)

Approved for public release; distribution unlimited.

17. DISTRIBUTION STATEMENT (of the abstract entered in Block 20, if different from Report)

18. SUPPLEMENTARY NOTES

19. KEY WORDS (Continue on reverse side if necessary and identify by block number)

Discrimination, Anelasticity, signal analysis, elastodynamics, wave propagation, explosion yield estimation

20. ABSTRACT (Continue on reverse side if necessary and identify by block number)

(over)

DD FORM 1 JAN 73 1473 EDITION OF 1 NOV 65 IS OBSOLETE

UNCLASSIFIED

SECURITY CLASSIFICATION OF THIS PAGE (When Data Entered)

In this report we describe specific research results in: (1) The theoretical basis for seismic event discrimination and for the inference of physical parameters describing seismic sources; (2) Observations of body wave magnitude residuals in the U.S. and Southern Canada and the implications for yield estimation at non-U.S. and/or U.S. test sites; (3) Inferences of magnitude-yield relationships for both U.S. and U.S.S.R. test areas, with applications of these relations to U.S. and Russian nuclear test observations, to obtain new yield estimates; (4) Studies of a variety of physical situations which would produce seismic observations for an earthquake making it appear "anomalous" (i.e., explosion-like) when viewed from the perspective of "standard" discrimination methods, and similarly physical situations were described for which explosions could appear earthquake-like, and which could also lead to large yield estimate errors.

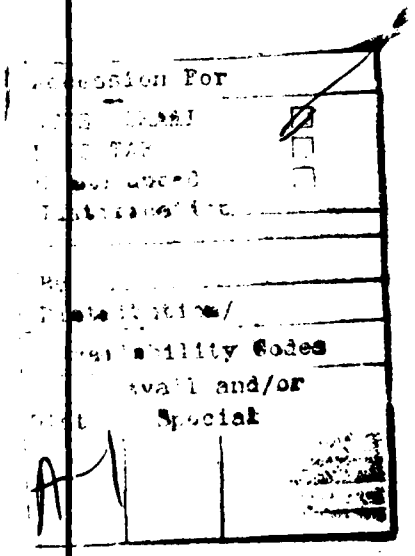

Research on Deterministic Methods of Seismic Source Identification

Summary of Annual Technical Report for October 1, 1982 - September 30, 1983

The objectives of the research being conducted under the current 2 year contract are to: (1) Develop and test methods of discrimination in the regional and teleseismic distance range using physical source parameter discriminants, (2) Pursue theoretical and observational studies of seismic sources; (3) To develop methods of theoretical seismogram synthesis in the near, regional and teleseismic distance ranges for structure and source definition; (4) To develop and apply advanced signal processing/analysis methods for discrimination and explosion yield estimation studies and; (5) to pursue near field studies of explosions and earthquakes for detailed source definition.

In this report we describe specific research results in: (1) The theoretical basis for seismic event discrimination and for the inference of physical parameters describing seismic sources; (2) Observations of body wave magnitude residuals in the U.S. and Southern Canada and the implications for yield estimation at non-U.S. and/or U.S. test sites; (3) Inferences of magnitude-yield relationships for both U.S. and U.S.S.R. test areas, with applications of these relations to U.S. and Russian nuclear test observations, to obtain new yield estimates; (4) Studies of a variety of physical situations which would produce seismic observations for an earthquake making it appear "anomalous" (i.e., explosion-like) when viewed from the perspective of "standard" discrimination methods, and similarly physical situations were described for which explosions could appear earthquake-like, and which could also lead to large yield estimate errors.

Some of the major conclusions drawn from the results described are: (1) That earthquake-explosion discrimination by $m_b - M_s$, at large to moderate magnitude levels, is due, in part, to basic differences in the high frequency

radiation from the two source types, as predicted, with explosions producing more high frequency seismic radiation than earthquakes with the same low frequency radiation. Further, because of this same spectral difference between the two types of seismic events, spectral discrimination, using variable frequency magnitude (VFM) methods, is very effective in distinguishing and identifying the two event types in the regional distance range and can be applied to very low magnitude levels (below $m_b \cong 3$). (2) Deviations of observed single station body wave magnitudes from the mean observed magnitude can be very large, of the order of one magnitude unit from the mean, and these deviations can also be strongly dependent on the azimuth from the station to the source, with variations as large as .5 magnitude units occurring as a function of azimuth. These variations are considered to be due to both focusing (defocusing) effects and variations of anelastic absorption between points of observation. The azimuthal variation at OB2NV, at the Nevada test site, is .22 magnitude units, while at RKON, on the Canadian shield, the variation with azimuth is .45 units; suggesting that use of these sites as analogs for the differences between NTS and Russian test sites requires additional assumptions about how the strong azimuthal variations are to be interpreted. If, however, azimuthal variations are averaged and these stations are used, then the predicted difference in m_b observations from Russian tests and NTS tests should be .31 magnitude units, with NTS having the lower *average* magnitude *if* the observing stations provide a reasonably uniform azimuth sampling of *both* test sits. (3) Russian test site body wave magnitude-yield relations, adjusted from NTS derived magnitude-yield relations to account for a transmission bias of slightly more than .3 magnitude units between NTS and Russian sites, give estimated yields for Russian tests (from 1968 to 1977) that are reasonably consistent with yields estimated using "universal" surface wave magnitude-yield relations. Further,

the estimated yields for Russian tests appear to be within the limitations of the test ban agreement. That is, within the uncertainties of the estimation methods, all the yield estimates obtained are less than, or about equal to, 150 kT. (4) Seismically anomalous events can (and do) occur under a variety of conditions, but it is possible to properly identify these events when appropriate seismic procedures are employed, with these methods being spectral discrimination methods which can be implemented for routine analysis.

I. Introduction

The objectives of the research being conducted under the current 2 year contract are to: (1) Develop and test methods of discrimination in the regional and teleseismic distance range using physical source parameter discriminants, (2) Pursue theoretical and observational studies of seismic sources; (3) To develop methods of theoretical seismogram synthesis in the near, regional and teleseismic distance ranges for structure and source definition; (4) To develop and apply advanced signal processing/analysis methods for discrimination and explosion yield estimation studies and; (5) to pursue near field studies of explosions and earthquakes for detailed source definition.

In this report we describe some of our work, and results, on the theory of earthquake source representation, as it relates to earthquake-explosion discrimination. In this regard, Section II and the Appendix 1 provide a description of a major part of our comprehensive study of the theoretical/observational basis for earthquake-explosion discrimination. In addition, in Section III, we summarize our observational results pertaining to measurements of magnitude variations for the U.S. and Southern Canada, and discus the relevance of these observations to magnitude bias due to upper mantle attenuation, as well as the relationship of these results to yield estimation for USSR underground tests. In a related study, described in Section IV, we

address the effects of variable coupling and attenuation as they relate to yield estimation for underground nuclear tests within the U.S. and the U.S.S.R., and then apply our inferences to the Russian and U.S. test data in order to obtain yield estimation results. In Section V we describe some of our investigations of the conditions under which "anomalous" events will occur, specifically for $m_b - M_s$ discrimination and VFM (variable frequency magnitude) discrimination.

II. Discrimination of Seismic Events

Several research projects have been pursued during the 1982-83 contract period. In this report we will emphasize our work on a comprehensive study of the theoretical foundations of seismic event discrimination (Archambeau and Evernden, 1984). These results are the first part of a comprehensive study of discrimination, with the complete study involving an integration of previous work on source theory, wave propagation theory and earth structure, including new material and results obtained under current AFOSR support. This work is an attempt to provide a complete explanation of empirically substantiated discrimination methods, and, in addition, to provide a basis for less verified or new discrimination methods. In the complete study, the theoretical predictions are compared to relatively large sets of observed data, in order to substantiate the predictions and confirm the models. Further, inferences of network capability for the detection and identification of explosions, including decoupled explosions, are also considered in an attempt to provide an accurate and realistic evaluation of U.S. capability for detection and identification of Eurasian events under a variety of conditions. Finally, consideration is also given to anomalous events, particularly anomalous explosions and the conditions under which it is expected that such events can be generated. In this regard, joint discrimination procedures are described that can be used to identify such events.

The first part of this study is included in the Appendix 1, wherein we provide the theoretical foundations for quantitative descriptions of earthquake generated seismic fields, along with specific spectral predictions, scaling laws, etc. These results form part of the framework within which we interpret discrimination methods, the other part being a similar quantitative representation of explosion generated seismic fields. Through the use of these theoretical predictions we are then able to interpret and understand observed discriminatory differences between earthquakes and explosions (Evernden and Archambeau, 1984). (These detailed comparisons of theory and observation will be discussed in our next report.)

We are also concerned with seismic source discrimination through the use of inferred physical parameters for seismic sources. In this investigation we consider it necessary to use formal inversion methods to obtain estimates of source parameters, such as stress drop, rupture length and rupture velocity. In this regard, inversion methods provide the necessary automated and objective methods that must be used, and we have therefore investigated approaches which involve moment tensors as well as new approaches to source inversion based on vector multipole formulations of the seismic radiation fields from explosions and earthquakes (Archambeau and Scales, 1984).

In this work it has been shown that the conceptual and physical basis for Gilbert's moment tensor representation (Gilbert, 1971) is faulty and that its criticism by Backus and Mulcahy (1976) is also in error. Further, it is found that the stress glut formulation and concept is without physical or mathematical (*i.e.*, logical) foundation. An alternative approach for the inversion of seismic data for source properties is given and it is shown that a vector multipole expansion of the seismic radiation field is appropriate, in that it provides a desired linear inversion for these coefficients from the observed data, as do

moment tensor components. In addition, the physical parameters defining the source, such as spatial stress changes, failure rate and failure zone dimensions, are explicitly related to the vector multipole coefficients and it is shown how these parameters can be obtained from the multipole coefficients through a non-linear inversion procedure.

In addition to a formal inversion approach, we have previously used relaxation source models in earth structure models to provide a basis of interpretation of the m_b and M_s data from earthquakes, in terms of failure zone dimensions and stress drop (Archambeau et al., 1983). In particular, we studied recorded earthquakes in the Aleutian region. During the present contract period this work was finalized and is being submitted for publication. We have begun a similar study of the magnitude data for the Japan-Kamchatka region during the current contract period and expect to finalize this work by the end of the contract period. Finally, we have begun studies of small earthquakes and explosions from the California-Nevada region using spectral methods to infer source stress-drop, dimension, etc. (Wilson and Archambeau, 1984). One of the principal results is that the average stress drops observed for large numbers of individual events show a definite dependence on rupture length, with small events giving much higher *average* stress drops than larger (longer) ones. This result strongly suggests that many smaller events involve failure at highly stressed single asperities, without failure zone propagation continuing very far outside the single asperity zone. On the other hand, larger events appear to involve failure connecting several or a large number of highly stressed asperities separated by zones of low tectonic stress. In such a picture, explosions appear as small rupture dimension events with very high stress drops (above the 4-5 kilobar level), while earthquakes of comparable effective failure zone lengt' s have s' ess drops significantly below the low kilobar level (below 1 kilo-

bar) and generally, as a population, have effective rupture dimensions that are much larger than explosions. Hence, a "physical parameter space" discriminant, involving stress drop *vs* maximum failure zone dimension, serves as another approach to event identification.

During the FY 1982-83 contract period we also continued our studies of spectral discriminants, in particular, the variable frequency magnitude discriminant employed in the study of Eurasian event data set. This latter effort was jointly conducted with Systems, Science and Software. The current effort involves finalization of this work, along with applications of new modeling techniques, of source and propagation effects, applied to provide a more detailed understanding of the observational results. The essential result obtained, however, is that VFM discrimination is very effective down to very low magnitude levels (at least to m_b = 3.0) and that its effectiveness is due to the fact that most explosions with the same low frequency spectral level as an earthquake will have a higher "corner frequency" than the earthquake, as well as a lesser P-wave spectral decay rate at frequencies above the corner frequency. Thus, this results in substantially greater high frequency generation for an explosion compared to an earthquake with the same low frequency spectral level for the direct P-wave, and this difference is exploited by the VFM method to provide the observed discrimination capability. The method is shown to be very effective in regional distance ranges where relatively high Q paths are available, particularly when very high frequency magnitudes (up to 10 Hz and beyond) are used.

III. Magnitude Bias Estimates for Yield Estimation

This work (Butler, 1983) involves body wave magnitude measurements at 1 Hz from a large set of selected events at all available U.S. stations, as well as at some stations in Canada. At a number of stations, including OB2NV at the Nevada test site, magnitude data was obtained at 3 azimuths, with each azimuth

data set analyzed separately. The results of this analysis are summarized in Figures 1 and 2. The conclusions that are apparent from the results of this study are that the relative body wave magnitude variations in the U.S. are large, with the range running at least from +.4 to -.4 magnitude units. Further, the spatial variation is, in many areas, extremely rapid, suggesting focusing and defocusing effects. In this regard, the variations of δm_b with azimuth at a particular station can be very large, with variations of as much as .4 magnitude units occurring, and with no apparent correlation with tectonic province for the large variations. In particular, the Nevada test site station OB2NV (on a granite stock), shows an azimuthal variation in δm_b of .22 magnitude units, and the site at RKON, which has been used as a station site comparable to Eurasian nuclear test sites, shows an azimuth variation of .45 magnitude units, with larger magnitudes to the north than to the south and northwest. These particular results strongly suggest that magnitude bias estimates, using OB2NV and RKON as representative NTS and Russian test site analogs, may be misleading and at the least ambiguous since different azimuthal sampling will give very different results. (*e.g.*, One could get values for the difference, δm_b (RKON) - δm_b (OB2), anywhere in the range from .74 to .07 depending on azimuth sampling.) If an average of the three azimuths is used, then δm_b (OB2) $\cong$ .14, while δm_b (RKON) $\cong$ .45, so that δm_b (RKON) - δm_b (OB2) $\cong$ .31. However, blind use of such an average in estimating magnitude bias for test sites is certainly suspect, unless one can show that the averaging removes local focusing-defocusing variations completely and that the average represents the basic anelastic absorption effect plus any regional focusing-defocusing due to deep (crust-upper mantle) structure. Even so, one would expect fairly wide ranging fluctuations in observations at different azimuths from tests at such sites. In any case, it is clear from the data that OB2 is not representative of the Nevada area nor the

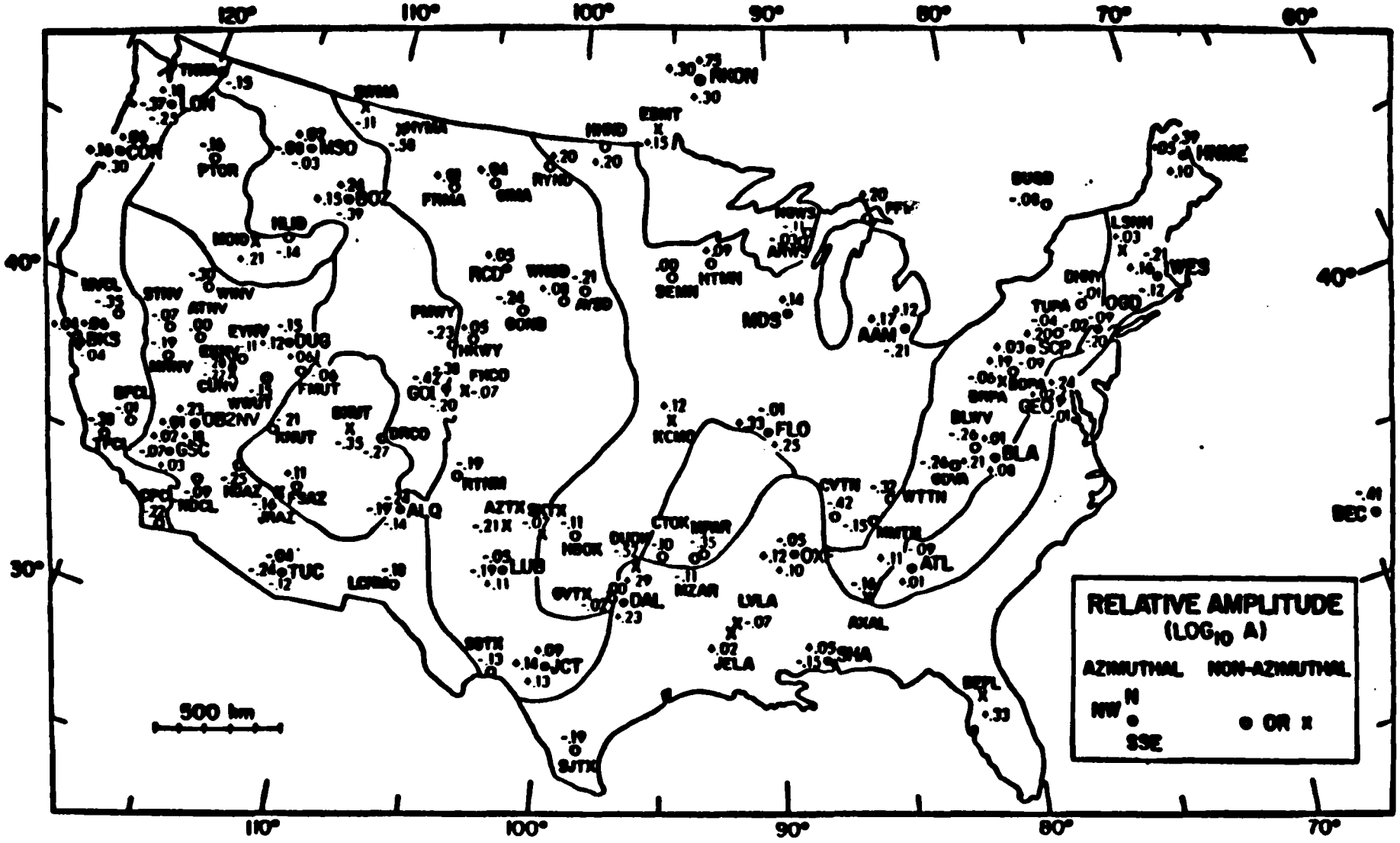

Figure 1. Distribution of stations and relative amplitude (δm_b) observations for the U.S. and Southern Canada. At some of the stations the data could be analyzed with respect to three distinct azimuths, the results of which are indicated by three values arranged at appropriate azimuths for these stations. (Butler, 1983)

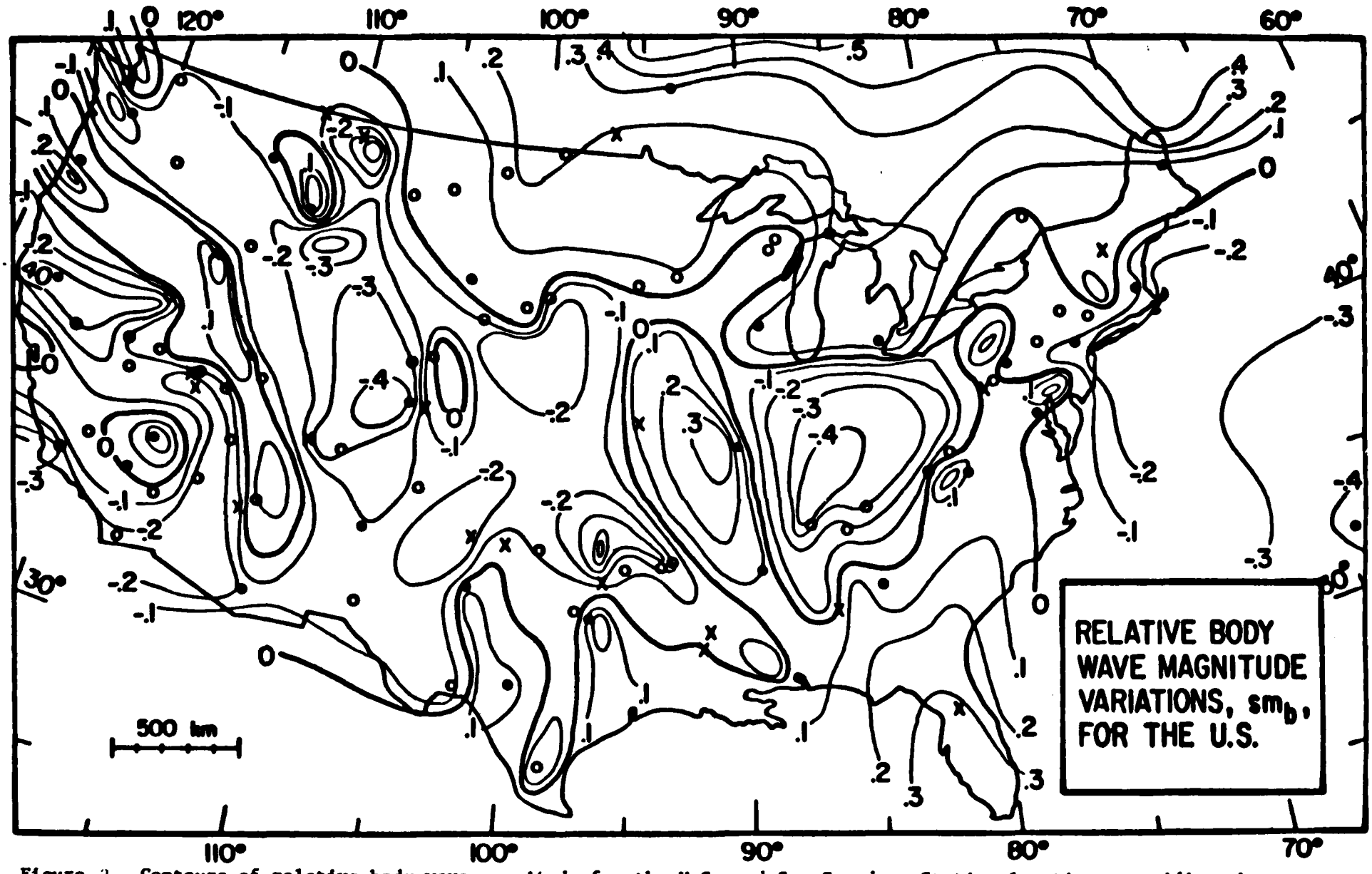

Figure 2. Contours of relative body wave magnitude for the U.S. and So. Canada. Station locations providing the data are indicated. Azimuthal data (3 directions) was available at stations indicated by the solid circles. The azimuthal variations observed at these stations was taken into account in the contouring. Where station coverage is sparse the contours are questionable, and must be viewed more as predictions rather than observations.

Basin and Range Province, and its anomalously high δm_b values relative to nearby stations probably represents strong focusing associated with the granite intrinsive at the site.

These results imply that extremely accurate yield estimates (to within, say, a 10% uncertainty) will most likely require detailed site information in view of the rapid, and somewhat unexpected, variations present within geologic provinces and sub-provinces. However, correlations of these observations with more readily available geophysical data (*e.g.*, gravity, heat flow, P delays, crustal thickness, near surface geology, P_n velocities,, elevation, etc.) may offer some hope of deducing magnitude variations for "random" sites.

IV. Teleseismic Yield Estimation with Applications to U.S. and U.S.S.R Test Data

The necessity of obtaining accurate and rather precise yield estimates from seismic data places a rather extreme burden on our methods of measurement and data analysis and, as well, on the basis of interpretation, of such data. As is well known, a large number of near site environmental factors, such as detailed material properties at the explosion site and the nature of tectonic stress fields, are capable of strongly perturbing the seismic field, and so this state of affairs makes accurate estimates of any single parameter such as yield extremely difficult, if not impossible, without a detailed understanding of all these (other) effects and the means of taking them into account in the analysis of the observed data. In addition, we are also well aware that variations in crust and upper mantle properties, including both structure and absorption properties, can lead to very strong fluctuations in the observed seismic data, resulting in biasing between different test sites. Until we have reasonably accurate determinations of these characteristics for potential underground test areas, it will be difficult to obtain yield estimates that are reliable to within a factor of two. Furthermore, the effects of anelastic absorption and scattering (focusing

and defocusing) are certainly frequency dependent and without fairly precise knowledge of the form of the frequency dependence for each, and the relative magnitudes of these effects at particular test locations, it is unlikely that very precise yield estimates can be obtained because of this uncertainty alone. Finally, it seems clear that much more precisely defined seismic magnitudes are required (or perhaps a different measurement or group of measurements which are carefully and precisely defined) in order to reduce observational subjectivity and associated variations in the measured data.

In addition to the effects of anelastic attenuation, it is clear that variations in material properties produce changes in the explosion coupling and so will produce different seismic wave fields for the same explosive yield. Figures 3 and 4, from Archambeau and Evernden (1983), show body and surface wave data (from Marshall et al.) which illustrates the approach required to obtain meaningful yield estimates. In particular, we have used high, intermediate and low coupling magnitude-yield curves to interpret this data, with these curves being based on results derived from explosion modeling in different types of materials. Further, the m_b versus yield curves shown are segmented into sections of different constant slope, this change of slope occurring at large yields when the corner frequency for the explosive generated P wave is less than 1 Hz. The upper curve, for non-NTS explosions in high coupling media, applies to Russian event data as well as U.S. Aleutian explosions. This curve, and associated data, indicates a clear shift above the high coupling NTS curve, of about .25 magnitude units. This then is a bias effect, which arises because of the differences between the NTS site transmission characteristics and the less attenuated transmission from other sites.

The data show considerable scatter about the magnitude yield curves, and this is considered to be due to: deviations from the mean material properties

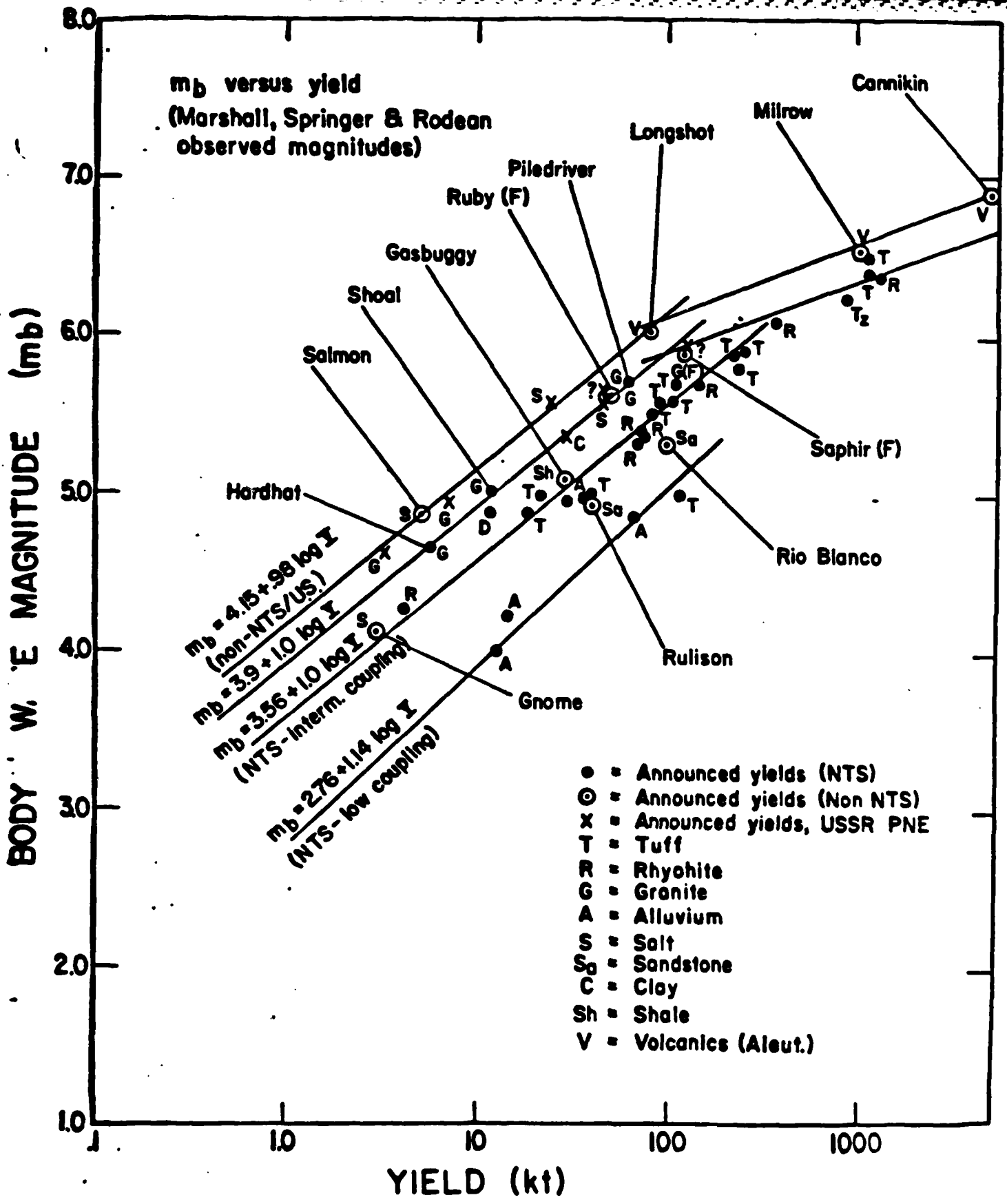

Figure 3. Observed body wave magnitude versus yield data (from Marshall et al.) interpreted using three coupling level m_b vs Y curves, which are based on modeling results. Note that yield curves generally consist of two segments of differing constant slope, these being due to magnitudes measured above the corner frequency for large yield events, and below the corner frequency for intermediate and low yield explosions.

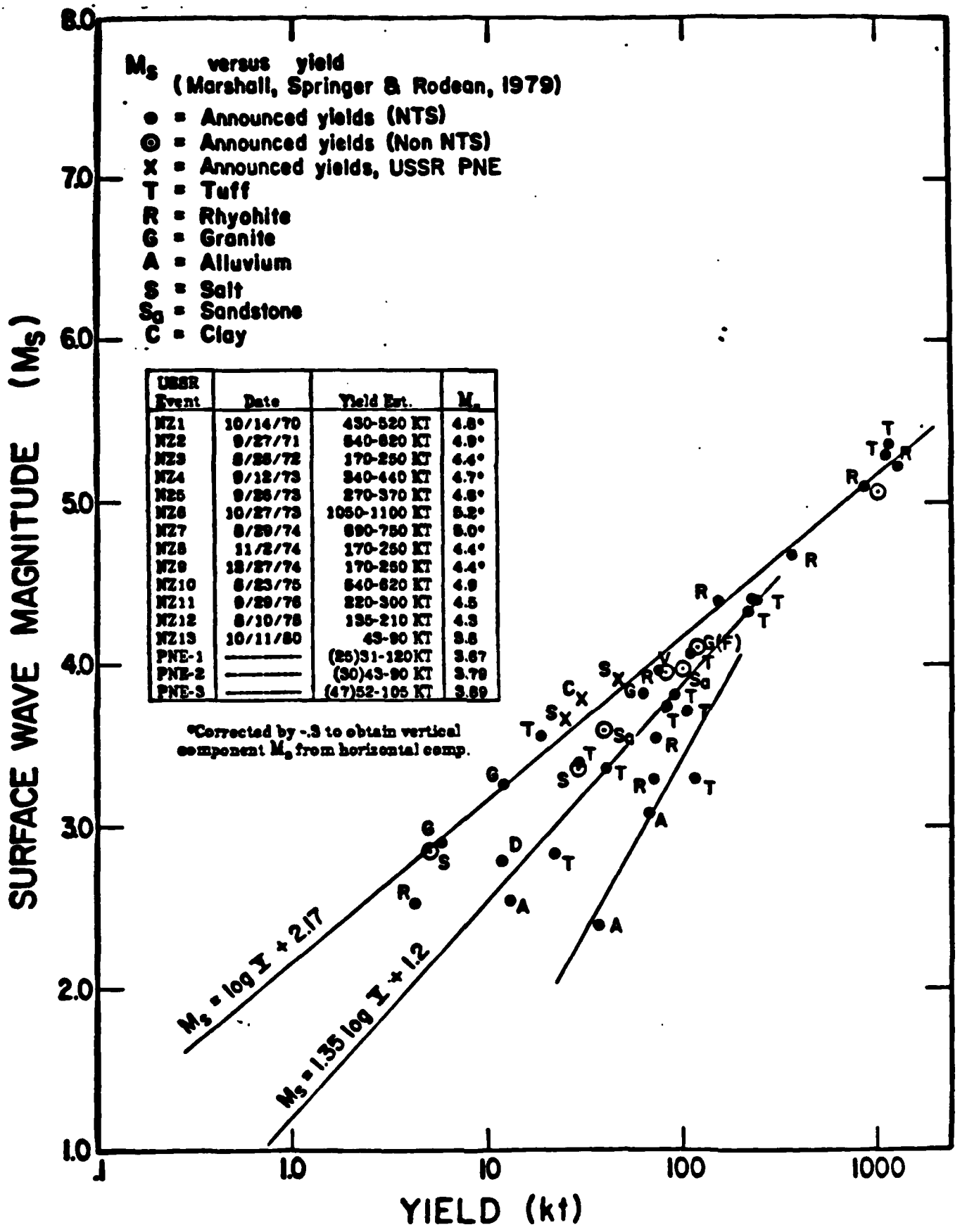

USSR Event	Date	Yield Est.	M_s
NZ1	10/14/70	430-520 KT	4.8*
NZ2	9/27/71	540-620 KT	4.9*
NZ3	8/26/72	170-250 KT	4.4*
NZ4	9/12/73	340-440 KT	4.7*
NZ5	9/26/73	270-370 KT	4.6*
NZ6	10/27/73	1050-1100 KT	5.2*
NZ7	8/29/74	690-750 KT	5.0*
NZ8	11/2/74	170-250 KT	4.4*
NZ9	12/27/74	170-250 KT	4.4*
NZ10	8/23/75	540-620 KT	4.9
NZ11	9/29/76	220-300 KT	4.5
NZ12	8/10/78	135-210 KT	4.3
NZ13	10/11/80	43-90 KT	3.8
PNE-1	———	(25)31-120KT	3.67
PNE-2	———	(30)43-90 KT	3.78
PNE-3	———	(47)52-105 KT	3.89

*Corrected by -.3 to obtain vertical component M_s from horizontal comp.

Figure 4. Observed surface wave magnitude versus yield data for NTS, non-NTS and USSR events with announced yields. The data is interpreted, as was the m_b vs Y data, using three coupling level M_s vs Y relations which are based on modeling results. All world wide data appears to be quite fit by these three coupling level curves of constant slope.

(implicitly) assumed for each of the three coupling level curves; local variations in the transmission characteristics arising from the shifts in explosion locations; and, finally, variations in m_b and M_s values due to tectonic release effects. The latter effect has been interpreted as being particularly strong for the Rulison and Rio Blanco events (Murphy, Archambeau and Shah, 1983), with the m_b values being considerably reduced by tectonic release having a double couple or fault plane equivalent corresponding to a 45° plane with normal equivalent faulting at the explosion hypocenter. (The actual tectonic release mechanism is thought to be stress relaxation in a prestressed zone around the (nearly spherical) shatter zone created by the explosion itself.)

As examples of the application of these current, somewhat preliminary results, to Russian explosion test site data, Figure 5 shows the inferred magnitude yield curves for Russian (shield) explosions with announced yields, along with French and U.S. data from the Aleutians, the latter two data sets considered to be comparable to data from Russian test sites in terms of roughly equivalent transmission characteristics. In particular, the anelastic absorption and other transmission characteristics are considered to be comparable. The empirical curves shown on this plot are obtained from the NTS curves shown earlier, with a .3 increase in the m_b value for a given yield. This value is based on the *average* δm_b value between an NTS test site (OB2NV) and the shield-like station at Red Lake Ontario (RKON), the result being obtained using the data shown in Figures 1 and 2. this value is also consistent with the rough magnitude of the inferred body wave magnitude difference between NTS and Aleutian events (.25 m_b units) indicated in Figure 3. The fit of the empirical curves shown in Figure 5 to the observed data is considered to be very good, with the high and intermediate coupling curves being in agreement with the observed data in a sensible and physically understandable manner.

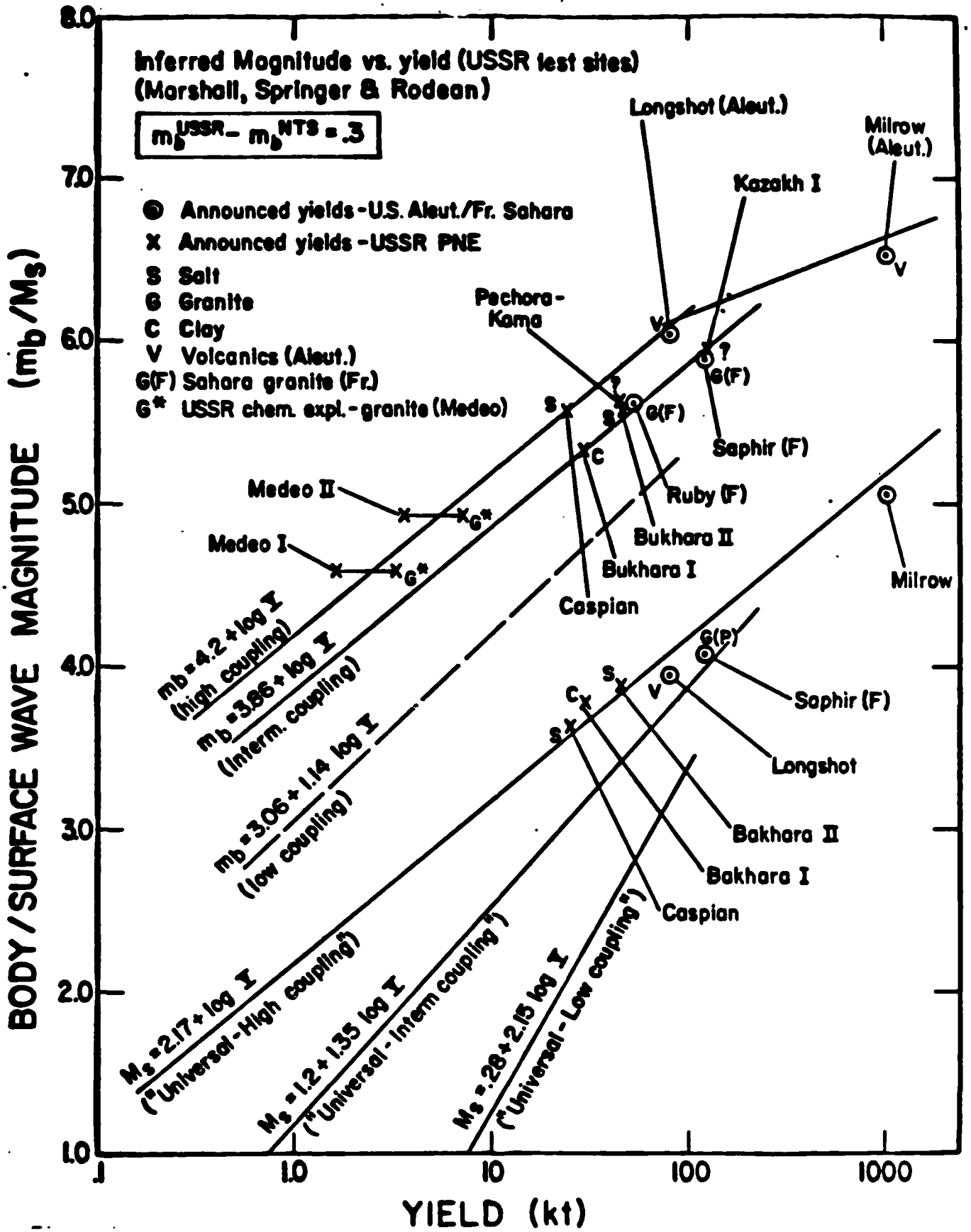

Figure 5. U.S. (NTS) body wave magnitude versus yield curves adjusted for differences in anelastic absorption between NTS and USSR test sites, compared to observed USSR events having announced yields. The lower set of three curves are the universal M_s vs Y curves with non-NTS surface wave magnitude data. Aleutian and French test data are also shown for comparison. The NTS body wave curves for high, intermediate and low coupling have all been shifted upward by .3 magnitude units. (Data from Marshall et al.)

The consequences of yield estimation based on magnitude-yield curves incorporating sensible corrections for strong biasing effects, such as differential absorption, variable coupling and tectonic release are indicated in Figures 6 and 7. Thus, with an uncorrected application of the NTS derived magnitude-yield relations to Russian test data one obtains yield estimates from conventional m_b and M_s data as indicated in Figure 6. As noted in the figure caption, there are several reasons why one expects such estimates to be systematically in error. On the other hand, Figure 7 shows estimates for the same set of Russian explosions when a bias correction in m_b values is applied to the NTS magnitude curves so as to account for the different transmission losses that are inferred between NTS and the Russian sites. Clearly, quite a different picture of Russian test activity is implied by Figure 7, compared to that inferred from Figure 6.

We expect that the residual scatter, about the one to one slope line corresponding to yield values which are the same from both m_b and M_s estimates, is mainly due to the unaccounted effects of tectonic release and local variations of transmission characteristics, which fluctuate about the mean for the Russian sites. In our future work we intend to attempt to significantly improve upon these yield estimates by more fully and accurately accounting for all three effects, and to provide a strong justification for the "corrections" that are used.

The yield estimates for U.S. underground tests, before and after the limited test ban agreement, were obtained using the NTS magnitude-yield curves shown earlier and these estimates may be compared to the results for the Russian tests. In this regard, the U.S. test data gives yield estimates with a distribution similar to the Russian results for the 1977-81 period. The somewhat greater scatter in the yield estimates for the Russian tests is thought to be due to the

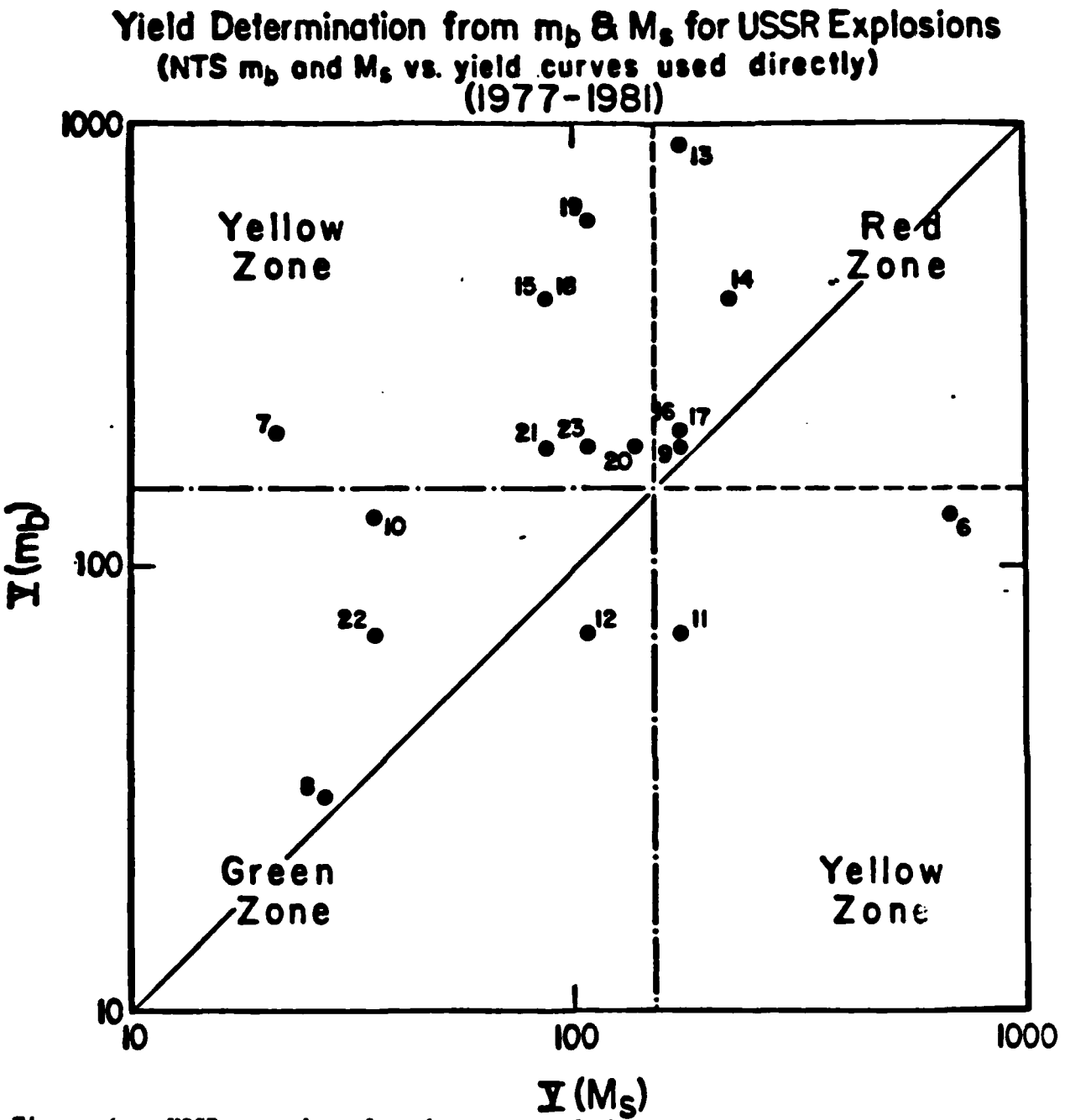

Figure 6 . USSR test data for the period of the limited test ban from 1977-1981. The yield estimate based on m_b is plotted vertically, while the M_S yield estimate is given on the horizontal scale. The NTS based m_b versus yield curve, uncorrected for site differences, was used to infer the body wave yields, $Y(m_b)$. The universal M_S versus yield curves were used for $Y(M_S)$. Use of the uncorrected m_b estimates of USSR yields produces biased $Y(m_b)$ results, with the yield estimates much too high for most events. Conversely, use of M_S uncorrected for tectonic release effects could result in $Y(M_S)$ too low for some events, and possibly $Y(M_S)$ too high for a few events.

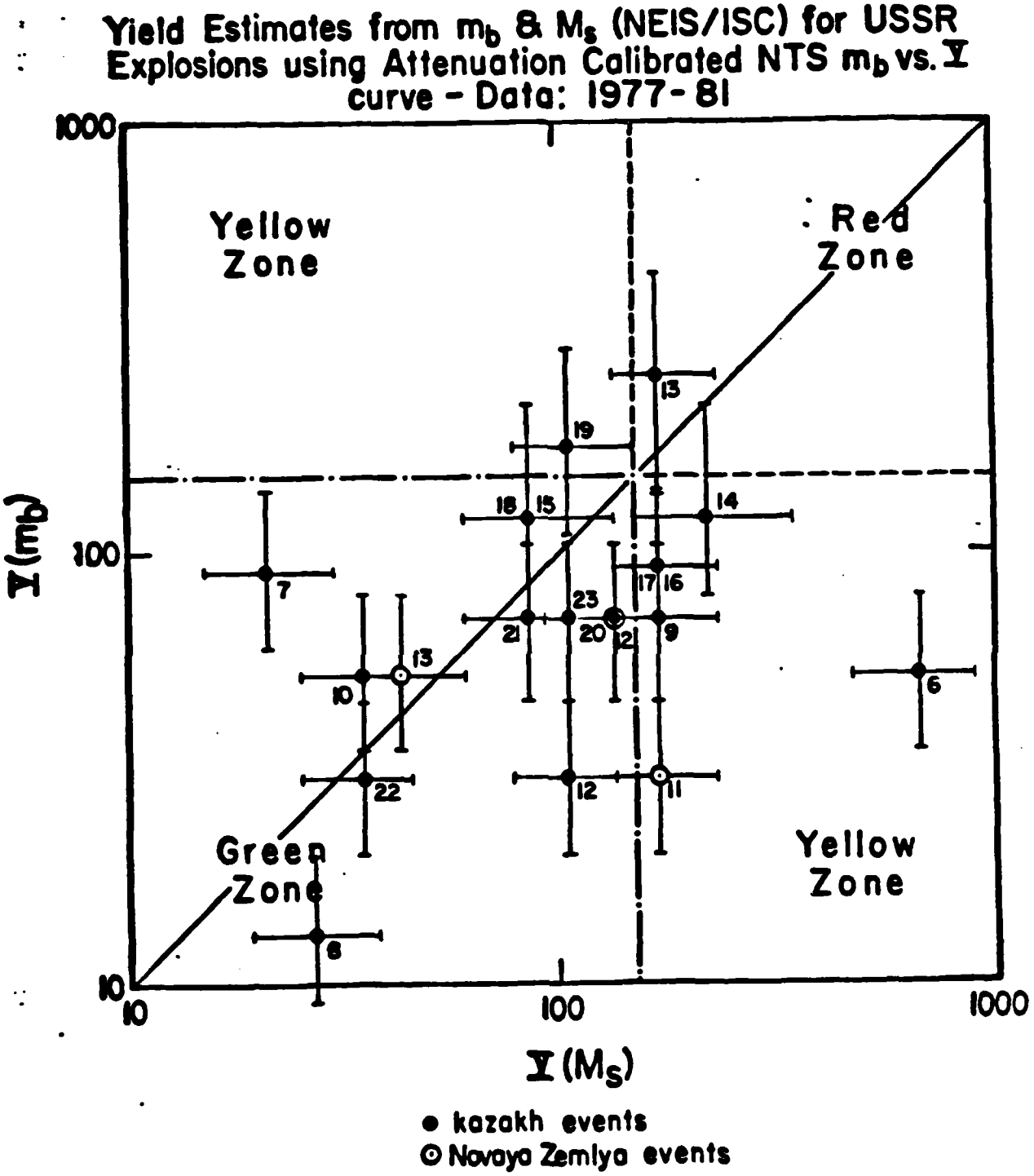

Figure 7. Yield estimates for the period 1977-81 using NTS magnitude versus yield curves corrected for differntial attenuation between NTS and Russian test sites (correction applied was .35 magnitude units for m_b). Yields based on M_s were obtained using "universal" M_s versus yield curves, with no correction for tectonic release effects.

greater perturbing effects of tectonic release for the Kazakh test site compared to NTS or the Novaya Zemlya sites. In particular, the Kazakh site appears to have a thrust type tectonic release equivalent while the NTS site is generally thought to produce strike-slip equivalent radiation, which only mildly perturbs the M_s values and has almost no effect on m_b values. On the other hand, a thrust mechanism can strongly bias M_s values and have nearly as large an effect on m_b (increases in m_b would be expected). As observed previously, we intend to more systematically investigate the effects of tectonic release on these yield estimates in an effort to provide a procedure for reduction or elimination of its effect for yield estimation.

V. "Anomalous Event" Conditions Leading to Discrimination Failure and Inaccurate Yield Estimates

It is rather easy to demonstrate that there are several complicating effects that can cause some of the standard earthquake-explosion discrimination methods, such as m_b *vs* M_s, to fail in particular circumstances. Further, biased yield estimates can be obtained when such magnitude data is used to estimate explosive yield. In particular, aside from the obvious failure that will occur for m_b *vs* M_s discrimination when earthquakes are grossly misclassified with respect to depth, it is shown that particular types of small earthquakes occurring at shallow depths, in the range from 5 to 25 km, will have anomalously low Rayleigh waves in the usual measurement range from 18 to 20 seconds. This "M_s null" occurs for small strike slip earthquakes, and is found to occur at *all* azimuths from this type of event. Further, as illustrated in Figure 10 small thrust earthquakes with dips at or near 45° produce similar "M_s nulls". These low M_s values will lead to earthquakes that appear very "explosion-like" in the $m_b - M_s$ discrimination plane.

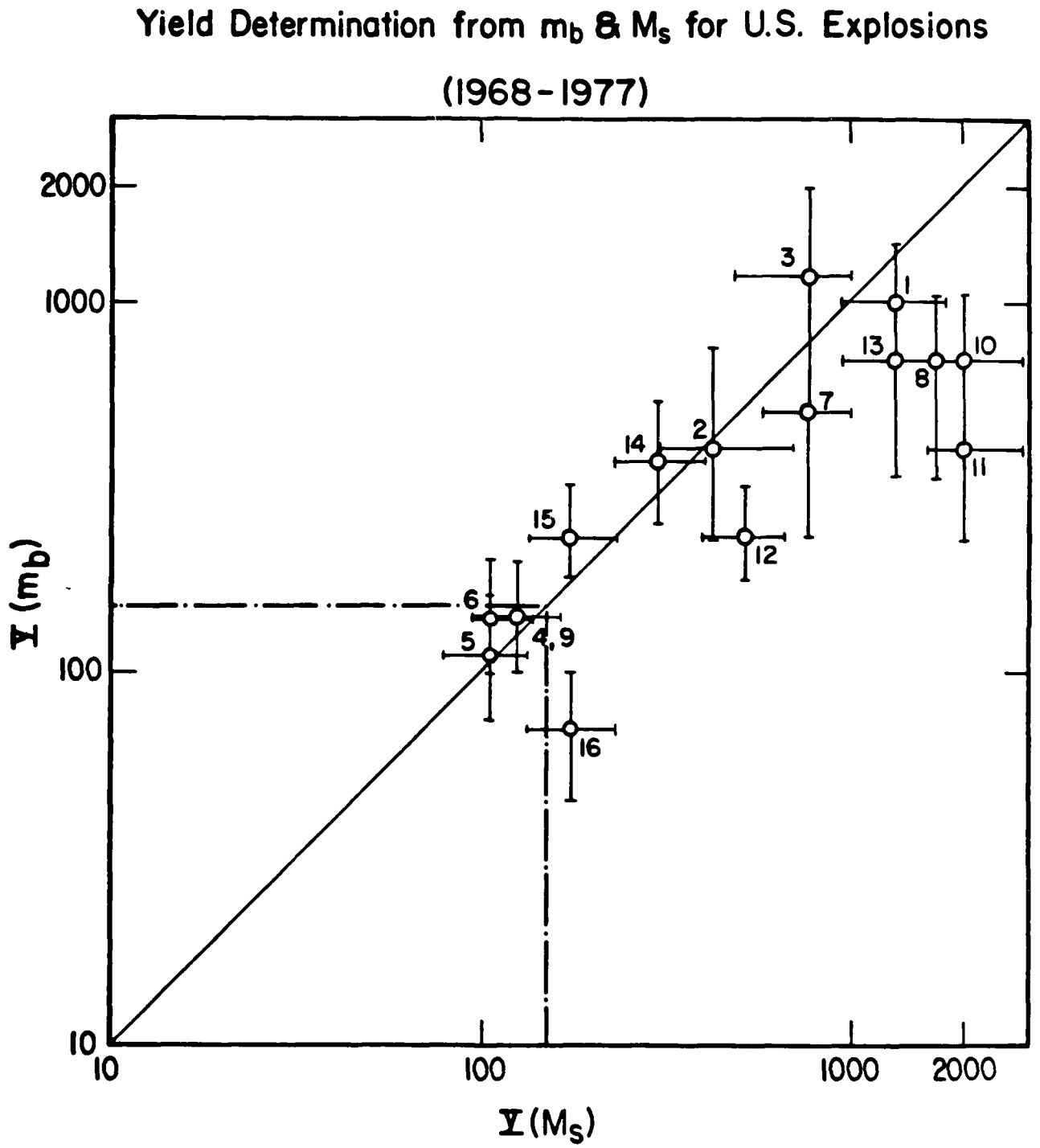

Figure 8. Yield estimates using both m_b and M_S for NTS underground explosions in the period 1968-77, prior to the limited test ban agreement.

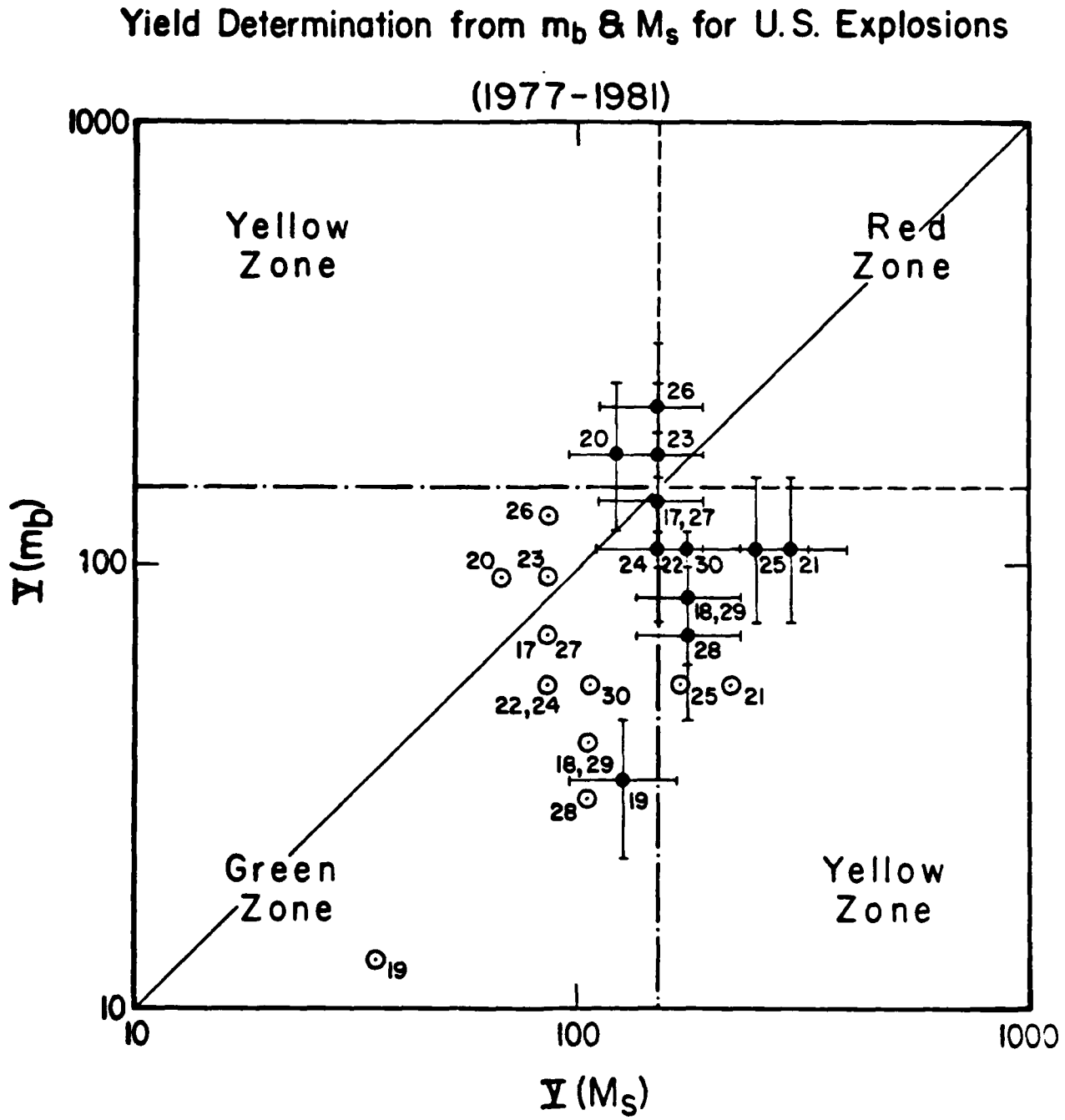

Figure 9. Yield estimates from both m_b and M_s data for NTS explosions during the period 1977-81. The solid circles correspond to estimates based on the intermediate coupling magnitude-yield curves for NTS while the open circles are yield estimates based on the NTS high coupling curves. The uncertainty lines indicated with the solid points are based on ±.15 deviations in both m_b and M_s data.

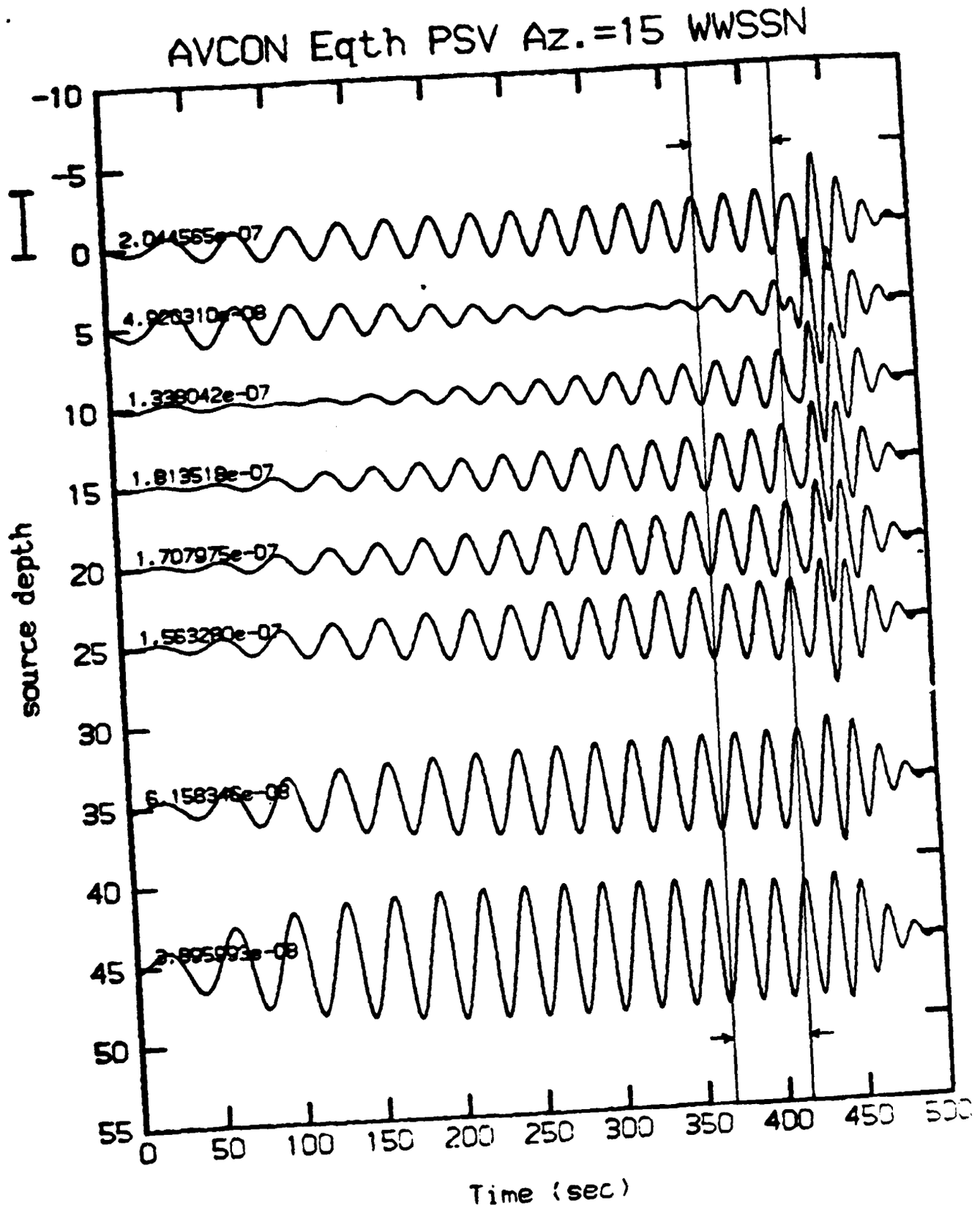

Figure 10 - Synthetic teleseismic Rayleigh waves for a 45° thrust point dislocation at various depths in an "average" continental structure (Model AVCON). The vertical lines indicate the time window within which Ms would be measured. The excitation of surface waves within the "Ms window" for the 5 km depth source will produce a "Ms null". This Ms null will occur at nearly all azimuths for small 45° thrust earthquakes.

A second complication that affects spectral discriminants at teleseismic distance ranges, and affects teleseismic explosive yield estimation as well, is the highly variable effective Q observed across continents, as well as similar variability across trench zones and oceanic ridges. For example, on the basis of results from Butler (1983), which are summarized in Section III, large variations in the observed effective Q occur within the continental U.S., not only from geologic province to province, but also within these provinces on a rather fine spatial scale. While part of these observed variations are undoubtedly due to complex velocity structure, which produces scattering and focusing effects, it is certain that the most important broad scale effect is due to upper mantle absorption, which occurs nearly exclusively within the upper mantle low velocity zone. As is well known, differences in the anelastic absorption and "scattering loss" processes between test sites can result in the necessity of recalibration of empirical magnitude-yield relations, to take into account the differences in absorption (the "Q bias") between test sites, as was discussed in Section IV. This, consequently, requires fairly detailed knowledge of the upper mantle characteristics at a test site, or reliance on other (robust) methods of yield estimation which are unaffected by upper mantle absorption. Thus, for accurate teleseismic yield estimation using "Q corrected" m_b, it would be necessary to have effective Q information for an area of interest that was at least as complete as that now available for the continental U.S.

In addition, low Q zones with associated high absorption can cause the high frequency spectra of explosions and earthquake P waves to be reduced below station noise levels near low Q regions, so that the spectral differences upon which variable frequency spectral discrimination is based cn be obscured by noise. Such effects on spectral magnitudes have been observed and correlated with the existence of anomalously low upper mantle Q zones in the vicinity of

particular events. (In this case, explosions will appear within the earthquake population in the spectral magnitude "parameter space.")

Theoretically it has been shown (Stevens, 1980) that zones of high initial prestress, at or near the failure zone for an earthquake, can give rise to peaked earthquake spectra and a significant enrichment of the high frequency part of the spectrum from the event. This is potentially a problem for both m_b *vs* M_s and spectral discrimination, since the high frequency enrichment could lead to enhanced m_b values at a fixed M_s level. However, it appears in reality that the stress levels in the earth at shallow depths are not generally high enough to cause serious difficulties for discrimination, and that only for quite deep earthquakes (100 km and deeper) is the effect likely to be very strong and only then, apparently, for some rather small percentage of earthquakes. In this regard, however, Figures 11 and 12 illustrate results of variable frequency magnitude (VFM) discrimination where this effect appears to occur.

Specifically, these figures show VFM discrimination results at Red Lake, Ontario and the LASA array in Montana for well recorded events from a large Eurasian data set. At RKON three deep earthquakes appear in the explosion population, plus one earthquake that is thought to be a shallow event. Nevertheless, a large number of deep and shallow earthquakes form a distinctly separate population distribution, which is well separated from the explosions. The LASA results, with fewer events well recorded, show that there is again a good representation of the explosion and earthquake populations with, however, one deep earthquake appearing in the explosion population. In both figures the earthquake populations are made up of earthquakes at all depths, from very shallow to very deep. Thus it appears that some earthquakes can violate this spectral discrimination criteria at a single station. However, it is also true that only very rarely does a particular earthquake fail the VFM

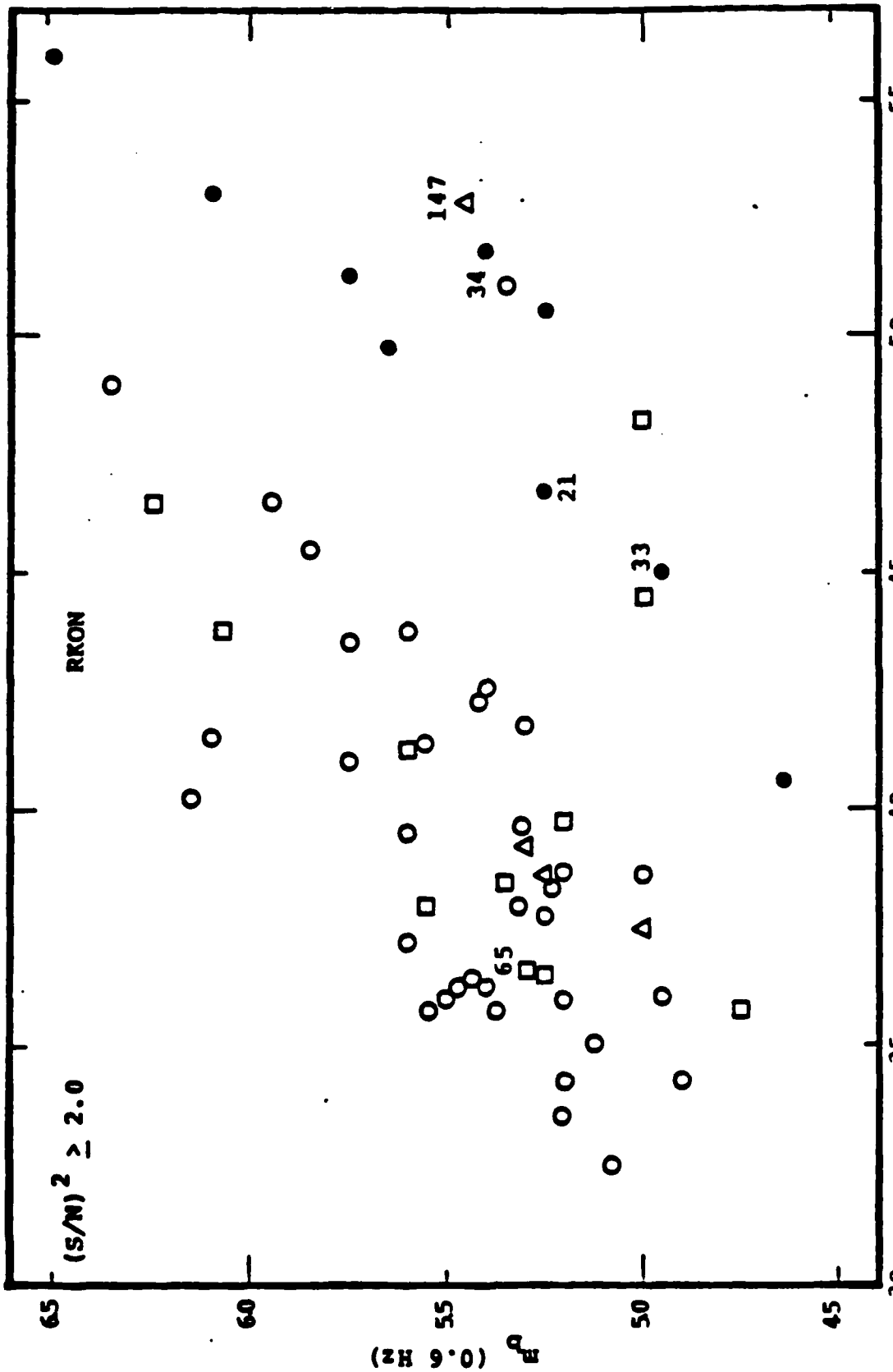

Figure 11. VFM discrimination at Red Lake Ontario, Canada results from events in Eurasia. Solid circles are presumed explosions, open circles shallow-earthquakes, open squares intermediate depth earthquakes and open triangles deep earthquakes.

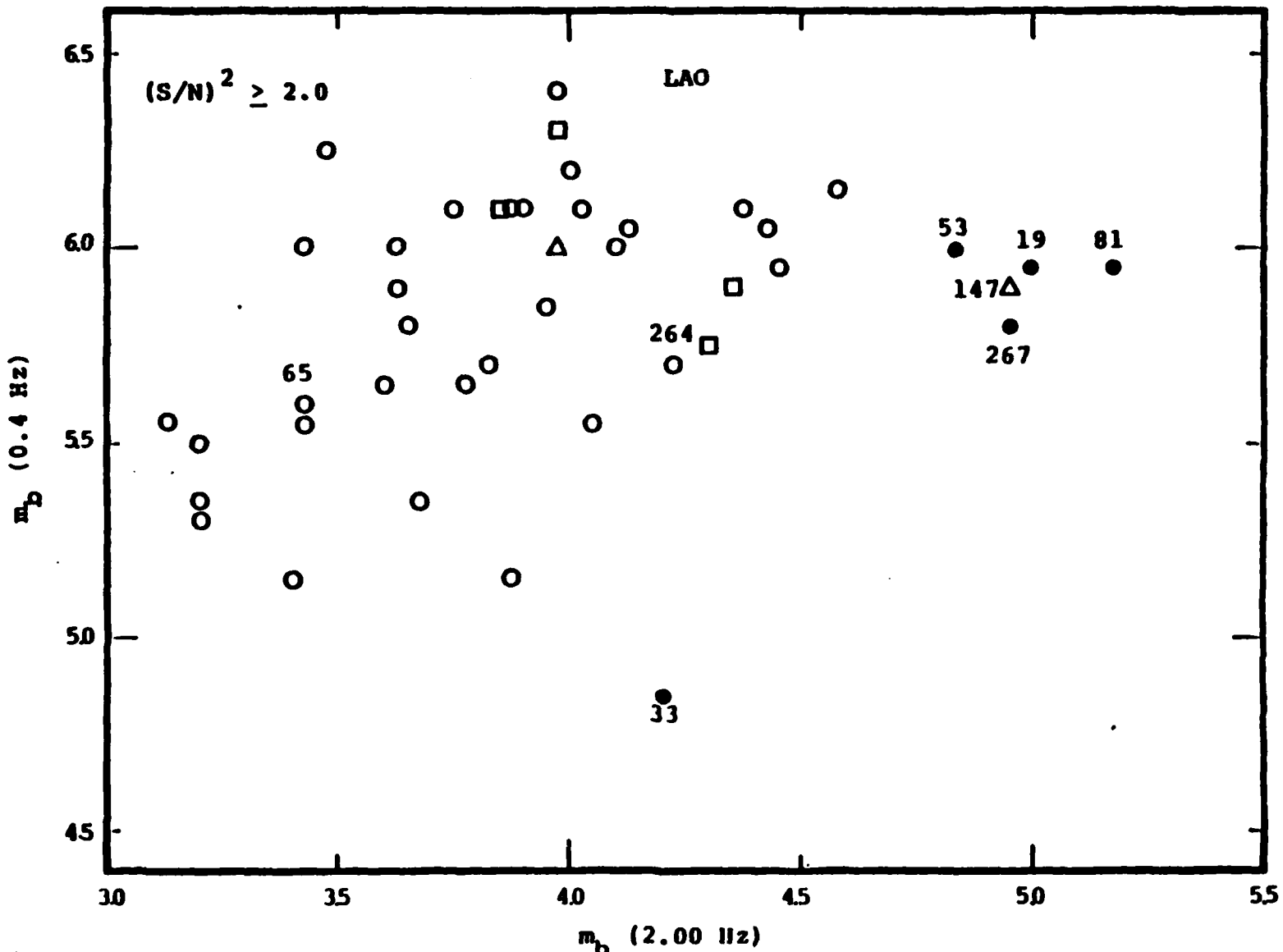

Figure 12. VFM discrimination results at the LASA array in Montana from events in Eurasia. Open symbols are earthquakes and solid circles are presumed explosions. Shallow earthquakes are indicated by circles, intermediate depth by squares, deep by triangles.

discrimination criteria over an entire set of stations and in the one instance where this occurred, the event in question was a very deep earthquake that appeared in explosion populations at many stations. (The event was in fact event No. 147 shown in these figures.) Thus, there appears to be occasional deep events having spectral properties that are explosion-like and that appear so at nearly all teleseismic stations. Nevertheless, almost all deep and shallow earthquakes appear distinctly different spectrally from explosions. Clearly, if these "anomalous" earthquakes are only deep earthquakes, then depth estimates for all events that appear "explosion-like" in the VFM plane will identify these "anomalous" events as deep earthquakes, with any shallow event in this population being a probable explosion.

Should there be more common occurrences of shallow earthquakes appearing in the explosion population, such as the one event considered to be an earthquake in the explosion population region in the VFM plane at RKON, then more elaborate (joint) discrimination procedures would be required to sort out the probable explosions, from events in the explosion population region in the VFM plane. However, based on the Eurasian events studied so far, no shallow earthquake that was "well" recorded (with signal to noise power larger than 2) at several stations has been found to appear explosion-like at a majority of the stations. Thus, occasionally, at one or two stations, a shallow earthquake will appear explosion-like, but on a multi-station identification basis, these events have been properly identified. (This means, however, that ***single*** station event identification by VFM spectral discrimination can result in misclassification of some shallow earthquakes as possible explosions unless other single station discriminants are also used which can help provide identification.)

Finally, a complicating effect of considerable significance is tectonic

release associated with explosions. As is well known, numerous Shagan River test site explosions show highly anomalous surface wave radiation involving large Love waves and "reversed" Rayleigh waves (i.e. reversed in polarity compared to explosion events in the same region that do not produce large Love waves). The effect can be explained by tectonic release equivalent to a thrust type tectonic shear stress field at the explosion site. Hence, it is clear that low frequency Rayleigh waves, and M_s measurements, can be very strongly affected. In fact the tectonic component can be much larger than the explosion component, so that yield estimation from M_s can be (very) strongly perturbed. In addition, as shown by Murphy, Archambeau and Shaw (1983), the direct P wave from the Rulison explosion in Colorado was strongly perturbed by induced tectonic release, such that the observed *mb* value was reduced by about .3 magnitude units. Therefore *both* M_s and m_b can be strongly perturbed by tectonic release effects making yield estimation using these magnitude measures more difficult. (Indeed, if the thrust oriented shear stress applies to the surface waves from the Shagan River events then, based on the Rulison results, this tectonic mechanism would also strongly perturb the m_b values for these events. The perturbation would, however, be such as to *increase* them by as much as several tenths of a magnitude unit, which is opposite to the decrease in m_b observed for Rulison.)

Solutions to most of these problems are not too difficult to find, once the mechanisms responsible for the anomalies are identified. Specifically, multivariant spectral magnitude discrimination using both body and surface wave magnitudes measured at a number of frequencies can eliminate or minimize the discrimination problems described earlier. Here the appropriate approach would be to rely upon body wave spectral magnitudes, such as $m_b(f_1)$ *vs* $m_b(f_2)$, for discrimination in the regional distance range, particularly for small

events, and to use $m_b(f_1)$ *vs* $M_s(f_2)$ (including the standard m_b *vs* M_s) at teleseismic distances, for the larger events (*e.g.*, for events with $m_b > 4.0$ to 4.5). In this case the "M_s null" for small events is avoided, since body waves are used for spectral discrimination of small events, and at regional distance ranges the upper mantle low Q absorption will not affect this crustal body wave discrimination procedure. For all larger events, which will involve failure over a fairly wide depth interval, the "M_s null" will not appear and m_b *vs* M_s will apply as a well verified discrimination procedure that is not so strongly perturbed, by upper mantle Q variations and other propagational effects, as to cause event identification failure. Here, the standard m_b *vs* M_s approach would be supplemented by using m_b *vs* M_s at a range of frequencies (*e.g.*, 1 Hz and .05 Hz, as is the practice now, but also at .5 Hz and .03 Hz, 1.5 Hz and .05 Hz, etc.) This latter multivariant m_b *vs* M_s approach can be used to increase the confidence level of teleseismic event identification, and also to supplement the body wave spectral discrimination at regional distances.

For accurate yield estimation of identified explosions in all situations, it is necessary to avoid Q biased measurements, or to correct for the "Q bias", and to explicitly remove contamination effects due to tectonic release, the latter when it occurs being evidenced by SH wave production at rather high levels at all frequencies. This can be accomplished by routinely measuring $M_S^L(f)$ (*i.e.*, Love wave magnitudes at several frequencies) as well as $M_S^R(f)$ (the normal Rayleigh wave magnitudes at various frequencies) and $m_b(f)$. When the Love wave magnitudes for identified (or suspected) explosions are low, then $M_S^R(f)$, with appropriate distance corrections applied, can be used to estimate yield in the usual manner. Since M_S^R based yield estimation avoids the strong upper mantle attenuation effects, it is to be preferred for yield estimation. However, m_b based yield estimates can simultaneously be obtained using a standard empiri-

cal relationship, and any "Q bias" for the explosion site region can be estimated by comparing the yield estimated from m_b to that obtained from M_s. (In this way a calibration for m_b *vs* yield for the site could be obtained.) For explosions showing moderately large M_S^L at the lower frequencies used for yield estimation, such as .05 Hz, then the observed M_S^R and M_S^L data must be jointly interpreted (e.g. within the theoretical framework of stress relaxation due to shatter zone induced tectonic release) to provide estimates of the physical parameters for the tectonic release source, in particular the effective shatter zone radius and the prestress magnitude and orientation. These parameters can then be used, again within the framework of the theory, to infer the magnitude of the explosive component for both M_S^R and m_b measurements. These corrected M_S^R and m_b values can then be used to infer the proper yield, again with M_S^R used as the primary means of yield estimation, so that "Q bias" effects are minimized. For very large observed M_S^L values associated with an identified explosion (*e.g.*, $M_S^L > M_S^R$ for $f \geq .05$ Hz), then it is possible that earthquake triggering could have taken place and, in this rare instance, an in-depth study of such a potentially complex event would be necessary to obtain an accurate explosive yield estimate.

VI. References

Archambeau, C. B., Applications of variable frequency magnitude data to the estimation of seismic source properties, *EOS, 59*, 1139, 1978.

Archambeau, C. B., Seismic evidence for strongly heterogeneous tectonic stress in the Earth; Abstract, Spring Meeting, American Geophysical Union, 1982.

Archambeau, C. B. and J. F. Evernden, Seismic discrimination of earthquakes and explosions, Part I. Theoretical Foundations, *Rev. Geophys. Space Phys.*, 1983.

Archambeau, C. B. and J. Savino, Discrimination of seismic events using body wave spectral magnitudes, *J. Geophys. Res.*, 1983.

Archambeau, C. B. and J. Scales, The physical significance of seismic moment tensor representations, *Geophys. J. Roy. Astr. Soc.*, 1983.

Archambeau, C. B. and M. Schnapp, Computer applications of quasi-harmonic decomposition to seismic signal detection and analysis, to be submitted to *Geophys. J. Roy. Astr. Soc.*, 1984.

Archambeau, C. B., T. C. Bache and C. A. Salvado, Estimation of non-hydrostatic stress in the Earth by seismic methods: Lithospheric stress levels along the Aleutian subduction zone, *Geophys. J. Roy. Astr. Soc.*, 1983.

Archambeau, C. B., C. Salvado and T. Bache, Estimation of tectonic stress by seismic methods: Lithospheric stress levels in the Alaska-Aleutian Arc Region, to be submitted to *Geophys. J. Roy Astr. Soc.*, 1984.

Archambeau, C. B., M. Schnapp, R. Goff, J. M. Savino, J. F. Masso, and K. Hamilton, Methods of seismic detection and analysis based on Quasi-Harmonic Decomposition (QHD), submitted to *Geophys. J. Roy. Astr. Soc.*, 1984.

Dilts, G., J. A. Scales and C. B. Archambeau, The transparent non-spherical elastodynamic source; Abstract, Spring Meeting, American Geophysical Union,

1982.

Evernden, J. F. and C. B. Archambeau, Seismic discrimination of earthquakes and explosions, Part II. Observational Methods and Results, *Rev. Geophys. Space Phys.*, 1984.

Harvey, D., Seismogram synthetics using normal mode superposition: The locked mode approximation method, *Geophys. J. Roy. Astr. Soc.*, *66*, 37-69, 1981.

Harvey, D., Mode superposition methods for prediction and analysis of complete seismic wave fields, Ph.D. Thesis, University of Colorado, Dept. of Geology/CIRES, 1984.

Savino, J. and C. B. Archambeau, Applications of variable frequency magnitude data to the estimation of seismic source properties, Abstract, Spring Meeting, Amer. Geophys. Union, 1978.

Savino, J. M., J. F. Masso and C. B. Archambeau, Discrimination results from the Priority I stations (U), Interim Report, ARPA Order No. 2251, Systems Science and Software Report SSS-CR-79-4026, May, 1979.

Savino, J. M., C. B. Archambeau and J. F. Masso, VFM Discrimination Results for the Priority II stations, Systems, Science and Software Special Technical Report, VSC-TR-81-29, July, 1980.

Scales, J. A. and C. B. Archambeau, The physical significance of moment tensor representations; Abstract, Spring Meeting, American Geophysical Union, 1982.

Marshall, P. O., D. L. Springer and H. C. Rodean, Magnitude corrections for attenuation in the upper mantle, *Geophys. J. R. Astr. Soc.*, *57*, 509-638, 1979.

Murphy, J. R., C. B. Archambeau and H. K. Shah, Magnitude/yield variability in the western United States: Analysis of the Rulison/Gasbuggy anomaly,

AFOSR Report, ARPA Order No. 4397, Systems, Science and Software report SSS-R-83-5978, Jan. 1983.

Appendix 1

Seismic Discrimination of Earthquakes and Explosions:

Part I - Theoretical Foundations

I. Mathematical Foundations

In the following sections we will wish to make use of a number of rather standard results in the mathematical theory of elasticity. In addition, we will use some new results, as well as specialized notation, which may not be immediately familiar to the reader. In order to present the more physical arguments and discussion that will follow, without the clutter involved with the parenthetical digressions required to define notation and develop certain mathematical results, we give a brief summary of the basic mathematical notation and results that will be needed later.

Basic Equations of Motion and Boundary Conditions

In order to develop the representations to be used in a systematic and logical fashion we begin with the basic equations of motion in an elastic/anelastic continuum, which simply are an expression of the conservation of momentum. These equations can be put into the form (Archambeau and Minster, 1978):

$$L_{\alpha\gamma}u_\gamma = \rho f_\alpha \; ; \; \alpha, \gamma = 1,2,3,4 \tag{1}$$

where the summation convention for repeated indices applies and where u_α are components of the displacement field and f_α the external force field density, with both of these fields written as four vectors for the convenience of expressing the equations of motion in compact form. In particular, these fields are defined to have the component form:

$$(u_\gamma) = (u_1, u_2, u_3, 0)$$

$$(f_\alpha) = (f_1, f_2, f_3, 0)$$

where the fourth component (the "time-like" component) is set to zero. In addition, the independent variable vector $\mathbf{x}$ is the four vector:

$$(x_\gamma) = (x_1, x_2, x_3, t)$$

with time t the fourth component in this notation. Further, in this notation $L_{\alpha\gamma}$ is the "elastic operator", and has the form:

$$L_{\alpha\gamma} \equiv \frac{\partial}{\partial x_\beta}\left[C_{\alpha\beta\gamma\delta}\frac{\partial}{\partial x_\delta}\right]$$

where

$$C_{\alpha\beta\gamma\delta} = \begin{cases} C_{\alpha\beta\gamma\delta} = -C_{ijkl}; (\alpha, \beta, \gamma, \delta) = (i, j, k, l) \\ C_{i4k4} = C_{44ik} = \rho\delta_{ik}; i, k = 1, 2, 3 \\ C_{\alpha\beta\gamma\delta} = 0; \text{ all other } \alpha, \beta, \gamma, \delta \end{cases}$$

Here the greek indices are always defined to run over the integer range from 1 to 4, with the regular latin indices i, j, etc., always defined to run over the integer range from 1 to 3. The tensor C_{ijkl} is the ordinary elastic tensor, which in the isotropic case is just:

$$C_{ijkl} = \lambda\delta_{ij}\delta_{ik} + \mu(\delta_{il}\delta_{jk} + \delta_{ik}\delta_{jl})$$

(This material tensor can incorporate anelastic effects if the Lamé constants λ and μ are generalized to represent operators, involving convolutions and derivatives with respect to time. See Archambeau and Minster (1978) for details.) Finally, ρ is the density for the material.

Thus the elastic tensor, when written in the expanded "four component" form, can be made to include inertial effects as well as rheological effects. The symmetry of this generalized elastic tensor is the same as that of the ordinary elastic tensor, in particular:

$$C_{ijkl} = C_{jikl} = C_{ijlk} = C_{klij}$$

and

$$C_{\alpha\beta\gamma\delta} = C_{\beta\alpha\gamma\delta} = C_{\alpha\beta\delta\gamma} = C_{\gamma\delta\alpha\beta}$$

This symmetry insures that angular momentum is conserved, as well as linear momentum, in the equations of motion.

A generalized stress tensor $\tau_{\alpha\beta}$ can be defined in terms of the generalized elastic tensor, where

$$\tau_{\alpha\beta} = C_{\alpha\beta\gamma\delta} \frac{\partial u_\gamma}{\partial x_\delta}$$

In terms of this tensor, the equations of motion become

$$\tau_{\alpha\beta,\beta} = \rho f_\alpha \,. \tag{2}$$

where the comma denotes the derivative with respect to the index β, that is:

$$\tau_{\alpha\beta,\beta} \equiv \frac{\partial}{\partial x_\beta} \tau_{\alpha\beta}$$

As is shown by Archambeau and Minster (1978), boundary conditions at or across *any* type of boundary within the medium are:

$$\left[\!\left[\tau_{\alpha\beta}\eta_\beta \right]\!\right] = 0; \mathbf{r} \in \partial V \tag{3}$$

where the double bracket notation is used to denote the change (or jump) in the quantity enclosed across the internal or external boundaries ∂V. That is, $\left[\!\left[\varphi \right]\!\right] = \varphi^{(1)} - \varphi^{(2)}$, where φ is any function or variable and the superscripts (1) and (2) are used to denote the value of φ when the surface is approached, in the limit sense, from opposite sides. Here η_β are the components of a space-time normal to a hypersurface in (x_k, t), and this four-vector has the form:

$$(\eta_\beta) = (n_1, n_2, n_3, -U_i^* n_i)$$

where n_i, $i = 1, 2, 3$, is the ordinary spatial normal to a surface of discontinuity in the continuum and

$$U_i^* = U_i - v_i \,,$$

where U_i are components of the velocity of the boundary[+] and v_i are the

[+]Since U is the velocity of a surface, it is defined to be continuous across that surface. Thus $\left[\!\left[U_i \right]\!\right] = 0$, for all i.

components of the velocity of the material particles. If the boundary moves with the particles and the particle velocity is continuous across the boundary, which is ordinarily the case for solid-solid boundaries, then the relative velocity components U_i^* all vanish, and the boundary condition (3) reduces to the regular condition of continuity of traction across a material boundary. Further, since the combination $U_i^* n_i$ appears in the expression for η_β, then $U_i^* n_i$ vanishes if only the normal components of **U** and **v** are equal and continuous at the boundary. This is the case for ordinary liquid-solid boundaries. However, in certain cases such as when the boundary in question is a moving phase change boundary, where the material on one side is in a different phase state from that on the other, then the boundary movement in space may be driven at a slower or faster rate than the particles are driven, and in this case $U_i^* n_i$ is non-zero. In particular, in the case of spontaneous failure in a solid under stress, the boundary of the failure zone expands with time and separates material regions in which the rheological properties are quite different. Further, the failure zone surface separates regions in which the material behaves nonlinearly (the interior) from the exterior linear region, where the linearized equations of motion (1) apply. The boundary of a failure zone usually expands at a rate that is very different than the local velocity of the material particles and, as shown by Archambeau and Minster (1978) and in later sections of this discussion, the rate of movement is much larger than the particle velocity, usually being of the order of the local shear velocity in the material. Therefore the boundary condition (3), which expresses conservation of momentum at a boundary, must be used in its most general form when we deal with failure processes, such as those involved in earthquake phenomena.

If we use the definition for the generalized stress and "elastic" tensors, then the boundary condition (3) can be put into the form:

$$\left[\!\left[\tau_{\alpha\beta}\eta_\beta \right]\!\right] = \left[\!\left[(\rho v_k v_l^* - T_{lk})\, n_l \right]\!\right] = 0$$

where T_{lk} is the ordinary stress tensor, that is

$$T_{lk} = C_{lkmn} u_{m,n}$$

in the exterior linear region, and where[+]

$$v_l^* = v_l - U_l = -U_l^*$$

Whereas (3) expresses the conservation of momentum across a boundary, the conservation of mass is insured by the condition (Archambeau and Minster, 1978)

$$\left[\!\left[\rho v_l^* n_l \right]\!\right] = 0 \qquad (4)$$

which holds in general, whether the boundary moves with the particles or not. If the boundary does, however, move with the particles, then conservation of mass is insured by

$$\left[\!\left[v_l n_l \right]\!\right] = 0$$

[+]It should be emphasized that **U** is, by definition, continuous across the boundary over which it is defined, in that $\left[\!\left[U_l \right]\!\right] = 0$, for all l. However, since components of **v** can be discontinuous, $U_l = v_l$ can *only* occur if **v** happens to be continuous in all its components on the surface over which **U** is defined.

so that (4) degenerates to the condition of continuity of the normal component of the particle velocity. If the boundary is assumed to be a "welded" solid-solid contact, then the tangential components of the particle velocity across the boundary are also continuous, and the (stronger) condition,

$$[\, v_k \,] = 0, \; k = 1, 2, 3,$$

applies. This is also often expressed in terms of the displacement field as

$$[\, u_k \,] = 0, \; k = 1, 2, 3 \,.$$

The conservation of energy at an expanding or moving boundary has the form (Archambeau and Minster, 1978):

$$[\, (\rho E v_i^{\bullet} - v_k T_{ik} + q_i)\, n_i \,] = 0 \qquad (5)$$

Here ρ is the density, E the total energy, q_i the components of the heat flux and T_{ik} the stress tensor. In most elastodynamic applications, including those involving failure processes, the heat flux term may be neglected since the changes due to heat flow are very small on the time scale associated with elastodynamic variations. Thus, for a "fast process" like failure in solids, the heat flux term in (5) is negligible. Further, the total energy, ρE, is the sum of the internal energy ρe, the kinetic energy $1/2 \rho v_k v_k$ and the potential energy due to conservative body forces, so that

$$E = e + 1/2 v_k v_k + \varphi$$

where φ is the potential for the body forces, defined by $f = -\nabla\varphi$. In the elastodynamic case, φ corresponds to the gravitation potential and changes in this quantity across boundaries, in particular across failure zone boundaries, are very small. Therefore

$$[\, E \,] \simeq [\, e \,] + 1/2 [\, v_k v_k \,]$$

is a good approximation for the change in E across material boundaries. When heat exchange and changes in the body force potential are neglected, then (5) is automatically satisfied when the momentum and mass conservation relations, (3) and (4), are satisfied, if there is no change or "jump" in the internal energy across the boundary. This is the situation with normal boundaries, defined by material contrasts in a layered medium, where the boundary moves with the material particles.

If there is energy absorption or release at a boundary, such as is the case for a failure process where energy is absorbed by the material in the transition to the more disordered (failed) state, then (5) is not automatically satisfied and the conservation of energy condition at the boundary constrains the rate at which the failure process can proceed. In particular, the energy absorbed per unit mass $[\, e \,]$ is characteristic of the material and the particular transition process which is occurring, and so is equivalent to a quantity analogous to a latent heat. For failure processes in solids (which may or may not involve first order phase transitions) the energy required for the process, per unit mass that undergoes failure, is denoted by L. Hence, we set: $[\, e \,] = L$, and the boundary condition in (5) can be put in the form:

$$\rho^{(1)}(L + 1/2 [\, v_k v_k \,])\, (U_i - v_i^{(1)}) n_i = - [\, v_k T_{ik} n_i - q_i n_i \,]$$

Here $\rho^{(1)}$ and $v_i^{(1)}$ refer to the material before transition, that is to the material outside the failure zone. We define the rupture rate U_R to be the rate at which the failure surface expands in the direction normal to itself, measured relative to the particle velocity in the material outside the failure zone. Thus

$$U_R \equiv (U_i - v_i^{(1)})n_i$$

Now, using the other conservation relations given in (3) and (4) to eliminate terms involving $[\![v_k]\!]$, it is shown by Archambeau and Minster (1978) that this relation is equivalent to:

$$U_R^2 - \frac{[\![q_k n_k]\!]}{\rho L} - \frac{[\![t_k t_k]\!]}{2\rho^2 L} = 0$$

where $\rho \equiv \rho^{(1)}$, and $t_k \equiv T_{ik} n_i$ is the traction. Here, of course, it is assumed that $L \neq 0$. If the heat flux is neglected then this gives:

$$U_R \simeq \left[\frac{[\![t_k t_k]\!]}{2\rho^2 L} \right]^{\frac{1}{2}} \tag{6}$$

which expresses energy conservation on a moving boundary along which energy absorption occurs due to a transition process, such as material failure.

The momentum and mass conservation relations, in the general case, may be combined into one relation by expanding (3), and by using (4) to eliminate terms. Specifically, the combined mass-momentum boundary relation is (Archambeau and Minster, 1978):

$$\rho [\![v_k]\!] U_R = - [\![t_k]\!] \tag{7}$$

where U_R, ρ and t_k are as defined above.

In general, any boundary along which energy absorption (or release) occurs will move at a rate that is different than the particle velocities on either side of the boundary, and in this case the general forms of the conservation laws expressed by (3), (4) and (6), or (6) and (7), are the appropriate boundary relations to be satisfied. Further, such moving boundaries make the dynamical system non-linear, since the movement or expansion of these boundaries depends on the elastodynamic field, via the (nonlinear) dependence of U_R on the particle velocities and tractions in (5) and (7). Thus, while the equations of motion in the medium exterior to a failure zone are linear, and are as indicated in (1), nevertheless the system of equations governing the elastodynamic fields in the linear zone outside the failure region consist of the linear differential equations *plus* the (nonlinear) boundary conditions on a rapidly moving, or expanding, boundary surface. The non-linear aspect of this elastodynamic problem is displayed explicitly by the Green's function integral equation for the displacement field u in the exterior (linear) region surrounding an expanding failure zone, since it incorporates, in a single equation, the equation of motion and boundary conditions at the failure surface, plus initial conditions.

Green's Functions and Integral Equations for Elastodynamic Problems

In order to obtain integral equations for the elastodynamic field, and exact and approximate solutions of these latter equations, we need to consider Green's functions, $G_k^m(\mathbf{x}, t; \mathbf{x}_0, t_0)$, corresponding to the k component of displacement in the medium, at a receiver point at $\mathbf{x}$ and time t, due to an impulse

force in the m coordinate direction, occurring at a source point at $\mathbf{x}_0$ and at time t_0. The Green's function to be considered must satisfy the inhomogeneous elastodynamic equation of motion along with the regular boundary conditions for a layered earth model. More specifically, the boundaries of the medium are taken to move with the material, so that there is not relative movement between particles and the boundary surface, but there may be slip at the boundary such as occurs at fluid-solid or fluid-fluid boundaries. In this latter case the tangential components of the particle velocity need not be continuous.

The Green's function of interest therefore is defined by the following system of equations:

$$\frac{\partial}{\partial t}\left[\rho \frac{\partial G_i^m}{\partial t}\right] - \frac{\partial}{\partial x_j}\left[C_{ijkl} \frac{\partial G_k^m}{\partial x_l}\right] = \Delta_i^m(\mathbf{x}, t; \mathbf{x}_0, t_0) \tag{8a}$$

with Δ_i^m a generalized delta function given by

$$\Delta_i^m = 4\pi\delta_{im}\, \delta(\mathbf{x} - \mathbf{x}_0)\, \delta(t - t_0)$$

Here $\delta_{im} = 1$ if $i = m$ and is zero otherwise, while $\delta(\mathbf{x} - \mathbf{x}_0)$ and $\delta(t - t_0)$ are Dirac delta functions. The appropriate boundary conditions for G_k^m are:

$$[\, g_k^m \,] = 0 \,;\, \mathbf{x} \in \partial V \tag{8b}$$

and, on welded solid-solid boundaries

$$[\, G_k^m \,] = \,;\, \mathbf{x} \in \partial V \tag{8c}$$

or, on liquid-solid and liquid-liquid boundaries

$$\left[\, \frac{\partial G_k^m}{\partial t} n_k \,\right] = 0 \,;\, \mathbf{x} \in \partial V \tag{8d}$$

Here g_k^m denotes the tractions on the boundaries of the medium, the latter denoted by ∂V, with n_k the components of the normal to such a surface. (The boundaries ∂V can be internal as well as external, with any of these being defined as surfaces across which the material properties are discontinuous.) The explicit form for the Green's traction is:

$$g_i^m = \left[C_{ijkl} \frac{\partial}{\partial x_l} G_k^m\right] n_j$$

The system of equations in (8) can be solved in closed form for media composed of layers with uniform properties, such as are usually used to model the earth. In particular, for a spherical earth model, consisting of concentric spherical shells, the Green's function satisfying the system of equations (8) in such a model is obtained by first applying the Fourier time transform to the system of equations (8), and then expressing the Green's function as an eigenfunction expansion with coefficients which are determined by the boundary conditions. The resulting system of algebraic equations can be solved using the Haskell-Thompson matrix method (*e.g.* Ben-Menahem and Singh, 1972) and this gives, for the transform of the Green's function:

$$\bar{G}_{ij}^{s}(\mathbf{x}, \mathbf{x}_0; \omega) = \sum_{l,m,n} \left[\frac{\psi_p^S(\mathbf{x}; \omega_{lm}^S)\, \bar{\psi}_q^S(\mathbf{x}_0; \omega_{lm}^S)}{\omega^2 - (\omega_{lm}^S)^2}\right.$$

$$+ \frac{\psi_p^T(\mathbf{x};\omega_{ln}^T)\,\bar{\psi}_q^T(\mathbf{x}_0;\omega_{ln}^T)}{\omega^2-(\omega_{ln}^T)^2}\Bigg] \tag{9}$$

where

$$\psi_p^S(\mathbf{x};\omega_{ln}^S) = D_{lm}(r;\omega_{ln}^S)\,\mathbf{P}_{lm}(\vartheta,\varphi)\cdot\mathbf{e}_p$$

$$+ E_{lm}(r;\omega_{ln}^S)\,\mathbf{B}_{lm}(\vartheta,\varphi)\cdot\mathbf{e}_p$$

$$\psi_p^T(\mathbf{x};\omega_{ln}^T) = F_{lm}(r;\omega_{ln}^T)\,\mathbf{C}_{lm}(\vartheta,\varphi)\cdot\mathbf{e}_p$$

Here ψ_p^S and ψ_p^T denote components of the spheroidal and toroidal eigenfunctions for the layered sphere, with ω_{ln}^S and ω_{ln}^T the associated eigenfrequencies. A bar over the eigenfunction denotes complex conjugation. The functions $\mathbf{P}_{lm}$, $\mathbf{B}_{lm}$ and $\mathbf{C}_{lm}$ are the vector spherical harmonics (*e.g.* Morse and Feshbach, 1953) and the radial functions D_{lm}, E_{lm} and F_{lm} can be expressed in closed form in terms of spherical Bessel functions, with coefficients expressed in terms of products of Haskell-Thompson matrices, (e.g., Ben-Menahem and Singh, 1972).

An entirely similar eigenfunction expansion for the Green's function in a layered half space can also be obtained (Archambeau and Stevens, unpublished manuscript, 1980). Therefore the Green's functions for quite detailed models of the earth can be expressed explicitly in terms of elementary functions.

As is well known, the system of equations defining the Green's function, that is, equations (8), may be used together with the elastodynamic equations (1) and appropriate boundary conditions, such as given in (6) and (7), to obtain an integral equation for the unknown elastodynamic displacement field in an elastic (or anelastic) medium. Such an integral equation incorporates the equations of motion along with the spatial boundary conditions and "initial values". This integral equation is usually called an "elastodynamic representation" theorem in the present context. In the case of an elastic/anelastic solid with an expanding failure zone, the usual development of the Green's function integral equation is not straightforward. Archambeau and Minster (1978) give the derivation for this case. The important differences between this derivation and the more standard results used in elasticity theory and seismology (*e.g.* DeHoop, 1957) are that the equilibrium stress field, for a medium which is in a state of initial stress, will change as an internal failure zone boundary grows. This gives rise to an "initial value" integral term that isn't present in the usual formulations in elastodynamics. In addition, the boundary conditions on the growing failure surface are of a more general form than those on a normal, "fixed", boundary, as was indicated earlier.

A form of the Green's function integral equation which accounts for these effects is shown by Archambeau and Minster (1978) to be:

$$4\pi u_\mu(\mathbf{x}) = \int_{-\infty}^{+\infty} dt_0 \int_V \rho f_\alpha(\mathbf{x}_0)\,G_\alpha^\mu(\mathbf{x},\mathbf{x}_0)\,d^3\mathbf{x}_0 - \int_{-\infty}^{+\infty} dt_0 \int_{\delta V} J_\beta^\mu(\mathbf{x},\mathbf{x}_0)\,\eta_\beta(\mathbf{x}_0)\,d\Omega_0$$

$$+ \int_{-\infty}^{+\infty} dt_0 \int_V \left[\rho\,\frac{\partial u_\alpha^0(\mathbf{x}_0)}{\partial t_0}\right]\frac{\partial G_\alpha^\mu(\mathbf{x},\mathbf{x}_0)}{\partial t_0}\,d^3\mathbf{x}_0 \tag{10}$$

Here the summation convention applies as always, and a four-vector notation is used, where all greek indices run over the range from 1 to 4. In this case we express ordinary spatial vectors as four vectors with the fourth ("time-like") component set to zero, such as for an ordinary displacement vector where:

$$(u_\mu) = (u_1, u_2, u_3, 0)$$

Similarly, all *ordinary* spatial tensors are "adjoined" with zeros for the "time-like" (index 4) components. Thus:

$$G_k^\mu = \begin{cases} G_l^m; \text{ if } \alpha \text{ or } \mu = 1,2,3 \\ 0; \text{ if } \alpha \text{ or } \mu = 4 \end{cases}$$

where the latin indices, such as l and m, run only over the range from 1 to 3.

The quantities η_β and J_β^μ, on the other hand, are four vectors with non-zero time-like components, and are defined by:

$$J_\beta^\mu = G_k^\mu \tau_{k\beta} - u_\alpha g_{\alpha\beta}^\mu$$

$$(\eta_\beta) = (n_1, n_2, n_3, -U_i n_i)$$

where*

$$\tau_{\alpha\beta} = C_{\alpha\beta\gamma\delta}(\mathbf{x}_0) \frac{\partial u_\gamma(\mathbf{x}_0)}{\partial x_\delta^0}$$

$$g_{\alpha\beta}^\mu = C_{\alpha\beta\gamma\delta}(\mathbf{x}_0) \frac{\partial G_\gamma^\mu(\mathbf{x}, \mathbf{x}_0)}{\partial x_\delta^0}$$

are the generalized stress tensors associated with the displacement u_γ and Green's displacement g_α^μ, respectively. Both $\tau_{\alpha\beta}$ and $g_{\alpha\beta}^\mu$ have non-zero "time-like" components, as well as "space-like" components. Here the coordinate components x_δ define a four-vector $\mathbf{x}$ such that

$$(x_\delta) = (x_1, x_2, x_3, t); \delta = 1,2,3,4$$

and $C_{\alpha\beta\gamma\delta}$ is the generalized elastic tensor, defined earlier in connection with equation (1), with the density as well as the ordinary elastic constants of the material as components. Thus this tensor includes inertial as well as elastic response coefficients. The space-time normal with components η_β have values equal to the ordinary components of $\mathbf{n}$, the spatial (outer) normal to the moving surface, plus a fourth, "time-like", component with a value equal to the negative of the normal component of the boundary velocity at this surface.

To obtain the (linearized) integral relation for the elastodynamic field $\mathbf{u}$, the equations of motion in the linearized form of (1) are used and, in addition, the generalized normal has been linearized by using $-U_i n_i$ as its fourth

*When necessary for notational clarity, we will write the source coordinates as $x_1^0, x_2^0, x_3^0, x_4^0$ in component form. These are to be interpreted as the components of $\mathbf{x}_0$. We shall also occasionally write $\mathbf{x}_0$ as $\mathbf{x}^0$ when necessary for consistency in notation.

component rather than the (proper) term - $U_i^* n_i$, with $U_i^* = U_i - v_i$ where v_i is a component of the particle velocity and U_i a component of the (absolute) velocity of the boundary. In the case of interest, wherein we are concerned with rupture zone growth rates, $|\mathbf{U}| \gg |\mathbf{v}|$, we can neglect the particle velocity relative to the rupture velocity, so $U_i^* n_i \simeq U_i n_i$. In this case then, the components of the generalized normal η_β can be expressed in a form that is explicitly independent of the elastodynamic field variables. The quantity $U_i n_i$ is usually called the "rupture velocity", and is defined as $U_R \equiv U_i n_i$. It is simply the rate at which the rupture surface expands in the direction normal to itself and defines the time history of expansion or growth of a failure zone.

The volume integrals in (10) are defined over the (linear) region *exterior* to any (nonlinear) failure zone, and this exterior volume is simply denoted by V. The surface integral is to be taken over the surface $\partial V'$ of the failure zone and all other boundary surfaces of the medium. Because the failure surface expands with time, at the rate U_R, then both the volume V and the surface $\partial V'$ are functions of the source time variable t_0.

The first integral in (10) involves the external body forces acting on the medium. In the elastodynamic case the only body force of any significance is gravity, and only the changes in the gravity field will affect the dynamic displacement field. These changes are very small relative to tectonic stress field changes for an earthquake source and can be neglected relative to other terms in (10). (See, for example, Archambeau and Scales, 1983).

The final integral term involves the derivative of the equilibrium displacement field $\mathbf{u}^*$ with respect to the source time variable t_0. When a failure boundary *forms* and expands with time in a stressed medium, as is the case with an earthquake source, then the equilibrium state for the medium must also change and this integral accounts for the dynamical effects produced by such changes. It plays the role of the initial value integral of the classical Green's function integral representation (*e.g.* Morse and Feshbach, 1953), but has a more general form in this case. The surface integral over the moving boundary $\partial V'$ accounts for scattering and absorption of energy at the moving boundary and it also has a more general form than arises in the classical case due to the relative movement of the boundary with respect to the material particles.

The expanded form of the integrand $J_\beta^* \eta_\beta$ in the surface integral can be shown, from the definitions given, to be:

$$J_\beta^* \eta_\beta = \left\{ G_i^m \left[\tau_{ik} - \rho \frac{\partial u_i}{\partial t_0} U_k \right] - u_i \left[g_{ik}^m - \rho \frac{\partial G_i^m}{\partial t_0} U_k \right] \right\} n_k$$

where u_i, τ_{ik} and n_k are the conventional spatial displacement, stress and surface normal, and similarly G_i^m and g_{ik}^m are the Green's displacement and stress. This quantity is identical to the classical result for a stationary boundary, except for the addition of the terms involving the boundary velocity function U. These latter terms account for the actual transport of material from one side of the boundary to the other. In the case of failure, the terms account for the envelopment of new material by the rapidly expanding failure zone.

In order to make direct use in (10) of the eigenfunction expansion for the Green's function given in (9), it is necessary to use the Fourier transformed (spectral) version of (10). Hence, with the Fourier transform operator with respect to the (*observer* or *receiver*) time variable t having the form:

$$F_t\{f(t)\} = \int_{-\infty}^{+\infty} f(t)e^{-i\omega t}\,dt = \tilde{f}(\omega)$$

with inverse

$$F_\omega^{-1}\{\tilde{f}(\omega)\} = \int_{-\infty}^{+\infty} \tilde{f}(\omega)e^{i\omega t}\,df = f(t)$$

where $\omega = 2\pi f$, then application to a *causal* Green's function (see, for example, Archambeau and Minster, 1978), $G_n^p(\mathbf{x};\mathbf{x}_0) \equiv G_n^p(x^k, x_0^k; t - t_0)$, gives:

$$F_t\left\{G_n^p(x^k, x_0^k; t - t_0)\right\} = e^{-i\omega t_0}\,\tilde{G}_n^p(x^k, x_0^k; \omega)$$

Here $\tilde{G}_n^p$ denotes the Fourier transform of G_n^p with respect to t. Since the transform is with respect to the time variable t, then this operator commutes with the integrals and derivatives taken with respect to x_0 and t_0, so that the operation can be taken inside the integrals appearing in (10). It is then not difficult to show that:

$$4\pi\tilde{u}_m(x^k, \omega) = \int_{-\infty}^{+\infty} e^{-i\omega t_0}\,dt_0 \int_{V(t_0)} \rho f_i \tilde{G}_i^m\,d^3x_0$$

$$- \int_{-\infty}^{+\infty} e^{-i\omega t_0}\,dt_0 \int_{\partial V(t_0)} \left\{\tilde{G}_i^m\left[\tau_{ik} - \frac{\rho\partial u_i}{\partial t_0}U_k\right] - u_i\left[\tilde{g}^m_{ik} + i\omega\rho\tilde{G}_i^m U_k\right]\right\} n_k\,d\alpha_0$$

$$+ i\omega \int_{-\infty}^{+\infty} e^{-i\omega t_0}\,dt_0 \int_{V(t_0)} \left[\rho\frac{\partial u_k^*}{\partial t_0}\right]\tilde{G}_k^m\,d^3x_0 \qquad (11)$$

As is clear from the expression of each integral term in (11), the terms correspond to Fourier transforms of integrals over a time dependent volume or surface integral. Here the transform turns out to be with respect to the *source* time variable t_0, rather than with respect to the receiver time t. If the dependence of the volume V and surface ∂V on t_0 can be neglected, and some fixed limits of integration used, then the transform operation can be moved inside the spatial integrals. In this case the result (11) simplifies to spatial integrals over products of Fourier transforms, as in the classical result with stationary boundaries. However, in general, the result (11) must be used essentially as it stands.

One formally rigorous approach in dealing with the evaluation of (11) in general circumstances is to (continuously) map the surface ∂V into some *fixed* surface that has a convenient shape, such as a sphere, and to thereby produce spatial integrals that have fixed limits with respect to t_0. In this case all the functions appearing in the integrand are also mapped into a new (time dependent) "space" and, in addition, the Jacobian of the mapping appears in the integrand. Then, however, the Fourier transform can be moved inside the integrals and applied directly to the resulting integrand. In this case a variety of approximations are possible since the Jacobian of the transformation can be expanded, as well as the Green's functions and other terms, in appropriate

functions to yield quite accurate analytical and numerical results. This latter approach, while complicated, has been pursued by Scales and Dilts (1983) and has provided initial results in several important cases involving ellipsoidal failure zone formation. In the present discussion we will be content to consider simpler (geometric) cases that can be approximated without recourse to the mapping theory, but that nevertheless contain the essential features of the theory of spontaneous elastodynamic sources (earthquakes).

In view of the length of the expressions for the integral representation of the elastodynamic field, it is convenient to introduce an inner product notation, along with the four-vector (space-time) representation, in order to condense the results and to highlight their physical significance.

Thus, defining inner products over the failure zone boundary, ∂V and the volume, V, exterior to that boundary, we can express the integral representation of the transformed dynamic field $\mathfrak{U}_m$ in (11) as:

$$\mathfrak{U}_m = \mathfrak{U}_m^{(G)} + \mathfrak{U}_m^{(S)} + \mathfrak{U}_m^{(R)} \tag{12}$$

with

$$\mathfrak{U}_m^{(G)} = F_{t_0}\left\{\langle \rho f_i, \tilde{G}_i^m \rangle_V\right\}$$

$$\mathfrak{U}_\mu^{(S)} = F_{t_0}\left\{\langle u_\alpha, \tilde{g}_{\alpha\beta}^\mu \eta_\beta \rangle_{\partial V} - \langle \tau_{\alpha\beta}\eta_\beta, \tilde{G}_k^\mu \rangle_{\partial V}\right\}$$

$$\mathfrak{U}_m^{(R)} = i\omega F_{t_0}\left\{\langle \rho \delta_{t_0} u_k^*, \tilde{G}_k^m \rangle_V\right\}$$

Here $\mathfrak{U}_m^{(G)}$ denotes the dynamical displacements associated with (gravitational) body force perturbations due to the failure process. As noted earlier, this term is very small compared to the displacement term $\mathfrak{U}_m^{(R)}$, associated with the relaxation of tectonic stress due to the spontaneous creation of a failure zone. The displacement term $\mathfrak{U}_\mu^{(S)}$ denotes the (secondary) displacement effects due to scattering from the (growing) failure surface. (The four vector notation is used to compress the expression for this term. However, $u_\mu^{(S)}$ is identical with $u_m^{(S)}$, $m = 1,2,3$ since the component with $\mu = 4$ is zero.)

The various inner products represent spatial integrals over the volume outside the failure zone or over its surface, so that for example:

$$\langle \rho \delta_{t_0} u_k^*, \tilde{G}_k^m \rangle_V = \int_{V(t_0)} \rho \left[\frac{\partial u_k^*}{\partial t_0}\right] \tilde{G}_k^m d^3x_0$$

Finally, F_{t_0} represents the Fourier transform operator with respect to the (source) time variable t_0, as defined earlier.

If, as was also noted earlier, the volume V and surface ∂V are independent of time variable t_0, then the operator F_{t_0} commutes with the inner product integrals and, in this special case,

$$\mathcal{U}_m^{(C)} = \langle \rho \tilde{f}_i \cdot \tilde{G}_i^m \rangle_V$$

$$\mathcal{U}_m^{(S)} = \langle \mathcal{U}_\alpha \cdot \tilde{g}_{k\beta}^m \eta_\beta \rangle_{\partial V'} - \langle \tau_{\alpha\beta} \eta_\beta \cdot \tilde{G}_k^m \rangle_{\partial V'}$$

$$\mathcal{U}_m^{(R)} = -\omega^2 \langle \rho \mathcal{U}_k^\beta \cdot \tilde{G}_k^m \rangle_V$$

where $\tilde{f}_i$, etc., are simple Fourier transforms of the variables in question. In this case, when the volume V and surface(s) $\partial V'$ are independent of time, then it is also true that the normal boundary velocity $U \cdot \mathbf{n}$ will be equal to the normal component of the particle velocity at the boundary. That is, there are no growing failure zone boundaries in this case. Therefore the rupture velocity $U_R = (U_i - v_i^{(1)}) n_i$ vanishes in the integral terms above, and these integrals immediately reduce to:

$$\left.\begin{aligned} \mathcal{U}_m^{(C)} &= \langle \rho \tilde{f}_i \cdot \tilde{G}_i^m \rangle_V \\ \mathcal{U}_m^{(S)} &= \langle \mathcal{U}_i \cdot \tilde{g}_{ik}^m n_k \rangle_{\partial V'} - \langle \tilde{T}_{ik}^m n_k \cdot \tilde{G}_i^m \rangle_{\partial V'} \\ \mathcal{U}_m^{(R)} &= -\omega^2 \langle \rho \mathcal{U}_k^\beta \cdot G_k^m \rangle_V \end{aligned}\right\} \qquad (13)$$

where T_{ik} and g_{ik}^m are the ordinary elastic stresses associated with the displacement u_i and Green's displacement function G_k^m. Since the medium does not, in this case, have an internal growing inclusion corresponding to a failure zone (or other phase change), then the equilibrium field will not change with the time variable t_0 even if the medium is initially stressed. In this case, $\partial_{t_0} u^* = 0$, and the relaxation displacement field vanishes. Hence, in this case only the first two integral terms in (13) are nonzero and the total displacement field is just the sum of these two terms. Written out explicitly we have, in this "standard" case:

$$\tilde{u}_m = \int_V \rho \tilde{f}_i \tilde{G}_i^m \, d^3 x_0 + \int_{\partial V'} \left\{ \mathcal{U}_i \tilde{g}_{ik}^m n_k - \tilde{G}_i^m \tilde{T}_{ik}^m n_k \right\} da_0 \qquad (14)$$

This is, in fact, the classical integral representation used by DeHoop (1957) and others in elastodynamic and seismological applications. As will be seen, this integral form for the elastodynamic problem has many uses, including the representation of dynamical dislocation fields and equivalent elastic sources. In these cases, and in many others involving elastic scattering problems, the first integral over the body forces f_i can be neglected. On the other hand, if one uses equivalent forces to represent a source, then this leading integral term gives the displacement field.

II. Basic Theory and Models of Earthquakes

It is generally agreed that the seismic radiation produced by an earthquake is a consequence of the relaxation of tectonic stress in the medium surrounding a zone of material failure. Thus, the origin of the energy of an earthquake is the stored strain energy within a large volume surrounding the (narrow) fracture zone and, in quantitative terms, the total energy release is the

difference between the equilibrium strain energies stored in the entire medium before and after the creation of the failure zone. The computation of this energy change is, in principal, accomplished by simply computing the strain energy stored in the prestressed medium *with* an inclusion (the failure zone) and subtracting it from the strain energy initially stored in the stressed medium without the inclusion. In both computations the prestress state is specified by requiring the stress field, *with or without the inclusion*, to assume a prescribed fixed form and value at great distances from the origin, where the finite failure zone is centered. (See Landau and Lifshitz, 1959; Archambeau, 1968 and 1973 or Eshelby, 1957 for examples of this computation in specific cases.)

The creation of a failure, when viewed in this way, can be shown to cause a net reduction of the strain energy stored in the medium. This difference in stored (potential) strain energy must necessarily be partitioned between seismic radiation and the energy required for the creation of the failure zone. Such a calculation, involving the differences between two equilibrium states, does not, however, tell us how this energy is partitioned between these two forms, nor does it tell us how the energy in the radiation field is distributed spectrally. That is, it says nothing about the manner in which the system goes, dynamically, from one equilibrium state to the other.

On the other hand, this fundamental energy computation forces us to recognize that the energy in the seismic radiation field comes from the release of stored energy from the *volume* surrounding the failure zone. Thus an earthquake is, quite literally, a volume source within which, or at the boundaries of which, our measurements are usually made. This simple observation, in itself, suggests that any direct *dynamical* formulation describing the seismic radiation from an earthquake will involve a volume source distributed over the medium surrounding a growing failure zone or fracture. This follows, of course, because the energy literally comes from the elastic region surrounding the failure zone and any direct dynamical formulation of the problem designed to predict the seismic radiation should show this explicitly.

Kinematical Representations

In contrast to dynamical representations of earthquakes, which must involve the physics of the failure process itself as well as stress wave radiation, kinematical dislocation sources are often used to represent an earthquake. This approach has considerable intuitive appeal since an earthquake, as well as changing the stress field in the medium, also produces a displacement "dislocation", or offset in the medium across the failure zone. Since a failure zone is usually very thin, often only a few millimeters in thickness, then the zone can easily be considered to be essentially a plane and the displacement to be discontinuous across this plane. Clearly, one may conceive of an earthquake as being *equivalent to* a displacement dislocation taking place along a plane (the "failure plane") with an "appropriate" time history. In this case, one has at ones disposal the knowledge that if a displacement is *specified* completely in terms of its space, time and magnitude history on such a plane, and if the (usual) boundary condition requiring continuity of tractions is assumed, then this is sufficient to prescribe the elastic wave field everywhere in the medium surrounding this "dislocation source". This, in fact, follows quite simply from the usual Green's function solution of the equations of motion in an elastic solid with *fixed* boundaries. (See, for example, Morse and Feshbach (1953), for basic Green's function solutions; or Aki and Richards (1980), for detailed dislocation solutions.) In particular, the displacement field (neglecting body forces) is given, in general, by[+]:

[+]The summation convention is to be applied to repeated indices throughout, so for example, $U_i n_i = U_1 n_1 + U_2 n_2 + U_3 n_3$. Here also, we use $t^+ = t + \varepsilon$, where t is the receiver time and $\varepsilon > 0$ is a small time increment which merely serves to avoid any singularities of G_{ij}^n.

$$4\pi u_m(\mathbf{x},t) = \int_0^{t^+} dt_0 \int_\Sigma \left[G_k^m t_k - u_k g_k^m \right] da_0$$

where G_k^m is the displacement Green's function, g_k^m the Green's function traction on the surface(s) Σ, given by

$$g_k^m(\mathbf{x},t;\mathbf{x}_0,t_0) = C_{ijkl}(\mathbf{x}_0) \frac{\partial G_i^m(\mathbf{x},t;\mathbf{x}_0,t_0)}{\partial x_0^j} n_l$$

with C_{ijkl} the elastic tensor, and where t_k and u_k are the traction and displacement components of the dynamic field. On a dislocation surface Σ_d, where the volume enclosed by the surface is allowed to vanish, the traction component differences across such a (two-sided) surface vanish by the assumption of continuity of the traction, and the surface integral giving the displacement field in the medium reduces to:

$$4\pi u_m(\mathbf{x},t) = \int_0^{t^+} dt_0 \int_{\Sigma_d} \Delta u_k g_k^m da_0 ,$$

where Δu_k is now the difference in displacement on the two sides of the dislocation surface Σ_d.

It is now evident that if the surface Σ_d is specified along with the displacement offset, both as functions of time and spatial position, then the integral can be evaluated and the field is given (predicted) at all receiver positions $\mathbf{x}$ and for all time t.

It is just as clear however, that all that is accomplished by the evaluation of this integral representation is to *propagate* the *assumed* displacements on the surface Σ_d to other points in the medium. Thus, by assuming a particular displacement space-time history one *prescribes* a kinematical description of the failure process. The problem with this is that we do not necessarily know how to do this, and even if we are fortunate enough to be able to guess a proper, or nearly proper displacement space-time history using intuitive concepts, we still do not know how to relate such an assumed displacement function to the basic physics of the process. Indeed, this inability to relate the assumed dislocation displacement to the fundamental dynamical variables associated with an earthquake immediately shows up in the computation of the energy changes due to a dislocation in a prestressed medium. In particular, Steketee (1958) demonstrated that the strain energy change in the medium due to creation of a dislocation is *independent* of the prestress and depends only on the displacement jump and, furthermore, that this energy change is always such as to *increase* the strain energy of the already stressed medium. This increase is precisely the opposite of what is required for an allowed *spontaneous* process. Taken together, the increase in strain energy and the independence from the initial stresses in the medium simply means that when displacements are *arbitrarily* specified on a boundary or dislocation surface, in a manner independent of the initial stresses, then work is done on the system in order to create the dislocation. The key here is that the dislocation displacement is imposed arbitrarily without relation to the initial stress state, or

subsequent time changes in this stress state. Further, because no changes in material properties occur in the idealized dislocation procedure, then there is no reason for the initial stresses to adjust and the dislocation field is simply linearly superposed on the initial field. Consequently, a dislocation representation for a spontaneous energy release source, such as an earthquake, is fundamentally unrelated to the basic physical processes actually occurring, that is, the dislocation displacement is not related to the dynamical changes of the stress field in the medium within the representation theory provided by the dislocation model. (To provide such a relation one has to solve the dynamical problem from first principles and then deduce from the solution the equivalent dislocation, with suitable definitions of how changes in the energy state of the system are to be interpreted.)

Dynamical, Relaxation Source, Representations

While a dislocation and other similar kinematical representations of earthquakes can certainly be useful in some instances, such equivalents are not very helpful if we wish to describe the source from first principles in terms of basic physical parameters and variables. We shall therefore consider the description of earthquakes from the point of view already suggested, namely as a volume source of elastic energy which is released as a consequence of failure. Further, since we recognize that this is an interactive process in which the readjustment of stress in the medium is accomplished dynamically in such a way as to strongly influence the growth of the failure zone, we seek a formulation of the problem that incorporates such interactions.

In this regard, the formulation of the full dynamical problem as an initial value problem, as described by Archambeau (1968) or Archambeau and Minster (1978) for example, provides a representation of the seismic radiation in terms of a volume integral over the region surrounding a growing failure zone. This theoretical representation, which is now termed 'relaxation source theory', shows that the actual (volume) source function for an earthquake corresponds to changes in the equilibrium *displacement* field in the medium surrounding a failure zone, where these changes arise from the growth of a new boundary (the failure zone boundary) in the medium. In particular, the Green's function integral representation for the dynamical description of *both* the failure zone growth and the associated seismic radiation due to relaxation of the equilibrium stress field is, from Archambeau and Minster (1978):

$$4\pi u_m(\mathbf{x},t) = \int_0^{t^+} dt_0 \int_{\partial V} \left\{ G_k^m \left[C_{ijpl} \frac{\partial u_i}{\partial x_j^0} + \rho \frac{\partial u_k}{\partial t_0} U_l \right] - u_k \left[C_{ijpl} \frac{\partial G_i^m}{\partial x_j^0} + \rho \frac{\partial G_k^m}{\partial t_0} U_l \right] \right\} n_l \, d\alpha_0$$

$$+ \int_0^{t^+} dt_0 \int_V \rho \frac{\partial u_k^*}{\partial t_0} \left[\frac{\partial G_k^m}{\partial t_0} \right] d^3x_0 \qquad (1)$$

with boundary conditions on the failure zone boundary, denoted by ∂V and with normal $\mathbf{n}$, given by

$$\rho U_R [v_k] = -[t_k] \, , \; (\textit{conservation of mass and momentum}) \qquad (2)$$

$$U_R^2 = [t_k t_k] / (2\rho^2 L) \, , \; (\textit{conservation of energy}) \qquad (3)$$

where $U_R = U_i n_i$ is the normal component of the velocity of rupture boundary growth and L is the energy per gram required to cause the material to undergo failure. The latter two equations, (2) and (3), are statements of conservation of momentum and energy, respectively, at the *moving* failure zone boundary and the bracket notation is used to denote the changes in particle velocity components, v_k, and traction components, t_k, across the failure zone boundary.

In the integral representation in (1) for the dynamic displacement field u_m at any point within the elastic region surrounding the failure zone, $G_k^m = G_k^m(\mathbf{x},t;\mathbf{x}_0,t_0)$ represents the Green's function (impulse response) for this elastic medium, with $\mathbf{x}$ and t denoting the receiver coordinates and time, while $\mathbf{x}_0$ and t_0 denote the independent set of source coordinates and time. The first integral term, involving the surface integral over the failure zone boundary, accounts for the interaction between the elastic wave field and the growing failure zone boundary. This interaction, or wavefield "scattering", is actually coupled to the boundary conditions of (2) and (3), since the rupture velocity, $U_R = U_i n_i$, is explicitly present in the integrand and also determines (implicitly) the limits of the surface integral, since the surface ∂V changes with time in a manner determined by the function U_R.

The second integral term over the entire elastic region, V, exterior to the failure zone involves the time rate of change of the *equilibrium* displacement field $\mathbf{u}^e(\mathbf{x}_0,t_0)$, measured relative to the initial displacement field associated with the prestress state of the medium. This integral therefore accounts for the primary radiation due to relaxation of stress in the medium surrounding the growing failure zone, and as the failure zone continues to grow then the source density term $[\partial \mathbf{u}^e / \partial t_0]$ in the integrand will be a non-zero and changing function of t_0, the *source time*. This integral term therefore corresponds to a (generalized) initial value contribution to the radiation field which arises from the continuous change in equilibrium that is required during the creation of a failure zone inclusion.

Special Relaxation Theory Models and "Instantaneous" Failure Sources

To relate this integral term to more familiar initial value problems it is instructive to consider the limiting case in which a spherical failure zone is created, in an initially stressed medium, at a rate equal to, or greater than, the intrinsic compressional velocity in the medium. This situation, although somewhat of an idealization, approximates the creation of the roughly spherical shatter zone by an underground explosion. In this case the shock wave produced by the explosion propagates at a speed near the compressional velocity in the solid and produces a zone of failure in the material at, essentially, a "supersonic" rate. If the medium is initially stressed, then no changes in the prestress state outside this failure zone can occur until *after* the complete formation of this zone, since any relaxation of stress proceeds (radially outward) at a rate which is less than, or just equal to, the rate at which the failure zone formation occurs. In this case the failure inclusion in the medium is, in effect, created instantaneously, insofar as relaxation of any prestress is concerned, since its speed of formation is greater than the speed with which information concerning its existence can be propagated. Thus, an initially stressed medium, which had been in equilibrium, suddenly finds itself in a state which is out of equilibrium, at say the time $t_0 = 0$, due to the presence of a newly created internal inclusion which has altered effective elastic properties. In this case the initial value for the displacement field is:

$$\mathbf{u}^e(\mathbf{x}_0,t_0) = \left[\mathbf{u}^{(0)}(\mathbf{x}_0) - \mathbf{u}^{(1)}(\mathbf{x}_0)\right] H(t_0)$$

where $\mathbf{u}^{(0)}$ is the initial displacement associated with the prestressed state of the medium without the failure zone inclusion, while $\mathbf{u}^{(1)}$ is the equilibrium displacement field in the medium with the failure zone present. Further, $H(t)$ is a step function, at $t_0 = 0$, arising from the "instantaneous" creation of the failure zone, so that $\mathbf{u}^*$ is zero before the failure zone is created at $t_0 = 0$, while it is constant in time and equal to $[\mathbf{u}^{(0)} - \mathbf{u}^{(1)}]$ after the zone is created. According to the initial value integral term in (1) then, the source density term $\partial u_k^* / \partial t_0$ will be a delta function at the time $t_0 = 0$. Thus, the initial value integral term in equation (1) takes the form

$$\int_0^{t^+} dt_0 \int_V \rho \left[\frac{\partial u_k^*}{\partial t_0} \left[\frac{\partial G_k^m}{\partial t_0} \right] \right] d^3x_0 =$$

$$\int_0^{t^+} \delta(t_0) \int_{V(t_0)} \rho \left[u_k^{(0)} - u_k^{(1)} \right] \frac{\partial G_k^m}{\partial t_0} \, d^3x_0 \, dt_0$$

$$= \int_{V(0)} \rho \left[u_k^{(0)} - u_k^{(1)} \right] \left[\frac{\partial G_k^m}{\partial t_0} \right]_{t_0=0} d^3x_0$$

where $V(0)$ denotes the volume integration limits at the time $t_0 = 0$, and so corresponds to the entire medium outside the failure zone. For all times $t_0 > 0$ the rupture boundary velocity U_R is zero, since the failure zone is fixed in size after its "instantaneous" formation. Therefore the boundary conditions in equations (2) and (3), for this special problem, reduce to the (standard) conditions that the tractions, t_k, are continuous; that is, to $[\![t_k]\!] = 0$. Likewise the terms in the surface integral involving $U_R = U_i n_i$ are absent; so for this "instantaneous" failure problem the general representation of the displacement field specified by equations (1) through (3) reduce to:

$$4\pi u_m(\mathbf{x}_0, t) = \int_0^{t^+} dt_0 \int_{\partial V(0)} \left[G_k^m \, t_k - u_k \, g_k^m \right] d\sigma_0$$

$$+ \int_{V(0)} \rho [\delta u_k^*] \left[\frac{\partial G_k^m}{\partial t_0} \right]_{t_0=0} d^3x_0 \qquad (4)$$

with the condition

$$[\![t_k]\!] = 0 \qquad (5)$$

across the boundary, ∂V, of the failure zone. Here, $\delta \mathbf{u}^* \equiv [\mathbf{u}^{(0)}(\mathbf{x}_0) - \mathbf{u}^{(1)}(\mathbf{x}_0)]$ and

$$t_k = C_{ijpl} \frac{\partial u_i}{\partial x_j^0} n_l$$

are the tractions on the surface with normal vector $\mathbf{n}$. Similarly,

$$g_k^m = C_{ijpl} \frac{\partial G_i^m}{\partial x_j^0} n_l$$

are Green's function tractions on the surface with normal n.

The equation (4), which provides a representation of the radiation field for this special relaxation source, is identical to the classical Green's function integral representation for an elastic medium with an initial displacement from final equilibrium equal to δu^*, and this problem is discussed in standard works in considerable detail (*e.g.*, Morse and Feshbach, 1953). The interpretation of the physical origins of the two integral terms making up the representation in (4) is that the surface integral describes scattering of the primary elastic radiation by the failure zone boundary (*e.g.*, reflections and refraction at the boundary), while the second integral, involving the initial value of the displacement field, represents the primary elastic field produced by the release of stored elastic energy from the entire medium external to the failure zone. Clearly, scattering effects will be of secondary importance for purposes of predicting the main features of the seismic radiation field from this relaxation source and to first order one expects the field to be predicted by the initial value term in (4). Therefore, to first order, we have the simple *solution*

$$4\pi u_m^{(1)}(\mathbf{x},t) = \int_{V(0)} \rho[\delta u_k^*] \left[\frac{\partial G_k^m}{\partial t_0}\right]_{t_0=0} d^3x_0 \qquad (6)$$

where $u_m^{(1)}$ denotes a first order solution obtained by neglecting the surface integration term in (4). To account, approximately, for the scattering effects we can use the first order solution for u_k and t_k in the surface integral term in equation (4), to obtain a second order approximate solution. That is, we have as an approximate solution which includes scattering effects:

$$4\pi u_m^{(2)}(\mathbf{x},t) = 4\pi u_m^{(1)}(\mathbf{x},t) + \int_0^{t^+} dt_0 \int_{\partial V(0)} \left[G_k^m t_k^{(1)} - u_k^{(1)} g_k^m\right] da_0 \qquad (7)$$

The detailed solution of (6) for a spherical failure zone can be found in Archambeau (1972), for example, and involves first specifying a prestress state for the medium and then solving the static boundary value problem for an inclusion, in the prestressed medium. This requires a solution of the equations of equilibrium such that the new equilibrium stress assumes the value of the prestress at large distances from the failure zone while satisfying continuity of traction and normal displacement across the failure zone boundary. Here, in particular, the material inside the failure zone is considered to have rheological properties that are quite different than those before failure. Solutions for static inclusion problems, for various boundary shapes, can be found in the literature (*e.g.*, Landau and Lifshitz, 1959; Neuber, 1946; Eshelby, 1957) or can be obtained from first principals in either analytical or numerical form. In any case, using the static solution so obtained to specify the initial value δu^* in (6), as the difference in the equilibrium states before and after the failure zone formation, and then expressing the Green's function as an eigenfunction expansion (*i.e.*, as an expansion in eigenfunctions for a layered spherical or flat-earth model, for example), allows the integral in (6) to be evaluated. Once $u_m^{(1)}$ is obtained from (6), then the second order solution $u_m^{(2)}$ can be obtained from (7), using the expansion for the Green's function and the same integration procedures as are used for (6).

It is appropriate to emphasize that the integral representation for the radiation field given by equation (4), along with the iterative form of solution given by (6) and (7), can be used to describe the seismic radiation from any *instantaneous* failure process with *any* boundary shape. That is, while a

spherical failure zone is one that is of practical interest and can effectively be produced instantaneously by an explosive shock wave, such a failure zone shape is only one of an infinite set of geometric possibilities that can be described by (4). Thus, while it is difficult to envision natural situations (including man made) where failure zones, other than explosive induced spherical (or near spherical), are produced at supersonic rates (or "instantaneously") nevertheless in the abstract we can use the "geometric generality" of the simple "instantaneous failure" representation in other ways, as we will show later, to provide an understanding and interpretation of the rather complex general representation in (1).

Interpretation of the General Relaxation Source Representation

The value of the "instantaneous failure" example is at least two fold: First it shows that the rather complicated representation given in (1), for a general spontaneous failure process, reduces in a natural and logical way to what is essentially a classical result with which we are familiar and for which there are alternate formulations that can be demonstrated to give the same result. In this regard Stevens (1981), has shown that the initial value formulation given by (4) can be put into the form of a stress pulse equivalent, wherein the initial value volume integral can be re-expressed as a surface integral over the failure zone boundary, and where the effective source function in this integral is now the stress difference between the initial and final equilibrium states at the boundary. This form is identical to the usual integral representation employed in crack theory. Further, when reformulated in this way, Stevens was able to solve for the seismic field produced by a spherical inclusion exactly, including all scattering effects. Further, his solution was obtained for an arbitrary (spatially variable) prestress condition, so that the solution has considerable generality. Comparison of this exact solution with the iterative solution procedure indicated by the equations (6) and (7), but with (7) repeated in successive approximations, showed that the iterative method is convergent and that the scattering term produced only a small correction to the relaxation term, as expected.

In addition to the verification of the general representation and its iterative solution in a special case, the "instantaneous failure" example can be used to provide insight into the structure and meaning of the general relaxation source representation. That is, the limiting process and logic used to generate the special case equations from the general representation of (1) through (3) can be turned around to enable us to see how the general formulas can be built from this special case. In particular, we can adopt the special instantaneous failure integral representation and associated solution as the fundamental or canonical problem to be used to build more general solutions. From this point of view the more general case of spontaneous failure at a finite rate can be thought of as a sequence of instantaneous failure processes of the canonical type, with each increment of failure zone growth occurring instantaneously after some interval of time δt_0 between successive instantaneous events. This corresponds to the approximation of a continuous growth rate by a sequence of small steps. If we add up, or superpose, the fields produced by each step-like change in the failure zone, then we will be able to obtain the total radiation field from the entire sequence. Proceeding with this approach, using (6) to represent the radiation induced by each increment of boundary growth and considering scattering (and other interactions) at the boundary as a second order effect, we get to first order:

$$4\pi u_m^{(1)}(\mathbf{x},t) = \sum_n \int_{V(t_n)} \rho \left[\delta u_k^a(t_n)\right] \left[\frac{\partial G_k^m}{\partial t_0}\right]_{t_0 = t_n} d^3x_0$$

where t_n, $n = 1,2,\cdots N$, denote the times at which incremental, instantaneous, growth of the failure zone occurs. Here $V(t_n)$ denotes the elastic volume *outside* the failure zone at the time t_n. Now we can explicitly introduce the time of separation between increments of instantaneous growth of the failure by observing that $t_n = t_{n-1} + \delta t_0$ and rewrite the previous superposition as:

$$4\pi u_m^{(1)}(\mathbf{x},t) = \sum_n \delta t_0 \int_{V(t_n)} \left[\frac{\delta u_k^e(t_n)}{\delta t_0}\right]\left[\frac{\partial G_k^m}{\partial t_0}\right]_{t_0=t_n} d^3x_0$$

Now we can pass to the limit in which δt_0 is infinitesimal and where the boundary growth also becomes infinitesimal, and with it the incremental changes in the equilibrium field δu_k^e. By this process we can simulate a continuous, and finite rate, failure process and we have, using the definition of an integral as the limit of the summation:

$$4\pi u_m^{(1)}(\mathbf{x},t) = \int_0^{t+} dt_0 \int_{V(t_0)} \rho \left[\frac{\partial u_k^e}{\partial t_0}\right]\left[\frac{\partial G_k^m}{\partial t_0}\right] d^3x_0$$

We observe now that this limit of a sequence of elementary initial value representations of the seismic radiation from instantaneous failure processes results in a total field representation that is precisely the same as the relaxation term in (1), which accounts for stress relaxation effects in the general case. Thus we arrive at an interpretation of the most important term in the general representation in terms of an elementary initial value source which has a well known solution, in particular the general source is just a "sum" of these elementary initial value sources.

The close relationship between the very simple "instantaneous failure" source and the more complicated integral representation for the general case, given in (1), can be exploited further by observing that the surface integral term represents scattering, or interaction of the primary field with this boundary discontinuity in both cases; albeit that the boundary interaction in the general case is more complex since it involves reflections, etc. from a *moving* boundary and simultaneous *absorption* of energy at this boundary, due to the energy required to produce a failure transition in the material. In spite of these differences however, we may approach the solution of the integral equation in (1) in precisely the same fashion as was done in the case of the simple "instantaneous failure", and so in analogy with the iterative approach leading to equations (6) and (7), we use, in the general case, the solution procedure:

$$4\pi u_m^{(1)}(\mathbf{x},t) = \int_0^{t+} dt_0 \int_{V(t_0)} \rho \frac{\partial u_k^e}{\partial t_0}\left[\frac{\partial G_k^m}{\partial t_0}\right] d^3x_0 \tag{8}$$

$$4\pi u_m^{(n)}(\mathbf{x},t) = u_m^{(1)}(\mathbf{x},t) + \int_0^{t+} dt_0 \oint_{\partial V(t_0)} \left[G_k^m\left[C_{ijkl}\frac{\partial u_i^{(n-1)}}{\partial x_j^0} + \rho\frac{\partial u_k^{(n-1)}}{\partial t_0}U_l\right]\right.$$

$$\left. - u_k^{(n-1)}\left[C_{ijkl}\frac{\partial G_i^m}{\partial x_j^0} + \rho\frac{\partial G_k^m}{\partial t_0}U_l\right]\right] n_l\, d\alpha_0 \tag{9}$$

where the index $n \geq 2$ is the order of the iteration carried out using (9), with

(8) the first order "starting approximation". Here the exact solution is, formally:

$$u_m(\mathbf{x},t) = \lim_{n\to\infty} u_m^{(n)}(\mathbf{x},t)$$

but in practice $u_m^{(2)}$, or even $u_m^{(1)}$, is a sufficiently good approximation for the seismic radiation field, just as was the case for the instantaneous failure. Hence the primary contribution to the radiation field arises from the generalized initial value term given by $u_m^{(1)}$, while corrections accounting for scattering and the energy adsorption required to drive the failure process are obtained using the iterative approximation prescribed by (9). The energy absorption manifests itself explicitly through the dependence of the integrals in (8) and (9) on the time varying limits of integration, which are determined by the rupture rate function U_R, and through the rupture rate dependent terms of the form $\rho v_k U_R$, with $v_k = \partial u_k / \partial t$ corresponding to the particle velocity, appearing in the surface integral in (9). The interpretation placed on these effects, which were not present in the instantaneous failure representation, is that there is strain energy absorption in addition to scattering from a moving failure zone boundary in this more complete description. Further, we do not prescribe the boundary movement, but instead the rupture rate is determined by the dynamical boundary conditions at the failure surface, given by equations (2) and (3). In this interpretation then, energy absorption arises because the dynamical radiation field itself "feeds" the failure process and supplies the necessary energy to create a larger failure zone. Thus, the strain energy is redistributed dynamically by wave propagation to the failure zone boundary and, in one or more locations, reaches levels high enough to supply the energy required to continue the failure growth process. When the failure transition occurs (albeit in a very narrow zone, but nevertheless in some finite volume of the material) then the local strain energy is absorbed in the process, essentially being used to convert the material to its "failed state".

In spite of the added complications associated with the interaction of the radiation field with the (nonlinear) failure process in the spontaneous failure representation, the approach to the solution of the integral representation for the radiation field is the same as for the instantaneous failure. That is, the first order solution $u_m^{(1)}$ is obtained by first solving the static boundary value problem for an inclusion of appropriate geometrical shape and rheological properties in an initially prestressed medium, so that u_k^0, the change in the equilibrium field, is obtained. This static field is expressed in a form that depends parametrically on the time, t_0, because of the dependence of the inclusion geometry (*i.e.*, rupture zone dimensions) on the failure velocity function. Thus, for example, the equilibrium field changes due to the creation of an ellipsoidal failure zone in a prestressed medium would depend parametrically on the ellipsoidal axes (a, b and c) of the inclusion, and these in turn would depend on the time integral of the rupture velocity in the axial directions, so that the change in the equilibrium field would be expressible in terms of a time variable t_0. The derivative of the equilibrium field with respect to this time parameter yields the required source term in (8), and with the Green's function expressed in terms of an eigenfunction expansion, then evaluation of the integral for $u_m^{(1)}$ is possible. Once $u_m^{(1)}$ has been obtained, in the analytic form of an eigenfunction expansion, then the iterative procedure expressed by (9), while algebraically cumbersome, is straightforward.

Implications from the Dynamical Boundary Conditions for Failure Growth

In order to solve this source problem using the approach described, or any other method for the solution of (1), it is clear that a determination or specification of the rupture velocity function $U_R(x_0,t_0)$ is necessary. As was indicated earlier, the boundary equations (2) and (3) serve as dynamical conditions for failure and therefore actually determine the rupture velocity function. In most *modeling* of earthquakes however, the boundary conditions have not been used explicitly to determine this function, but instead a rupture velocity function has been specified (or assumed) having a form that was based on a combination of simple observation and elementary analysis of the failure boundary conditions. (See, for example, Archambeau, 1968 and Minster, 1973).

Archambeau and Minster (1978) show formally, however, that if a *complete loss of shear strength and no essential change in compressibility* characterizes the material after failure, which is a rather plausible assumption, then the boundary relations in (2) and (3) give a relation of the form:

$$U_R \left[v_k \right] = \left[\frac{\mu}{\rho C_s} v_k \right] \tag{10}$$

where v_k are particle velocity components and C_s denotes a signal velocity characterizing stress wave propagation in the medium surrounding the failure surface. If the rigidity inside the failure zone is essentially zero and if the failure process is considered to be driven by a shear wave, so that $C_s \simeq \sqrt{\mu/\rho}$, then this relation gives:

$$U_R \simeq \sqrt{\mu/\rho} \tag{11}$$

with μ and ρ denoting the shear modulus and density in the medium outside the failure zone.[*] Therefore, under the reasonable assumption of loss of shear strength in the material involved in the failure process, it is found that the rupture rate will be close to the local shear velocity within the medium. This result appears quite consistent with observations which suggest that the highest rupture rates are, in fact, close to the shear velocity.

Another result that provides insight into the failure dynamics, as expressed by the conservation equations at the failure boundary, can be obtained from the energy relation (3) which states that

$$\rho U_R^2 = \frac{\left[t_k t_k \right]}{2\rho L} \tag{12}$$

Now we note that the previous result states that $U_R \simeq v_s \equiv \sqrt{\mu/\rho}$ when the process of failure, characterized by a particular energy of transition L_0, results in a complete loss of shear strength. Thus for this process

$$\rho U_R^2 = \rho v_s^2 = \frac{|\Delta\sigma|^2}{2\rho L_0} \tag{13}$$

[*] If a change in compressibility is allowed during the failure transition, then this result is modified and it is possible for the rupture rate to become "trans-sonic", that is, to have a value between the shear and compressional velocities in the medium. It is felt that transitions of this sort are unlikely, or at least rare and confined to failure transitions at great depth in the earth.

which follows from the general energy equation, where we have used $|\Delta\sigma|$ to represent the quantity $\sqrt{[\![t_k t_k]\!]}$ which, in itself, is a measure of the magnitude of stress drop across the failure boundary. Because of the lack of shear strength in the failure zone for this process, then $|\Delta\sigma|$ represents a "total stress drop" (that is, the maximum possible shear stress change) at the boundary.

Now for some other process of failure that may operate in some thermodynamic environments in the earth, a complete loss of shear strength may not occur, or the material may be characterized by plastic or viscous properties allowing the retention of shear tractions. In this case the energy equation still applies in the form given by (12), with U_R and the traction jump in general different from those in (13). But we can use (13) as a means of normalizing the general case relation given by (12), so as to obtain a scaling law relating "partial shear stress drops" to the condition of total stress drop, characterized by $|\Delta\sigma|$. That is, if we divide equation (12) on both sides by the result in (13) we get:

$$U_R \simeq v_s \frac{[\![t_k t_k]\!]^{\frac{1}{2}}}{|\Delta\sigma|} \left[\frac{L_0}{L}\right]^{\frac{1}{2}} \tag{14}$$

Thus we find that the rupture rate scales as the ratio of the partial to total (shear) stress drops, and is always directly proportional to the local shear velocity of the material surrounding the failure zone. We also observe that U_R will depend on the square root of the transition energy ratios when the process of failure, resulting in a partial stress drop, is fundamentally different than the failure process resulting in complete loss of shear strength. However, in this regard, we might reasonably make the assumption that the same fundamental process is normally responsible for all occurrences of failure in the earth, and that the differences in stress drop are due to relatively subtle changes in mineralogy, water content and local temperature, which result in different rheological characteristics among similar earth materials subject to the same process of failure. In this case we would have $L = L_0$, and transition energy differences would not mediate the normalized rupture rate equation, given by (14). Under this assumption then, we get the simple scaling relation

$$U_R \simeq v_s \frac{|\Delta\sigma_p|}{|\Delta\sigma|} \tag{15}$$

where we have introduced $|\Delta\sigma_p|$ to represent the magnitude of the "partial stress drop" quantity $[\![t_k t_k]\!]^{\frac{1}{2}}$.

These results allow us to make several generalizations concerning earthquake dynamics and to also simplify the analytical modeling of these sources of seismic waves. In particular, total loss of shear strength in the material after failure implies total stress drops and rupture rates at or near the local shear velocity. The converse of this result, namely that rupture rates near or at the shear velocity necessarily require total loss of shear strength (and total shear stress drops) has not been shown, but certainly this would be a plausible interpretation of high rupture rate observations. Further, it is found that rupture velocities U_R scale linearly with the magnitude of the stress drop, so that the larger the partial stress drop, the larger the rupture rate, until the limits of total stress drop and rupture rates equal to the shear velocity of the medium are reached.

We observe further, however, that the stress drop and traction jumps appearing in all the relations describing conditions at the failure boundary, in particular, equations (14) and (15), are *dynamical* quantities and actually correspond to transient tractions, or stresses, at the points on the failure boundary surface where active failure is taking place. These stress changes may be very large due to dynamical stress concentration effects in the vicinity of the expanding edge of the failure zone and, while clearly related to the ambient background tectonic stress, could be one or even two orders of magnitude larger than the ambient stress level. Therefore to relate an equation like (15) to ambient quasi-static tectonic stresses, it is necessary to assume that the transient dynamic stress concentrations occurring at the front of a failure zone, which are responsible for failure, are directly related to the (local) ambient stress level. The simplest assumption would be that the general shape and curvature of the failure surface is the same for all conditions of failure, in which case the dynamic stress levels are always (for all failure modes) *directly proportional* to the ambient stress levels. With such an assumption, the ratio of the partial to total dynamic stress drops is equal to the ratio of the changes in the ambient (quasi-static) stress levels for partial and total stress drop. In this case a relation like (15) can be used to estimate ambient tectonic stress levels, since it can be rewritten in the form

$$U_R \simeq v_s \frac{|\overline{\Delta\sigma}|}{|\sigma_a|} \tag{16}$$

where $|\overline{\Delta\sigma}|$ is the quasi-static change in the ambient stress field under conditions of a partial stress drop and $|\sigma_a|$ denotes the ambient stress level, which arises from the total stress drop condition.

Physical Processes and Stress Level Requirements for Failure in the Earth

If assumptions required to arrive at the result given in (16) are appropriate, in particular if the mechanism of failure has the same energy requirements whether the stress drop is total or partial and if the dynamical stress load causing failure is strictly proportional to the quasi-static ambient stress for any failure process, then the relation provides the means of estimating the ambient stress from simultaneous observations of the rupture rate and the seismically observed stress drop. Such estimates cannot, however, be literally interpreted as being the stress levels that directly cause failure, since it is the dynamic stress concentrations that produce failure once the process is initialed and, quite certainly, it is intense quasi-static stress concentrations that initiate failure in the first place. That this must be true follows from an elementary consideration of the energy requirements for reasonable processes of failure in the earth.

Specifically, we observe that direct and indirect estimates of the average stress change in the quasi-static stress field due to earthquakes are in the range near 100 bars (10^8 dynes/cm^2) and are, at most, from 300 to 500 bars (*e.g.* Archambeau *et al.*, 1983). Further, the highest rupture rates observed are near the shear velocity, so, using (16), we estimate that ambient deviatoric stresses are at most of the order of 500 bars, and usually closer to 100 bars in regions with strong earthquake activity. Now if stress levels of such low magnitude actually were directly responsible for failure, then from (13), we would have for the energy per unit volume, ρL_0, required for failure, the estimate:

$$\rho L_0 \simeq \frac{1}{2}\frac{|\Delta\sigma|^2}{\rho v_s^2} \leq \frac{1}{2}\frac{(5\times 10^8)^2}{3(3\times 10^5)^2} = 4.6\times 10^5 \ ergs/cm^3$$

But this implies an energy for failure in the earth that is extremely low in comparison with energy requirements for even trivial changes in the thermodynamic state of the material. For example, the energy required to raise the temperature of one gram of water by one degree centigrade, in, say, a water saturated rock, is 10^7 ergs, which is already 25 times greater than the failure energy estimated from the largest ambient stress field changes. Further, when we consider the energy required for a material phase change such as shear melting, then even in the presence of water which would reduce the melting point considerably, the latent heats involved are of the order of 10^9 ergs/cm^3 and larger, and so the energy required for failure by melting would be of the order of, at least, 10^9 ergs/cm^3. This energy is nearly four orders of magnitude larger than the failure energy estimate based on ambient stress field changes.

Similarly, if we consider the ambient strain energy, W_a, stored in the medium per unit volume, and take the change in this quantity after failure to be an estimate of the energy per unit volume available for *initiation* of failure, then if the average ambient stresses determine failure energies, we would have to have

$$\rho L_0 \sim [\, W_a \,] = [\, \frac{1}{2\mu} \bar{\sigma}_{ij}^{(0)} \bar{\sigma}_{ij}^{(0)} \,] \,.$$

Here, as previously, ρL_0 is the energy per unit volume required for failure and $\bar{\sigma}_{ij}^{(0)}$ is the *average* tectonic stress. Hence, with the average ambient stress taken to be 500 bars as an extreme, we have, for a total loss of shear strength at the failure boundary:

$$\rho L_0 \sim [\, W_a \,] \simeq 5 \times 10^6 \; ergs / cm^3$$

Thus, with this quite different method of estimating the energy for failure, we obtain essentially the same, very low, transition energy estimate when reasonable estimates of the largest average ambient stresses are used.

Clearly, one conclusion that must be made is that the failure energy inferred, using reasonable upper limits for ambient stress field changes resulting from earthquakes, is so small that it cannot be a valid estimate for the energy required for failure in the earth. Nevertheless, it is even more certain that tectonic stresses must be responsible for failure in the earth and so we are forced to conclude that stress concentration effects, both transient, during failure growth, and quasi-static, prior to failure initiation, are the relevant stress levels supplying, the very local, high energy levels required for failure.

Indeed, in the dynamical situation, where we are concerned about the energy required for continued failure growth, the failure zone already exists and it can be viewed as an inclusion in the medium having drastically different elastic properties than the surrounding rock. Such an inclusion will produce very large stress concentrations in the surrounding medium in the near vicinity of that part of its surface having large curvature, for example near the edges of an ellipsoidally shaped failure inclusion. For a growing inclusion corresponding to the expanding failure zone, the stress concentrations are dynamically changing and transient, but certainly very large at the ends of a long thin failure transition zone with a width of a few millimeters. Indeed, for such an inclusion, stress concentration factors of 10 to 100 could be expected. In this case, the initial tectonic energy, which as we have seen has a low value per unit volume, is focused by the failure zone itself. Here, the strain energy is dynamically transferred through the propagation of stress waves from other parts of the medium to the ends of the failure zone. We know that this spatial

redistribution of internal energy is assured because the system is totally governed by the necessity of maintaining dynamical equilibrium with the inclusion zone and so must satisfy boundary conditions at the failure inclusion surface that demand stress distributions that approach those for the static limit, these being characterized by large stress levels at inclusion edges. Therefore, the process of stress relaxation, acts to increase the stress levels and strain energy levels near the high curvature edges of the inclusion and to decrease the stress and strain energy elsewhere, with the very local and large energy increases at the inclusion edges being accounted for by part of the energy reduction in the rest of the medium and with the "excess" strain energy reduction being radiated to the far field. Now the energy momentarily stored at the edges of the inclusion must be large enough to supply the energy required for failure and when this occurs the failure zone will grow.

The dynamical condition for failure growth at a rate U_R is, in fact, given by equation (12), so that we can estimate the magnitude of the transient stress concentration required to continue the failure process at some specified rate. In particular, if we consider failure progressing at or near the shear velocity in the medium with total loss of shear strength occurring, then the magnitude of the dynamical (shear) stress drop $|\Delta\sigma|$ must be given by

$$|\Delta\sigma| \equiv \sqrt{[\![t_k t_k]\!]} = \rho v_s \sqrt{2L_0} \tag{17}$$

where, as in equation (13), we have used $|\Delta\sigma|$ to represent the square root of the traction jump across the failure surface.

Since the failure process requiring least energy will be initiated first and will prevent stress concentrations adequate to trigger other failure processes requiring higher activation energies, we must consider the process with the lowest energy value, L_0, in order to estimate $|\Delta\sigma|$. In this regard, it seems that the lowest energy process that has been proposed as a mechanism leading to failure is a temperature increase in a water saturated rock medium sufficient to drive the local effective stress to zero. Under the supposition of very low tensile strength for the material, then only a small tensional stress would result in failure. This phenomenological mechanism, proposed by Raleigh and Evernden (1982) on the basis of quite a different set of arguments than those considered here, would require the presence of free water and very low permeability in the rock. However, both conditions are likely for the material in tectonically active regions. (Arguments for free water and high pore pressure based on geochemical and other evidence are given, for example, by Fyfe *et al.*, 1978.)

For this phenomenological mechanism to operate it is necessary to also propose a secondary mechanism that would rapidly convert the transient elastic strain energy at the edge of the failure zone to heat and produce the required increase in water temperature. Such a mechanism would quite certainly have to be a microscopic process, activated by the high dynamic stress levels. Numerous mechanisms are actually possible, particularly when we recognize that the material is extremely heterogeneous on a microscopic level and, therefore, would be expected to contain microscopic stresses from 10 to 100 times the local average stress, which is already at a much higher level than the ambient tectonic stress (by another factor of from 10 to 100) due to the "stress focusing" at the edge of the failure zone. Thus we can expect extremely high stresses at the edges of grains and pores which will activate highly dissipative flow and cracking in the material on the microscopic level. In fact, it would be likely, or at least possible, that the material could locally melt if water wasn't

present, but in the presence of free water then the heat produced by the non-linear and highly dissipative processes would rapidly raise the fluid temperature and with it the fluid pressure. During this process the high microscopic strain energy levels, and the average local strain energy level, would drop rapidly as non-linear plastic flow relaxed the stress. When the local interstitial fluid pressures reached the level of the maximum principal stress in the rock matrix or exceeded it, then the already locally weakened and microscopically flowing material could catastrophically yield, or fail, with the localized zones of flow and microfracture connecting throughout an element of material volume.

This particular process of failure would have a relatively low energy of activation, that is a low failure transition energy L_0. In this regard, Raleigh and Evernden (1982) estimate that the pressure increase required in the water would be of the order of the average ambient tectonic stress, since the water would be initially at a pressure about equal to the least principal stress in the rock matrix. Therefore a pressure increase of the order of 100 bars would be required. This would occur with about 5°C increase in temperature. Now if the transient strain energy stored in an element of volume at the edge of the failure zone is essentially all converted to heat by the microscopic processes of plastic flow and microfracture (with associated stress relaxation due to this deformation and flow) then the amount of energy required to raise the temperature by 5°C in a water saturated rock matrix is about equal to the total energy required for failure, that is, equal to L_0 in our notation. Thus, for this process

$$L_0 \simeq (5°C)\,(4 \times 10^7\ ergs/cal)\,(.25\ cal/gm/°C) = 5 \times 10^7\ ergs/gm$$

where .25 cal/gm/°C is a representative specific heat for the predominantly rock medium. Certainly this is a low energy when compared to the energy per gram required for melting, which is of the order of 10^9 ergs/gm or larger.

Now, given that this process requires an energy, L_0 of about 5×10^7 ergs/gm, then we can use the relation (17), which expresses energy conservation at the expanding failure surface, to obtain an estimate of the magnitude of the stress concentration required for the failure process. That is, we require

$$|\Delta\sigma| = \rho v_s \sqrt{2L_0} \sim 3(3 \times 10^5)\sqrt{10^8} \simeq 9\ kb$$

Thus, when the ambient tectonic stress is of the order of 100 bars, then stress concentration factors of the order of 100 are required in order to achieve the required transient stress levels in the lower kilobar range. This can only be achieved with thin failure zones, so that even this relatively low energy process of failure demands stress concentrations of such high levels, relative to the ambient stress, that only thin failure zones are predicted to be possible. Such thin transition zones are, of course, what are observed for earthquakes, where new fault zones are commonly observed to be of the order of millimeters in thickness. Therefore, in this regard at least, these inferences are consistent with observation. We also note that the inferred kilobar stress levels are of the same order as are observed in rock mechanics experiments for failure at high dynamic strain rates.

The probable situation that must occur *prior* to the initiation of failure is likely to be similar to the description of the dynamical growth of the failure zone. In this case, however, there is no pre-existing failure surface and no (rapid) dynamical stress readjustments taking place to concentrate the stress. However, it is clear that some process of stress concentration is necessary in order to initiate failure in view of the previous energy considerations. In this

case, with quasi-static stresses involved, it is likely that much lower stress levels are sufficient to activate non-linear creep and flow processes on a microscopic level, particularly when water is present. Therefore pre-existing heterogeneities within the medium, on a macroscopic scale, could serve to concentrate the very slowly increasing average tectonic stress, eventually to a level required for activation of creep and micro-scale fracture processes. Since these mechanisms would be expected to be activated in a heterogeneous manner spatially, then the resulting spatially non-uniform local weakening and flow of the material could be expected to increase the stress levels even further at those points where the material was stronger and more resistant to such deformation. At such points stress levels could reach higher levels on a shorter time scale and new microscopic processes, requiring higher stress levels, could be activated. At some stage, with the assumed presence of stronger zones allowing the eventual concentration of quite high stress levels, one would expect that a new increment of load accumulation within the highly stressed strong zones would exceed the threshold for activation of a new set of microscopic deformation mechanisms. This could trigger rapid and intense deformation and weakening, producing a small very weak zone which would serve as a stress concentrating inclusion on a macroscopic scale. Once this occurred then the dynamical process described earlier could serve to continue the growth of such a zone, sustained by the elastic energy released from the surrounding medium and concentrated at the inclusion edges. In this view of the initiation and growth of a failure zone then, it might be expected that there would commonly be a "starting time period" during which the failure growth was relatively slow. This time period of initiation could, however, be quite short in duration, with dynamical stress concentrations rapidly driving the failure growth rate to the shear velocity level.

As a final observation, it is appropriate to point out that the rupture rate, U_R, can be expected to be highly variable spatially. Thus, for example, while the shear velocity appearing in the equations specifying U_R can be nearly constant spatially, the traction or stress magnitude jumps, and the ratios for partial and total stress drop magnitudes, can be expected to vary in a manner related to the heterogeneous spatial variations of the ambient stress field. In addition, the partial stress drop magnitude might be expected to vary in a manner dependent on relatively subtle material properties (*e.g.*, water content and/or mineralogy). Therefore these results suggest that while the dynamics of the spontaneous failure processes resulting in earthquakes obey some (superficially) simple basic relations, these same relations, when combined with our knowledge of the heterogeneous makeup of the medium, predict that the failure process can be very complex, with highly variable rupture rates and stress changes not only possible, but quite likely to occur. Therefore we expect, and in fact observe, that large earthquakes involving large spatial rupture zones will be very complex and produce seismic radiation fields that reflect highly variable stress drops and rupture rates along the failure zone. Indeed many large events look, seismically, like multiple events with "bursts" of seismic radiation observed from different areas of the failure zone as it expands with variable speed. Further, it is likely that small events would have the same character, but with such extreme variations taking place on a smaller spatial scale and thus on a shorter time scale, so that these effects would be seen in the seismic radiation at higher frequencies, and likely to be observed only in the near or regional distance ranges from the event.

Relaxation Theory Models for Earthquakes

The results relating the rupture rate to the intrinsic shear velocity in the medium and the stress drops occurring during failure have significant implications for modeling of this type of seismic source. Specifically, we can simplify the computations implied by (8) and (9) very substantially if we can initially specify the rupture velocity function in a manner consistent with the boundary conditions, rather than be forced to calculate this function using the boundary conditions (2) and (3) jointly with the field relations (8) and (9).

Thus, since the rupture rate can be simply related, by equations (14) or (15), to the intrinsic medium properties and the dynamical stresses under some rather reasonable general assumptions, the following approach has been used in modeling earthquakes for purposes of predicting the properties of the radiated seismic field (see also Archambeau and Scales, 1984, for additional details):

(1) An initial prestress field is specified and, for convenience in handling the required integral evaluations in the dynamical solution, the field is described analytically in terms of the associated initial displacement, expressed in vector spherical harmonics.

(2) A failure zone geometry and time history of evolution is specified in terms of a rupture rate function U_R, with U_R prescribed in a form compatible with one of the equations (14), (15) or (16).

(3) Static solutions for the equilibrium displacement field of an inclusion, having the geometry specified in step (2), are obtained either numerically or, when possible, analytically. The solution is expressed in terms of a vector spherical harmonic expansion, so that it has an analytical expression compatible with that used for the initial displacement field, and such that the integrals in (8) and (9) may be most easily evaluated.

(4) The expansion, in vector harmonics, of the rate of change of the equilibrium field (*i.e.*, the expansion of the quantity $\partial \mathbf{u}^e(\mathbf{x}_0, t_0)/\partial t_0$ where $\mathbf{x}_0$ and t_0 are the *source* coordinates and time variables) is then used, in the integral result (8), to evaluate the initial value radiation field $u_m^{(1)}$. This field is expressed in vector spherical wave functions, and may then be used as a "starting solution" in (9) to obtain higher order approximations for the field, given by $u_m^{(n)}$. In all of this, U_R is employed in the form *specified* in step (2).

This (approximate) solution procedure can be specified quantitatively using the formalism developed in the section on "Mathematical Foundations". In this regard the static initial displacement, as well as the equilibrium displacement field in the vicinity of an embedded inclusion, are solutions of the static elastic equation

$$\nabla^2 \mathbf{u} + \frac{1}{1-2\sigma} \nabla(\nabla \cdot \mathbf{u}) = 0$$

where σ is Poisson's ratio for the material. We can treat the medium, as an approximation, as uniform and extending to great distances from an inclusion of variable size, such that its dimensions are relatively small (or very small) when computing the initial displacement field, but larger and of variable dimensions when computing the equilibrium field for the expanding failure zone. We then take the origin of coordinates at the center of the initial (small) inclusion, and at the same point for computation of the growing inclusion solutions.

Further, we require the stress field to assume a *prescribed* functional form or value at great distances from this origin such that, whatever the size of the inclusion, the equilibrium stress field must approach this value (or functional form) at great distances from the inclusion.

In this case all the equilibrium displacement fields, including the initial displacement field associated with the prestress state, can be expressed in the form:

$$\mathbf{u}(\mathbf{x}_0) = \sum_{l,m} \left[\alpha_{lm}\mathbf{M}^-_{lm}(\mathbf{r}_0) + \beta_{lm}N^-_{lm}(\mathbf{r}_0) + \gamma_{lm}\mathbf{F}_{lm}(\mathbf{r}_0)\right] + \mathbf{u}^{(0)}(\mathbf{x})$$

where $\mathbf{u}^{(0)}$ is the displacement associated with the stress prescribed at great distances from the origin. Here $\mathbf{M}^-_{lm}$, $\mathbf{N}^-_{lm}$ and $\mathbf{F}^-_{lm}$ are exterior vector harmonics, which are eigenfunctions of the Navier equation for the static displacement field. In particular, with $\gamma = 4(1-\sigma)$,

$$\mathbf{M}^-_{lm} = r_0^{-(l+1)}\sqrt{l(l+1)}\mathbf{C}_{lm}(\vartheta_0, \varphi_0)$$

$$\mathbf{N}^-_{l+1,m} = r_0^{-(l+2)}\left[\sqrt{l(l+1)}\mathbf{B}_{lm}(\vartheta_0, \varphi_0) - (l+1)\,\mathbf{P}_{lm}(\vartheta_0, \varphi_0)\right]$$

$$\mathbf{F}^-_{l-1,m} = r_0^{-l}\left[\frac{(\gamma-l)}{\gamma}\sqrt{l(l+1)}\,\mathbf{B}_{lm}(\vartheta_0, \varphi_0) + \frac{(\gamma+l-1)}{\gamma}\,l\,\mathbf{P}_{lm}(\vartheta_0, \varphi_0)\right]$$

The vector functions $\mathbf{P}_{lm}$, $\mathbf{B}_{lm}$ and $\mathbf{C}_{lm}$, are the classical vector spherical harmonics. The coefficients α_{lm}, β_{lm} and γ_{lm} are constants which depend on the dimensions of the inclusion and for the growing inclusion, therefore, these coefficients are parametrically dependent on time, since the dimensions of the inclusion are prescribed by the rupture rate, U_R, and change with time according to the time integral of U_R.

The initial value field $\mathbf{u}^*$ is defined as the difference between the equilibrium field for the growing inclusion (at any time) and the initial value field. Thus, using the previous general expression for these equilibrium fields we have, after subtraction,

$$\mathbf{u}^*(\mathbf{x}) = \sum_{l,m} \left[\alpha^*_{lm}\mathbf{M}^-_{lm}(\mathbf{r}) + \beta^*_{lm}\mathbf{N}^-_{lm}(\mathbf{r}) + \gamma^*_{lm}\mathbf{F}^-_{lm}(\mathbf{r})\right] \tag{18a}$$

where

$$\left.\begin{aligned}\alpha^*_{lm}(t_0) &= \alpha_{lm}(t_0) - \alpha^{(0)}_{lm}\\ \beta^*_{lm}(t_0) &= \beta_{lm}(t_0) - \beta^{(0)}_{lm}\\ \gamma^*_{lm}(t_0) &= \gamma_{lm}(t_0) - \gamma^{(0)}_{lm}\end{aligned}\right\} \tag{18b}$$

These coefficients, as noted, are (implicit) functions of the source time variable t_0. Here $\alpha^{(0)}_{lm}$, etc. are the constant coefficients associated with the solution for the static prestress condition prior to failure zone growth, while $\alpha_{lm}(t_0)$, etc., are the coefficients in the solution for the inclusion of dimension determined by the failure zone growth rate function U_R.

With the rupture rate *prescribed*, or approximated, for example, by a functional relation such as (from equation 16),

$$U_R = v_s \frac{|\overline{\Delta\sigma}|}{|\sigma_a|}$$

where v_s is the elastic shear velocity and $|\overline{\Delta\sigma}|$ is the magnitude of the (partial) stress drop at the failure boundary while $|\sigma_a|$ is the magnitude of ambient stress at the same point just before failure, then we can prescribe the evolution of failure growth and consequently the time dependence of the coefficients in (18). (This prescription of the time dependence of the equilibrium field coefficients is in numerical terms when the failure zone inclusion has a general geometrical shape.) Clearly, if we take the stress drop magnitude $|\Delta\sigma|$ to be proportional to the ambient stress $|\sigma_a|$ then U_R is a constant and proportional to the shear velocity. This approach has been often used in the past, and some results using this hypothesis are discussed later. On the other hand the stress drop can (reasonably) be taken to depend non-linearly on the ambient stress, for example $|\Delta\sigma| \simeq C_0 |\sigma_a| + C_1 |\sigma_a|^2$, with C_0 and C_1 constants. In this case the rupture rate would vary directly with the ambient stress level, that is we would have

$$U_R \simeq v_s \left[C_0 + C_1 |\sigma_a| \right]$$

In this case the rupture growth would speed up in zones of high initial stress. As will be pointed out later, there is some observational evidence that this occurs.

In any case, based on plausible hypotheses, it is possible to define a rupture rate compatible with energy and momentum conservation and to thereby determine a time history of the failure zone development, and to also express this time history in terms of variations for the equilibrium field expansion coefficients α°_{lm}, β°_{lm} and γ°_{lm} in the equilibrium field $\mathbf{u}^{\circ}$.

Now we have that the dynamic field is approximated, to first order, by the relaxation integral term given in (8). In terms of the Fourier transformed version of this field, using the results and inner product notation given in the section on "Mathematical Foundations" (equation 12), we have

$$4\pi \tilde{U}_j^{(1)} = i\omega F_{t_0} \left\{ \left\langle \rho \partial_{t_0} u_k^{\circ}, \tilde{G}_k^j \right\rangle_V \right\} \tag{19}$$

where f_{t_0} denotes Fourier transform operator with respect to t_0, the source time. Here, using the previous results for $\mathbf{u}^{\circ}$, we have that

$$\rho \partial_{t_0} \mathbf{u}^{\circ} = \sum_{l,m} \left[\rho \frac{\partial \alpha^{\circ}_{lm}}{\partial t_0} \mathbf{M}^{\bar{}}_{lm}(\mathbf{r}_0) + \rho \frac{\partial \beta^{\circ}_{lm}}{\partial t_0} \mathbf{N}^{\bar{}}_{lm}(\mathbf{r}_0) + \rho \frac{\partial \gamma^{\circ}_{lm}}{\partial t_0} \mathbf{F}^{\bar{}}_{lm}(\mathbf{r}_0) \right]$$

Further, the transformed Green's function $\tilde{G}_k^m(\mathbf{r}, \mathbf{r}_0; \omega)$ has the eigenfunction expansion given in the section on "Mathematical Foundations" (equation 9):

$$\tilde{G}_k^j(\mathbf{x}, \mathbf{x}_0; \omega) = \sum_{l,m,n} \left[\frac{\psi_j^s(\mathbf{r}, {}_n\omega_l^s)\, \bar{\psi}_k^s(\mathbf{r}_0, \omega_l^s)}{\omega^2 - ({}_n\omega_l^s)^2} \right.$$

$$\left. + \frac{\psi_j^T(\mathbf{r}, {}_n\omega_l^T)\, \bar{\psi}_k^T(\mathbf{r}, {}_n\omega_l^T)}{\omega^2 - ({}_n\omega_l^T)^2} \right]$$

with ψ^s and ψ^T spheroidal and toroidal vector eigenfunction for a layered spherical earth model, expressible in terms of linear combinations of the classical vector spherical harmonics $\mathbf{P}_{lm}$, $\mathbf{B}_{lm}$ and $\mathbf{C}_{lm}$, multiplied by Haskell-Thompson matrices involving spherical Bessel functions.

Using these expansions in the approximate solution, in (19), for the dynamic field then leads to+

$$\tau\pi\mathbf{u}^{(1)}(\mathbf{x},\omega) = i\omega \sum_{l,m,n} \sum_{l',m'} \int_{-\infty}^{+\infty} \frac{\partial}{\partial t_0} \begin{bmatrix} \alpha_l^s{}_{m'} \\ \beta_l^s{}_{m'} \\ \gamma_l^s{}_{m'} \end{bmatrix} \left\{ \left\langle \rho \begin{bmatrix} \mathbf{M}_{l'm'}^{-\dagger} \\ \mathbf{N}_{l'm'}^{-\dagger} \\ \mathbf{F}_{l'm'}^{-\dagger} \end{bmatrix} \bar{\psi}^s(\mathbf{r}_{0,n}\omega_l^s) \right\rangle_{V(t_0)} \frac{\psi^s(\mathbf{r}_n\omega_l^s)}{\omega^2 - (_n\omega_l^s)^2} \right.$$

$$\left. + \left\langle \rho \begin{bmatrix} \mathbf{M}_{l'm'}^{-\dagger} \\ \mathbf{N}_{l'm'}^{-\dagger} \\ \mathbf{F}_{l'm'}^{-\dagger} \end{bmatrix} \cdot \bar{\psi}^T(\mathbf{r}_{0,n}\omega_l^T) \right\rangle_{V(t_0)} \frac{\psi^T(\mathbf{r}_n\omega_l^T)}{\omega^2 - (_n\omega_l^T)^2} \right\} \exp^{-i\omega t_0} dt_0 \tag{20}$$

Here the inner product form is used to denote both a vector inner product and a functional inner product corresponding to an integration over the volume $V(t_0)$; that is:

$$\left\langle \rho \begin{bmatrix} \mathbf{M}_{l'm'}^{-\dagger} \\ \mathbf{N}_{l'm'}^{-\dagger} \\ \mathbf{F}_{l'm'}^{-\dagger} \end{bmatrix} \cdot \psi^s(\mathbf{r}_{0,n}\omega_l^s) \right\rangle_{V(t_0)} =$$

$$\left[\int_{V(t_0)} \rho \mathbf{M}_{l'm'}^{-} \cdot \psi^s \, d^3x_0, \int_{V(t_0)} \rho \mathbf{N}_{l'm'}^{-} \cdot \psi^s \, d^3x_0, \int_{V(t_0)} \rho \mathbf{F}_{l'm'}^{-} \cdot \psi^s \, d^3x_0 \right]$$

We have also used matrix forms in (20) to be able to write the results in more compact, yet explicit, form. Here and elsewhere the dagger (†) denotes the transpose of a matrix. Thus, in (20), the expanded matrix and inner products when written out give:

$$\frac{\partial}{\partial t_0} \begin{bmatrix} \alpha_l^s{}_{m'} \\ \beta_l^s{}_{m'} \\ \gamma_l^s{}_{m'} \end{bmatrix} \left\langle \rho \begin{bmatrix} \mathbf{M}_{l'm'}^{-\dagger} \\ \mathbf{N}_{l'm'}^{-\dagger} \\ \mathbf{F}_{l'm'}^{-\dagger} \end{bmatrix} \cdot \psi^s \right\rangle = \frac{\partial \alpha_l^s{}_{m'}}{\partial t_0} \int_{V(t_0)} \rho \mathbf{M}_{l'm'}^{-} \cdot \psi^s \, d^3x_0$$

$$+ \frac{\partial \beta_l^s{}_{m'}}{\partial t_0} \int_{V(t_0)} \rho \mathbf{N}_{l'm'}^{-} \cdot \psi^s \, d^3x_0 + \frac{\partial \gamma_l^s{}_{m'}}{\partial t_0} \int_{V(t_0)} \rho \mathbf{F}_{l'm'}^{-} \cdot \psi^s \, d^3x_0,$$

and analogously for the term involving the toroidal eigenfunctions.

The inner product integrals over $V(t_0)$ can be evaluated using the orthogonal properties of the vector spherical harmonics $\mathbf{P}_{lm}$, $\mathbf{B}_{lm}$ and $\mathbf{C}_{lm}$, since both

+ The summation convention is applied only to coordinate indices, while explicit summation is specified, when appropriate, for the "mode indices", l, m, n and l', m'.

the eigenfunctions and the vector solid harmonics are linear combinations of these functions. In particular, for a thin failure zone the inner products can be approximated by the relation:

$$\left\langle \rho \begin{bmatrix} \mathbf{M}_{i'm'}^{-} \\ \mathbf{N}_{i'm'}^{-} \\ \mathbf{F}_{i'm'}^{-} \end{bmatrix}^{\dagger} \cdot \psi^{s}(r_0, {}_n\omega_l^{(s)}) \right\rangle_{V(t_0)} = \begin{bmatrix} {}_S W_{i'm'n}^{(1)} \\ {}_S W_{i'm'n}^{(2)} \\ {}_S W_{i'm'n}^{(3)} \end{bmatrix}^{\dagger} \delta_{ll'} \delta_{mm'} \tag{21}$$

where the "weight functions" ${}_S W_{lmn}^{(P)}$ involve only integrals over the radial coordinate, which are, in general, functions of the source time variable t_0 due to the time dependence of the region of integration $V(t_0)$. Here the symbols $\delta_{ll'}$ and $\delta_{mm'}$ are Kronecker delta functions having zero value unless $l = l'$ and $m = m'$. Thus the eigenfunction expansion of the radiation field for a growing thin failure zone becomes, using (20) and the previous relation:

$$4\pi \tilde{\mathbf{u}}^{(1)}(\mathbf{r}, \omega) = i\omega \sum_{l,m,n} \left\{ \left[\int_{-\infty}^{+\infty} \begin{bmatrix} \partial_{t_0}\alpha_{lm}^{*} \\ \partial_{t_0}\beta_{lm}^{*} \\ \partial_{t_0}\gamma_{lm}^{*} \end{bmatrix} \begin{bmatrix} {}_S W_{lmn}^{(1)}(t_0) \\ {}_S W_{lmn}^{(2)}(t_0) \\ {}_S W_{lmn}^{(3)}(t_0) \end{bmatrix}^{\dagger} e^{-i\omega t_0}\, dt_0 \right] \frac{\psi^{s}(r, {}_n\omega_l^{S})}{\omega^2 - ({}_n\omega_l^{S})^2} \right.$$

$$\left. + \left[\int_{-\infty}^{+\infty} \begin{bmatrix} \partial_{t_0}\alpha_{lm}^{*} \\ \partial_{t_0}\beta_{lm}^{*} \\ \partial_{t_0}\gamma_{lm}^{*} \end{bmatrix} \begin{bmatrix} {}_T W_{lmn}^{(1)}(t_0) \\ {}_T W_{lmn}^{(2)}(t_0) \\ {}_T W_{lmn}^{(3)}(t_0) \end{bmatrix}^{\dagger} e^{-i\omega t_0}\, dt_0 \right] \frac{\psi^{T}(r, {}_n\omega_l^{T})}{\omega^2 - ({}_n\omega_l^{T})^2} \right\} \tag{22}$$

The structure of this eigenfunction expansion for the source radiation field has some noteworthy features, in particular the weight functions ${}_S W_{lmn}^{(P)}$ and ${}_T W_{lmn}^{(P)}$ are all *independent* of the source properties since they only involve inner product integrals of the spherical earth eigenfunctions with solid vector harmonics. (Thus, for a given earth model, they only need be calculated once, and can be used for any source calculation.) All the source information is carried in the coefficients involving time derivatives of the equilibrium field expansion coefficients α_{lm}^{*}, β_{lm}^{*}, γ_{lm}^{*}. These coefficients are, therefore, the fundamental "descriptors" of the source and, in an inversion procedure designed to infer source properties, are the unknowns to be determined.

We can consider the entire Fourier transform of the matrix product of the weight functions times these coefficients to be the transform of a scalar function. That is, we can define

$$\tilde{\alpha}_{lmn}^{S}(\omega) = \int_{-\infty}^{+\infty} \begin{bmatrix} \partial_{t_0}\alpha_{lm}^{*} \\ \partial_{t_0}\beta_{lm}^{*} \\ \partial_{t_0}\gamma_{lm}^{*} \end{bmatrix} \begin{bmatrix} {}_S W_{lmn}^{(1)}(t_0) \\ {}_S W_{lmn}^{(2)}(t_0) \\ {}_S W_{lmn}^{(3)}(t_0) \end{bmatrix}^{\dagger} e^{-i\omega t_0}\, dt_0 \tag{23a}$$

$$\tilde{\alpha}_{lmn}^{T}(\omega) = \int_{-\infty}^{+\infty} \begin{bmatrix} \partial_{t_0}\alpha_{lm}^{*} \\ \partial_{t_0}\beta_{lm}^{*} \\ \partial_{t_0}\gamma_{lm}^{*} \end{bmatrix} \begin{bmatrix} {}_T W_{lmn}^{(1)}(t_0) \\ {}_T W_{lmn}^{(2)}(t_0) \\ {}_T W_{lmn}^{(3)}(t_0) \end{bmatrix}^{\dagger} e^{-i\omega t_0}\, dt_0 \tag{23b}$$

and rewrite the result (21) in the simple form:

$$4\pi\tilde{\mathbf{u}}^{(1)}(\mathbf{r},\omega) = i\omega \sum_{l,m,n} \left[\frac{\tilde{\alpha}^{S}_{lmn}(\omega)}{\omega^2 - ({}_n\omega_l^S)^2} \psi^S({\mathbf{r}}_m {}_n\omega_l^S) + \frac{\tilde{\alpha}^{T}_{lmn}(\omega)}{\omega^2 - ({}_n\omega_l^T)^2} \psi^T({\mathbf{r}}_m {}_n\omega_l^T) \right] \tag{24}$$

In the time domain the inverse Fourier transform, with respect to the time variable t, is easily obtained using the residue theorem, by noting that the integrand on the right side in (22) has simple poles at $\pm {}_n\omega_l^S$ and $\pm {}_n\omega_l^T$. This gives:

$$4\pi u^{(1)}(\mathbf{r},t) = -\sum_{l,m,n} \left[\tilde{\alpha}^{S}_{lmn}({}_n\omega_l^S)\, \psi({\mathbf{r}}_m {}_n\omega_l^S) \cos {}_n\omega_l^S t \right.$$

$$\left. + \tilde{\alpha}^{T}_{lmn}({}_n\omega_l^T)\, \psi({\mathbf{r}}_m {}_n\omega_l^T) \cos {}_n\omega_l^T t \right] \tag{25}$$

Clearly, from (24) and (25) the coefficients $\tilde{\alpha}^{S}_{lmn}$ and $\tilde{\alpha}^{T}_{lmn}$ are the quantities that may be determined from observations. Then the relations in (22) are those that can be used to infer first order source properties from observations. Here the weight functions are known while the "equilibrium coefficients" are to be determined in such an "inversion" procedure. On the other hand, computation of the "equilibrium coefficients" for a particular source geometry and time evolution is all that is necessary to completely specify a theoretically predicted dynamic field from source.

In case the integrals for the weight functions, defined in (21), are over a region which is fixed in time, then the weight functions will also be independent of the source time t_0. For some source geometries this will be a good approximation, or will be, in other special cases, exact. In any case, when these weight functions are independent of t_0, or nearly so, then (23) simplifies to:

$$\begin{aligned} \tilde{\alpha}^{S}_{lmn}(\omega) &\simeq i\omega \begin{bmatrix} \tilde{\alpha}^{*}_{lm} \\ \tilde{\beta}^{*}_{lm} \\ \tilde{\gamma}^{*}_{lm} \end{bmatrix} \begin{bmatrix} S W^{(1)}_{lmn} \\ S W^{(2)}_{lmn} \\ S W^{(3)}_{lmn} \end{bmatrix}^{\dagger} \\ \tilde{\alpha}^{T}_{lmn}(\omega) &\simeq i\omega \begin{bmatrix} \tilde{\alpha}^{*}_{lm} \\ \tilde{\beta}^{*}_{lm} \\ \tilde{\gamma}^{*}_{lm} \end{bmatrix} \begin{bmatrix} T W^{(1)}_{lmn} \\ T W^{(2)}_{lmn} \\ T W^{(3)}_{lmn} \end{bmatrix}^{\dagger} \end{aligned} \tag{26}$$

This is a particularly simple result which is easily applied for the inference of source properties from observations or for the direct computation of theoretically predicted radiation fields from source models.

From our previous considerations of the elastic wave radiation from earthquakes, we have that corrections to the first order result given by (24) are obtained by computing the "scattering integral", given in equation (12) in the section on "Mathematical Foundations", or from integrals such as (9) in the present section. In terms of the inner product notation, the second order solution which accounts for "scattering" (and absorption of energy) on the failure surface is given by:

$$u_k^{(2)}(\mathbf{r},\omega) = \tilde{u}_k^{(1)}(\mathbf{r},\omega) + F_{t_0} \left[\langle u_d^{(1)}, \tilde{g}^{k}_{d\beta} \eta_\beta \rangle_{\partial V} - \langle \tau_{d\beta}^{(1)} \eta_\beta, \tilde{G}^{m}_{a} \rangle_{\partial V} \right]$$

Here all the functions on the right side are known since the eigenfunction expansions are used in all the transformed Green's tractions and displacements, while (23)-(25) explicitly specify $u_d^{(1)}$ and $\tau_{dj}^{(1)}$ from their definitions. While this form can be manipulated into an expansion like that for the first order field $\dot{u}_m^{(1)}$ from the source (Archambeau and Stevens, unpublished, 1980) it is not worthwhile to give these complicated results here, since they do not need to be used in the subsequent discussion. That is, we need only consider the first order predictions of the elastic radiation from earthquakes relative to explosion sources in order to quantify their differences.

The results given here have all been expressed in terms of expansions in the eigenfunctions of a spherical earth model. Similar results can be obtained for plane layered earth models, wherein the expansions are in terms of eigenfunctions in plane layered geometries (Archambeau and Stevens, unpublished, 1980). This expansion form is suitable for predictions (and source property inversion studies) when the source to receiver distances are less than a few thousand kilometers.

Results from model calculations using this type of approximation procedure have provided predictions of seismic radiation from theoretical sources that are reasonable dynamical approximations of earthquakes. An important feature of these models is that they are expressed in terms of the fundamental physical variable controlling the dynamics of these natural sources and so it is possible to infer both the basic properties of the seismic field and its variations in terms of such physical parameters as those describing the final dimensions of the failure zone, its rate of formation and prestress. As distinct from kinematic representations, these dynamical solutions do not involve any assumptions of the time history of the displacement or stress field at the failure surface, or "fault plane". The dynamical modeling does, however, require specification of the initial stress field and some general assumptions regarding the physics of the failure process involved, such as the assumption of the loss of shear strength in the material after failure.

One of the simplest models that can be investigated is one in which the initial prestress is taken to be uniform in the medium and the rupture rate to be constant and near the medium shear velocity. Various rupture zone geometries have been considered for this uniform prestress case, all of them corresponding to some type of ellipsoid of revolution generated by simultaneous expansion and translation of spherical failure zones (*e.g.* Archambeau, 1968; Minster, 1973). While this type of model is the most elementary that can be considered, it does allow the radiation fields to be evaluated analytically, so that the dependence of the seismic field on the various source parameters can be evaluated and described by analytic means. Most important, however, is the fact that we can expect predictions from these elementary models to provide a description of the essential first order features of the seismic radiation associated with natural earthquakes. Further, we also expect that the relaxation source theory, when considered in the limit in which a spherical rupture zone is created "supersonically", will provide a good first order determination of the seismic radiation released tectonically by an underground explosion in an initially stressed medium. (For details of the modeling of explosion induced tectonic release see, for example, Archambeau and Sammis, 1970; Archambeau, 1972.)

Analytical Results for Simple Relaxation Theory Models of Tectonic Sources

To illustrate the procedure used to construct relaxation theory models and to provide an example of the (analytical) form of the seismic field produced by such models, we will summarize the mathematical results for the simple translating and expanding spherical failure zone models.

In order to simplify matters, while nevertheless maintaining sufficient generality for purposes of describing important properties of the seismic field, we will consider a *homogeneous, pure shear* initial stress field as a representation of the (average) prestressed state of the medium. Further, this prestress field will explicitly be assumed to be uniform to great distances from the coordinate origin (i.e., the point of initial failure in the medium) and so, in effect, to be uniform to infinity. This will allow us to extend the source region, and specifically the integration over the zone in which stress relaxation takes place, to infinity and to thereby simplify the Green's function representation of the tectonic source. (In some of the past work on relaxation source representations, for example, by Archambeau (1968, 1972) and Minster (1973), the region in which relaxation of a *homogeneous* prestress was allowed to contribute to the seismic radiation field was restricted to a spherical volume of radius R_s. This was done on the grounds that, in the earth, the prestress was not homogeneous and that the zone of initial stress was in any case finite and not infinite as is implicitly assumed when a homogeneous initial stress is used. While these observations concerning the prestress must certainly be true, the approximation of the situation in the earth by the use of a "cutoff" in the homogeneous prestress model is not a very accurate one. In particular, subsequent work by Stevens (1981) has shown that failure induced relaxation of heterogeneous prestress does produce seismic radiation having spectra that are similar to that predicted using a homogeneous prestress along with the "R_s cutoff factor", but it cannot be said that the approximation gives an accurate representation of the low frequency radiation, nor does it show the high frequency complexities that can occur when the prestress is strongly heterogeneous. Therefore, in the present discussion we will develop the radiation field predictions for the completely homogeneous prestress case, which provides a good first order representation for earthquake radiation fields, and then discuss some of Steven's results, among others, for the non-homogeneous case, contrasting them with results from the homogeneous case in order to show how a spatially confined, heterogeneous initial prestress modifies the predictions.)

For the case of a homogeneous pure shear prestress the mathematical description can be developed in terms of the dilatation and rotation potentials, and is relatively simple.[+] Specifically, the dilatation, χ_4, and vector rotation fields, χ, are defined by

[+]The use of these "physical potentials" is limited to the pure shear prestress case and cannot usually be used to represent more general cases, where the prestress is arbitrary. This is because these potentials, when obtained from (27), do not always represent the entire elastic field in the static case, so that the static values of the dilatation and rotation potentials do not fully describe prestress or equilibrium stress states in all situations. It happens, in the pure shear prestress case, that the static dilatation and rotation potentials can completely represent the equilibrium stress state, but this is a special case. In the general prestress case the displacement field itself must be used along with the appropriate dynamical Green's function integral equation, with results as given earlier. If potentials are to be used, however, then the Lamé potentials, defined by $\mathbf{u} = \nabla\vartheta + \nabla \times \boldsymbol{\psi}$, are required. In the latter case the Lamé potentials ϑ and $\boldsymbol{\psi}$ satisfy ordinary wave equations and the analysis proceeds in the same way as it does for the dilatation and rotation, with formal results that are only different by constant factors.

$$\left.\begin{aligned} \chi &= (\chi_1, \chi_2, \chi_3) = \frac{1}{2}\nabla \times \mathbf{u} \\ \chi_4 &= \nabla \cdot \mathbf{u} \end{aligned}\right\} \tag{27}$$

The equation of motions for an isotropic and homogeneous medium, with negligible body forces acting, is

$$\partial_t^2 \mathbf{u} = v_p^2 \nabla \chi_4 - 2v_s^2 (\nabla \times \chi) \tag{28a}$$

with v_p and v_s the compressional and shear velocities in the medium. Therefore the equation of motion can be used to compute the acceleration from these potentials. If the Fourier transform with respect to time is applied to this relation, then the relation is:

$$\tilde{\mathbf{u}} = -\left[\frac{1}{k_p^2}\right]\nabla\tilde{\chi}_4 + \left[\frac{2}{k_s^2}\right]\nabla \times \tilde{\chi} \tag{28b}$$

where $k_p = \omega / v_p$ and $k_s = \omega / v_s$ are wave numbers for compressional and shear waves. Thus displacement transforms can be computed from the potential transforms using this relation.

It is not difficult to show that the equation of motion is satisfied if the *Cartesian components* of χ and the scalar potential χ_4 all satisfy wave equations of the same form (Archambeau, 1968). In particular, the potentials must satisfy:

$$\nabla^2 \chi_\alpha - \frac{1}{v_\alpha^2}\partial_t^2 \chi_\alpha = 0 \tag{29}$$

where $\alpha = 1, 2, 3, 4$ and

$$(\chi_\alpha) = (\chi_1, \chi_2, \chi_3, \chi_4)$$

is used to denote any one of the four potentials. Here also

$$(v_\alpha) = (v_s, v_s, v_s, v_p)$$

is the corresponding shear or compressional velocity associated with the individual potentials.

The advantage of the use of these potentials is that the eigenfunction solutions of the wave equations in (29) are scalar wave functions with well known properties (see, for example, Morse and Feshbach, 1953) and are easily manipulated, as opposed to the much more complicated and cumbersome vector wave functions associated with the elastic equations of motion. Further, as will become apparent, the radiation field is conveniently separated into purely compression waves (χ_4) and shear waves (χ) by this potential decomposition.

The Green's function solution of (29) corresponding to the volume relaxation source term, or initial value integral term denoted by $u_n^{(1)}$ in equation (8), is simply (Archambeau, 1968):

$$\chi_\alpha^{(1)}(\mathbf{r}, t) = \frac{1}{4\pi v_\alpha^2}\int_0^{t^+} dt_0 \int_{V(t_0)} \left[\frac{\partial \chi_\alpha^*}{\partial t_0}\right]\frac{\partial \Gamma^{(\alpha)}}{\partial t_0}\, d\mathbf{r}_0 \tag{30}$$

where $\Gamma^{(\alpha)}(\mathbf{r},t;\mathbf{r}_0,t_0)$ is the scalar Green's function for the wave equation. The volume integral is over $V(t_0)$, the volume outside the failure zone. This result is completely analogous to the first order solution ($u_m^{(1)}$) discussed earlier and given in equation (8). The potential χ_α^* appearing in this integral solution corresponds to the change in the equilibrium value of the potential χ_α, as a function of the *source time* variable t_0, due to the (spontaneous) creation and growth of the failure zone. This function is completely analogous to the equilibrium displacement function $\mathbf{u}^*$, and can, in the present case, be computed from it, using the potential definitions.[+]

The limit on the integral over the source time, t_0, is $t^+ = t + \varepsilon$, with $\varepsilon > 0$ and small, where ε is introduced simply to avoid singular points in the Green's function. However, if $t_0 > \tau_0$, with τ_0 the total time duration for formation of the failure zone, then χ_α^* does not vary for such t_0 values, since the failure zone does not change or grow, and then the derivative of χ_α^* will vanish. Therefore the integral over the source time t_0 has an upper limit equal to τ_0 when $t > \tau_0$. In general we will consider the case in which the observer time t, measured relative to the beginning of failure, is larger than the time τ_0. In this case we will replace the limit by τ_0 and explicitly note that this representation is valid for $t > \tau_0$.

The use of the index (α) with the Green's function is to indicate that slightly different Green's functions must be used for the rotation potential components, χ_j, $j = 1, 2, 3$, than is used for the dilatation potential χ_4. In particular, to compute the direct radiation field from a relaxation source, we can use the infinite space Green's function, and in this case:

$$\Gamma^{(\alpha)}(\mathbf{r}, t; \mathbf{r}_0, t_0) = \frac{\delta(\tau^*/v_\alpha - t^*)}{\tau^*}$$

where $\delta(x)$ denotes a Dirac delta function and

$$\tau^* = |\mathbf{r} - \mathbf{r}_0|$$

$$t^* = t - t_0$$

with $\mathbf{r}$ and t receiver coordinates and time. Here the Green's function for $\alpha = 1, 2, 3$ involves the shear velocity in $\Gamma^{(\alpha)}$, while the compressional velocity is used when $\alpha = 4$.

The Fourier transformed integral solution corresponding to (30) is obtained by taking transforms with respect to the *observers time* t. Thus

$$\tilde{\chi}_\alpha^{(1)}(\mathbf{r},\omega) = \int_{-\infty}^{+\infty} \chi_\alpha^{(1)}(\mathbf{r},t)\, e^{-i\omega t}\, dt$$

is the transformed potential. Applying this operation to (30), and taking account of the properties of the Dirac delta function, we have for $t > \tau_0$:

$$\tilde{\chi}_\alpha^{(1)}(\mathbf{r},\omega) = \frac{i\omega}{4\pi v_\alpha^2} \int_0^{\tau_0} e^{-i\omega t_0}\, dt_0 \int_{V(t_0)} \left[\frac{\partial \chi_\alpha^*}{\partial t_0}\right] \frac{e^{-ik_\alpha \tau^*}}{\tau^*}\, d\mathbf{r}_0;\ t > \tau_0 \qquad (31)$$

[+] As noted earlier, the dilatation and rotation potentials do not always completely describe the equilibrium state $\mathbf{u}^*$ when the potential definitions in (27) are used for *static* field computations.

This spectral representation is most useful for the evaluation of the potentials, as compared to the time domain representations, and (31) is generally the form that has been used. (See, for example, Archambeau, 1964, 1968 and Minster, 1973.)

The integral representation of the potentials can be evaluated using a procedure which is equivalent to that described earlier for approximate solutions for the source displacement field. This procedure is, as before, an approximation to the complete dynamical solution, wherein we *specify* the rupture growth, rather than solve for it using the boundary conditions and the equation of state for the material. (Further, for this example, only the initial value field $\chi_\alpha^{(1)}$ will be obtained, with the scattered field contributions given by $\chi_\alpha^{(n)}$ with $n \geq 2$ completely neglected.)

One way of specifying failure zones is indicated in Figure 1. In particular, the simple spherical zone can be made, to expand and translate in such a way that the time evolution of a natural or explosion induced failure process can be approximated. (Clearly, a thin disk or ellipsoid would be a more preferable geometric shape to use for simulation of an earthquake failure zone, rather than a sphere. However, the moving expanding sphere has the advantage of giving relatively simple closed form analytical results for the potentials, while the other geometries produce much more complex and cumbersome results. Further, as indicated by Minster (1973), when comparisons are made, the radiation field predictions for models with "thin failure zone" geometries do not differ in any fundamental way from those using a *tangentially expanding sphere* with the same final dimensions and growth characteristics.)

For a spherical zone at any time t_0, we can parameterize the failure zone in terms of two functions of time: $d(t_0)$, a function describing the movement of the center of the sphere relative to a fixed coordinate system, and $R(t_0)$, the time dependent radius of the sphere, as indicated in Figure 1. By adjusting the time dependence of these two functions, we can obtain time evolutions such as those illustrated in the three lower insets in Figure 1. (This parameterization is equivalent to a full specification of the rupture velocity function, U_R, as a function of time and position.) Of the three models shown, the uniformly expanding sphere has been used to model tectonic release effects associated with explosions in prestressed media (*e.g.*, Archambeau, 1972) while the tangentially expanding sphere and moving sphere models have been used to approximate earthquake failure zones by Minster (1973) and Archambeau (1968), respectively. Of the latter two model types, the tangentially expanding model leads to the most accurate approximate representation for earthquakes.

Now the equilibrium displacement field in the elastic medium surrounding a spherical cavity in a homogeneously prestressed medium is, from Landau and Lifshitz (1959) for example:

$$u_i^e = \frac{R_0^3}{\mu(7-5\sigma)} \left\{ 5(1-\sigma)\, \sigma_{ik}^{(0)} \frac{\partial}{\partial x_k'} \left[\frac{1}{r'}\right] - \frac{R_0^2}{4}\, \sigma_{kl}^{(0)} \frac{\partial^3}{\partial x_i' \partial x_k' \partial x_l'} \left[\frac{1}{r'}\right] \right.$$

$$\left. - 5/4\, \sigma_{kl}^{(0)} \frac{\partial^3}{\partial x_i' \partial x_k' \partial x_l'}\, r' \right\}$$

Here, $\sigma_{ik}^{(0)}$ is the constant prestress existing prior to the introduction of the cavity, σ is Poissons ratio, μ is the elastic rigidity of the medium and R_0 is the radius of the spherical cavity. If we specify the prestress to be a constant pure shear field, with:

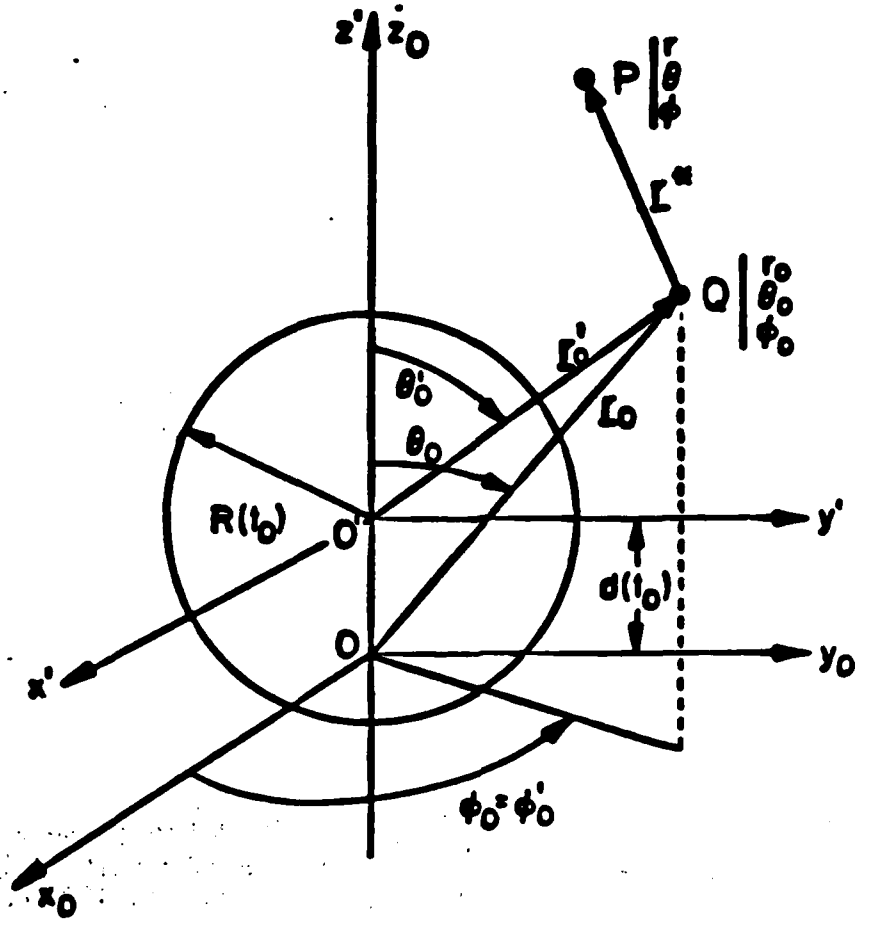

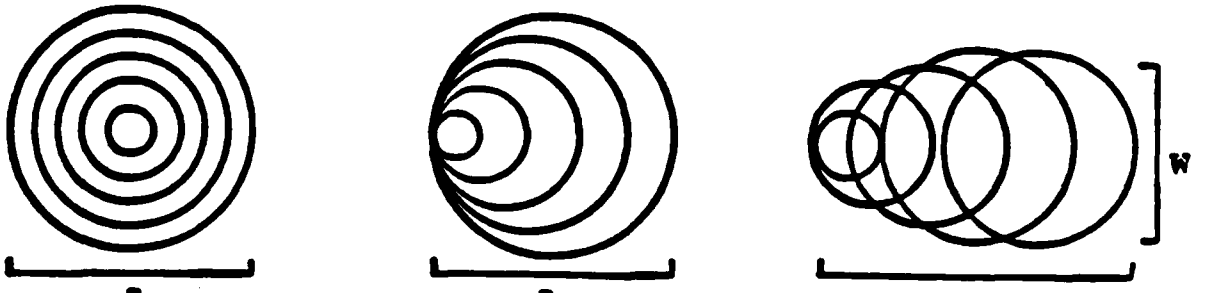

UNIFORMLY EXPANDING SPHERE
$d(t_0)=0$

TANGENTIALLY EXPANDING SPHERE
$d(t_0)=R(t_0)$

MOVING SPHERE
L/W = 1.6

$d(t_0)>R(t_0)$

Figure 1. Coordinate systems used to describe the geometry of a translating and expanding sphere. The primed coordinate system moves with the center of the sphere while the fixed coordinates, with origin (O), are used to locate source points Q in the system r_o, θ_o, ϕ_o and observer points P in the system r, θ, φ. The lower three insets illustrate three geometric models for failure zones using translating/expanding spheres.

$$\sigma_{11}^{(0)} = \sigma_{22}^{(0)} = \sigma_{33}^{(0)} = 0$$

then this solution can be used to represent the equilibrium displacement field around a spherical inclusion in which the shear strength vanishes ($\mu = 0$ inside) and in which the compressibility matches that of the medium outside the inclusion. In this case, the associated potentials χ_α^s can be shown from (27) to have the form, in the coordinates r'_0, ϑ'_0, φ'_0 in the frame 0' in Figure 1:

$$\chi_\alpha^s(r'_0, t_0) = \left[\frac{1}{r'_0}\right]^{s} \sum_{m=0}^{s} \left\{ a_{sm}^{(\alpha)} \cos m\varphi'_0 + b_{sm}^{(\alpha)} \sin m\varphi'_0 \right\} P_s^m(\cos\vartheta'_0) \qquad (32)$$

where the coefficients $a_{sm}^{(\alpha)}$ and $b_{sm}^{(\alpha)}$, $\alpha = 1, 2, 3, 4$, are:

$$\left[a_{sm}^{(\alpha)}(t_0)\right] = \frac{5[(1-\sigma) - \delta_{\alpha 4}\sigma]}{\mu(7-5\sigma)} R^3(t_0) \begin{bmatrix} -\frac{3}{2}\sigma_{23}^{(0)} & -\frac{1}{2}\sigma_{12}^{(0)} & -\frac{1}{4}\sigma_{23}^{(0)} \\ \frac{3}{2}\sigma_{13}^{(0)} & 0 & -\frac{1}{4}\sigma_{13}^{(0)} \\ 0 & \frac{1}{2}\sigma_{23}^{(0)} & \frac{1}{2}\sigma_{12}^{(0)} \\ 0 & \sigma_{13}^{(0)} & 0 \end{bmatrix}$$

$$\left[b_{sm}^{(\alpha)}(t_0)\right] = \frac{5[(1-\sigma) - \delta_{\alpha 4}\sigma]}{\mu(7-5\sigma)} R^3(t_0) \begin{bmatrix} 0 & 0 & \frac{1}{4}\sigma_{13}^{(0)} \\ 0 & \frac{1}{2}\sigma_{12}^{(0)} & -\frac{1}{4}\sigma_{23}^{(0)} \\ 0 & -\frac{1}{2}\sigma_{13}^{(0)} & 0 \\ 0 & \sigma_{23}^{(0)} & \frac{1}{2}\sigma_{12}^{(0)} \end{bmatrix}$$

with $\delta_{\alpha 4} = 0$ if $\alpha \neq 4$, and $\delta_{\alpha 4} = 1$ if $\alpha = 4$. Here the potential function index (α) numbers the rows vertically from 1 to 4 in the matrices, while m = 0, 1, 2 is the column index running from left to right. (This result is given by Archambeau (1964, 1968) with a multiplicative factor of 1/2 missing from the rotation potential coefficients. Minster (1973) gives the correct results, but omits a minus sign from the coefficient $a_{22}^{(2)}$. The result given here is from Harkrider (personal communication), who gives the general result for $\sigma_{11}^{(0)} \neq \sigma_{22}^{(0)} \neq \sigma_{33}^{(0)} \neq 0$ In this general case the following additional coefficients are non-zero in the matrices $a_{sm}^{(\alpha)}$ and $b_{sm}^{(\alpha)}$: $a_{21}^{(2)} = \frac{1}{2}(\sigma_{11}^{(0)} - \sigma_{33}^{(0)})$, $a_{20}^{(4)} = \frac{1}{2}(2\sigma_{33}^{(0)} - \sigma_{11}^{(0)} - \sigma_{22}^{(0)})$, $a_{22}^{(4)} = \frac{1}{4}(\sigma_{11}^{(0)} - \sigma_{22}^{(0)})$, $b_{21}^{(1)} = -\frac{1}{2}(\sigma_{22}^{(0)} - \sigma_{33}^{(0)})$, and $b_{22}^{(3)} = \frac{1}{4}(\sigma_{22}^{(0)} - \sigma_{11}^{(0)})$. In the case of a pure shear initial stress, these coefficients all vanish.)

With this description of a "spherical inclusion equilibrium field, we can express the equilibrium field at any source time t_0, for any of the failure zone evolutions in Figure 1, by using an appropriate radius function $R(t_0)$. The field so expressed will, however, be in the *moving* coordinate system, with origin 0' and spherical coordinates r', ϑ', φ'.

The movement of this coordinate frame is a simple translation relative to the fixed coordinates with origin 0, and is described by the function $d(t_0)$.

Thus, to use this description of the equilibrium field χ_a^e in the integral representation of the dynamic radiation field, in (31), it is necessary to either express the field χ_a^e in terms of the coordinates of the *fixed* reference frame $(r_0, \vartheta_0, \varphi_0)$ and evaluate (31) as it stands, or to evaluate the integral representation for the dynamic field in the *moving* frame, with source coordinates $(r_0', \vartheta_0', \varphi_0')$ and observer coordinates $(r', \vartheta', \varphi')$, and to then transform the dynamical results back to the *fixed* reference frame. The former procedure was used by Archambeau (1968), while Minster (1973) used the latter. We shall follow Minster's procedure since the results are somewhat more general and compact than the alternate expansion.

The first step in evaluating (31) is to express the infinite space Green's function in the integrand in terms of spherical wave-functions referenced to the coordinate system which moves with the expanding spherical zone of failure. This is a classical result (*e.g.*, Morse and Feshbach, 1953), and has the form:

$$\frac{e^{-ik_a r^*}}{r^*} = -ik_a \sum_{l=0}^{\infty} (2l+1)\, P_l(\cos\gamma') \begin{cases} j_l(k_a r_0')\, h_l^{(2)}(k_a r') \,; r' > r_0' \\ j_l(k_a r')\, h_l^{(2)}(k_a r_0') \,; r' < r_0' \end{cases}$$

where $(r', \vartheta', \varphi')$ are source point coordinates in the moving frame, corresponding to the point Q in the figure. The angle γ' is measured between the vectors $\mathbf{r}'$ and $\mathbf{r}_0'$. (The vector $\mathbf{r}'$, from the origin 0' to the observer's point P is not shown in Figure 1, but vectors $\mathbf{r}$ and $\mathbf{r}'$ to the point P have the same relationship to the coordinate systems at 0 and 0' as do the vectors $\mathbf{r}_0$ and $\mathbf{r}_0'$ for the source point Q). The Legendre function, involving the angle γ', has the expansion (Morse and Feshbach, 1953)

$$P_l(\cos\gamma') = \sum_{m=0}^{l} (2-\delta_{m0})\, \frac{(l-m)!}{(l+m)!}\, P_l^m(\cos\vartheta')\, P_l^m(\cos\vartheta_0')\, \cos m(\varphi' - \varphi_0')$$

which involves the basic observer and source point coordinate angles ϑ', φ' and ϑ_0', φ_0'. Here δ_{mn} denotes a Kronecker delta function. Hence, these two expansions allow us to express the Green's function in separated form in terms of the source and observer coordinates in the moving frame. Now, using this Green's function expansion and the solution for χ_a^e, the equilibrium potential field for the spherical inclusion as expressed in (32), we get, from (31), the integral solution:

$$\tilde{\varepsilon}_a^{(1)}(r',\omega) = \frac{k_a^2}{4\pi v_a} \sum_{l=0}^{\infty} \sum_{m=0}^{2} (2l+1) \int_0^{\tau_0} \frac{dR^3(t_0)}{dt_0}\, e^{-i\omega t_0}$$

$$\left\{ \int_0^{\pi} \int_0^{2\pi} \left[a_{gm}^{(a)} \cos m\varphi_0' + b_{gm}^{(a)} \sin m\varphi_0' \right] P_g^m(\cos\vartheta_0')\, P_l(\cos\gamma')\, \sin\vartheta_0'\, d\vartheta_0'\, d\varphi_0' \right.$$

$$\left. \cdot \left[h_l^{(2)}(k_a r') \int_{R(t_0)}^{r'} \frac{j_l(k_a r_0')}{r_0'}\, dr_0' + j_l(k_a r') \int_{r'}^{\infty} \frac{h_l^{(2)}(k_a r')}{r_0'}\, dr_0' \right] \right\} dt_0$$

for the dynamic field due to relaxation effects, for observer times $t > \tau_0$, where τ_0 is the time necessary for the complete formation of the failure zone. Here

we have factored out the time dependence term from the multiple coefficients $a_{\ell m}^{(\alpha)}$ and $b_{\ell m}^{(\alpha)}$ in (32), so that $a_{\ell m}^{'(\alpha)}$ and $b_{\ell m}^{'(\alpha)}$ are the time independent coefficients defined by:

$$\left[a_{\ell m}^{(\alpha)}(t_0)\right] = R^{\beta}(t_0)\left[a_{\ell m}^{'(\alpha)}\right]$$

$$\left[b_{\ell m}^{(\alpha)}(t_0)\right] = R^{\beta}(t_0)\left[b_{\ell m}^{'(\alpha)}\right]$$

Observing that the orthogonality of the Legendre functions is such that:

$$\int_0^{2\pi}\int_0^{\pi} P_l(\cos\gamma')\, P_\ell^m(\cos\vartheta_0')\begin{bmatrix}\cos m\varphi_0'\\ \sin m\varphi_0'\end{bmatrix}\sin\vartheta_0'\, d\vartheta_0'\, d\varphi_0' =$$

$$\frac{4\pi}{2l+1} P_l^m(\cos\vartheta')\begin{bmatrix}\cos m\varphi'\\ \sin m\varphi'\end{bmatrix}\delta_{l2}$$

where

$$\delta_{l2} = \begin{cases}0, & l \neq 2\\ 1, & l = 2\end{cases}$$

then we have that

$$\tilde{\chi}_\alpha^{(1)}(r',\omega) = \frac{k_\alpha^2}{v_\alpha}\sum_{m=0}^{2}\int_0^{\tau_0}\frac{dR^{\beta}(t_0)}{dt_0}\, e^{-i\omega t_0}\cdot\left\{\left[a_{2m}^{'(\alpha)}\cos m\varphi'\right.\right.$$

$$\left.+\, b_{2m}^{'(\alpha)}\sin m\varphi'\right] P_2^m(\cos\vartheta')\left[h_2^{(2)}(k_\alpha r')\int_{R(t_0)}^{r'}\frac{j_2(k_\alpha r_0')}{r_0'}\, dr_0'\right.$$

$$\left.\left.+\, j_2(k_\alpha r')\int_{r'}^{\infty}\frac{h_2^{(2)}(k_\alpha r_0')}{r_0'}\, dr_0'\right]\right\} dt_0$$

The spatial integrals involving the spherical Bessel function and Hankel function are standard integrals which may be evaluated from:

$$\int_a^b (r_0)^{-(l+1)}\, j_l(k_\alpha r_0)\, r_0^2 dr_0 = \frac{j_{l-1}(k_\alpha a)}{(k_\alpha a)^{l-1}} - \frac{j_{l-1}(k_\alpha b)}{(k_\alpha b)^{l-1}}$$

$$\int_a^b (r_0)^{-(l+1)}\, h_l(k_\alpha r_0)\, r_0^2 dr_0 = \frac{h_l^{(2)}(k_\alpha a)}{(k_\alpha a)^{l-1}} - \frac{h_l^{(2)}(k_\alpha b)}{(k_\alpha b)^{l-1}}$$

Using these relations and the Wronskian relation for the spherical Hankel and Bessel functions given by (*e.g.*, Abramowitz, 1964):

$$j_l(k\tau)\, h_{l-1}^{(2)}(k\tau) - h_l^{(2)}(k\tau)\, j_{l-1}(k\tau) = -\frac{i}{k^2\tau^2}\,.$$

then we can put the result for $\tilde{\chi}_a^{(1)}$ into the form:

$$\tilde{\chi}_a^{(1)}(r', \omega) = \frac{k_a^2}{v_a} \sum_{m=0}^{2} \int_0^{\tau_0} \frac{j_1(k_a R(t_0))}{k_a R(t_0)} \left[\frac{dR^0(t_0)}{dt_0}\right]$$

$$\cdot \left\{\left[a_{2m}^{(a)} \cos m\varphi' + b_{2m}^{(a)} \sin m\varphi'\right] P_2^m(\cos\vartheta')\, h_2^{(2)}(k_a r')\right\} e^{-i\omega t_0}\, dt_0$$

$$+ \left[\frac{1}{i\omega}\right] \int_0^{\tau_0} \frac{1}{r'^2} \left[\frac{da_{2m}^{(a)}}{dt_0} \cos m\varphi' + \frac{db_{2m}^{(a)}}{dt_0} \sin m\varphi'\right] P_2^m(\cos\vartheta')\, e^{-i\omega t_0}\, dt_0 \qquad (33)$$

where, in the final integral term, we have reintroduced the original multiple coefficients, $a_{2m}^{(a)}(t_0)$ and $b_{2m}^{(a)}(t_0)$, associated with the equilibrium field χ_a^*.

Now we observe that the final integral is not a propagating field but actually corresponds to the Fourier transform of the changing initial value field χ_a^*, times the Fourier transform of a step function which accounts for the factor of $\left[\frac{1}{i\omega}\right]$ multiplying the integral. Thus this term results from the time dependence of the initial value field as the failure zone is created and corresponds to the change in the potential due to the changing reference state. These reference state changes are, by choice, measured relative to the (fixed or static) final equilibrium state in the formulation of the original integral solution given in (22), and so this term accounts for the fact that this final equilibrium is not achieved until dynamic relaxation of the stress has taken place everywhere in the medium. Hence, the term functions to keep track of the instantaneous equilibrium state relative to this final reference state.

The first integral term in the expansion for $\tilde{\chi}_a^{(1)}$ is a propagating wave field, in view of the presence of the spherical Hankel function, and corresponds to the radiation field that would be measured. We are therefore interested in the detailed form of this field from the dynamical standpoint, rather than in the second integral term, and will simply omit the second integral from further consideration.

The form of the dynamical term in $\tilde{\chi}_a^{(1)}$ is that of a quadrupole radiator in a *moving* coordinate frame $(r', \vartheta', \varphi')$. However, the coordinates in the moving frame implicitly depend on the source time t_0, since the moving frame is defined to have its origin at the center of the expanding/translating sphere with radius and position depending on t_0 in some parametric fashion. To bring out this dependence explicitly, and to evaluate the integral over the source time t_0, we need to express the wave field in the *fixed* coordinate system (r, ϑ, φ) indicated in Figure 1. That is, we must transform the expression for the quadrupole radiation field in the moving frame to an equivalent multipole field in a fixed reference frame. To do this we can use the addition theorem for spherical wave functions, as employed by Minster (1973). In particular, for the translation by $d(t_0)$ of the moving frame along the z axis of the fixed reference frame, as shown in Figure 1, Minster shows that the spherical wave function of order $l = 2$ transforms between the moving and fixed frames according to:

$$h_2^{(2)}(k_a r')\, P_2^m(\cos\vartheta') \begin{bmatrix}\cos m\varphi' \\ \sin m\varphi'\end{bmatrix} = (-1)^m \sqrt{\frac{4\pi(2+m)!}{5(2-m)!}} \sum_{l=0}^{\infty} \sum_{\nu=|l-2|}^{l+2}$$

$$c_1(\nu, l\,|\,2, m)\, j_\nu(k_\alpha d(t_0))\,(-1)^m \sqrt{\frac{2l+1)\,(l-m)!}{4\pi(l+m)!}}\, h_l^{(2)}(k_\alpha r)\, P_l^m(\cos\vartheta) \begin{bmatrix}\cos m\varphi \\ \sin m\varphi\end{bmatrix}$$

when $r' > d(t_0)$.

Here the coefficients $c_1(\nu, l\,|\,2, m)$ are related to Clebsch-Gordan coefficients, where in general

$$c_1(\nu, l\,|\,n, m) = (-1)^\nu i^{\nu+l-n}(2\nu+1)(2l+1)^{\frac{1}{2}}(2n+1)^{-\frac{1}{2}} \cdot (l\,\nu m\,0\,|\,n\,m)\,(l\,\nu 0\,0\,|\,n\,0)$$

The symbols $(l\,\nu m\,0\,|\,n\,m)$, etc., on the right are the Clebsch-Gordan coefficients, and since they are tabulated (*e.g.*, see Edmonds (1957) or Abramowitz and Stegun (1965)), their computation presents no problem. The relation, as noted, is valid when $r' > d(t_0)$. When $r' < d(t_0)$, corresponding to the very near field distance range, then another form of this expansion must be used (see Minster, 1973 for details). However, our main interest is in the far, or intermediate, distance range, so that the expansion given here is sufficient.

Substitution of the expansion for the "moving quadrupole field" in terms of a fixed reference frame, wherein a translational aspect of rupture zone growth is included, gives finally:

$$\tilde{\chi}_\alpha^{(1)}(\mathbf{r}, \omega) = \sum_{l=0}^{\infty} \sum_{m=0}^{\min(2,l)} \left[A_{lm}^{(\alpha)}(\omega)\cos m\varphi + B_{lm}^{(\alpha)}(\omega)\sin m\varphi\right] \cdot P_l^m(\cos\vartheta)\, h_l^{(2)}(k_\alpha r) \tag{34a}$$

when $r > d(t_0)$ and $t > \tau_0$. Here

$$\begin{bmatrix}A_{lm}^{(\alpha)}(\omega) \\ B_{lm}^{(\alpha)}(\omega)\end{bmatrix} = \frac{k_\alpha^2}{v_\alpha} \sum_{\nu=|l-2|}^{l+2} (-1)^{\nu+1} i^{\nu+l}\, \frac{(2\nu+1)(2l+1)}{5} \cdot \sqrt{\frac{(l-m)!\,(2+m)!}{(l+m)!\,(2-m)!}}\,(l\,\nu m\,0\,|\,2\,m)$$

$$(l\,\nu 0\,0\,|\,2\,0) \cdot \int_0^{\tau_0} e^{-i\omega t_0} \left[\frac{dR^3(t_0)}{dt_0}\right] \frac{j_1(k_\alpha R(t_0))}{k_\alpha R(t_0)}\, j_\nu(k_\alpha d(t_0))\, dt_0 \begin{bmatrix}a_{2m}^{\prime(\alpha)} \\ b_{2m}^{\prime(\alpha)}\end{bmatrix} \tag{34b}$$

We have, therefore, that the radiation field due to the relaxation effects associated with failure, when expressed in terms of the potentials $\chi_\alpha^{(1)}$ corresponding to the scalar dilatation ($\alpha = 4$) and vector rotation ($\alpha = 1, 2, 3$), is a multipole field whose coefficients $A_{lm}^{(\alpha)}$ and $B_{lm}^{(\alpha)}$ are (independent) functions of frequency, which depend on the growth rate of the failure zone through the functions $R(t_0)$ and $d(t_0)$ for the particular parameterization used here, as well as upon the initial stress state of the medium and its elastic properties. Clearly, the case considered here is special, since it has been assumed from the onset that the prestress was uniform and pure shear and that the failure zone was of a type described by a translating and expanding sphere. However, it is nevertheless true that the radiation field from *any* source can be expressed in the form of (34a), and it is only the multipole coefficients that change form as a function of the detailed nature of the source.

The specific form of the result obtained in (34) will depend on the choice of the functions $R(t_0)$ and $d(t_0)$. Once this choice has been made, the evolution of the failure zone is completely defined and the integral in (34) can be evaluated. This integral is seen to be a Fourier transform, involving products of spherical

Bessel functions. In general it is evaluated numerically by the Fast Fourier Transform (FFT) method. (See Minster, 1973, however, for methods of analytical evaluation.) Limiting analytical forms of the integral, at large or small values of frequency ω for example, can be obtained without much difficulty in specific cases of interest and Minster (1973) provides examples. We shall use these results later, in the section on "Scaling Laws", to provide a description of the seismic radiation in terms of basic event parameters, such as rupture rate, prestress and failure zone dimensions.

The case of rupture zone evolution illustrated in Figure 1 are among those that have been used to model tectonic radiation effects from both earthquakes and underground explosions. As mentioned earlier, of the models illustrated in Figure 1, the tangentially growing spherical failure zone model produces radiation field predictions that are considered to most accurately approximate earthquake radiation fields. In this case the choice for $R(t_0)$ and $d(t_0)$ is constrained by:

$$d(t_0) = R(t_0)$$

and; for uniform growth, consistent with the uniform prestress, then

$$d(t_0) + R(t_0) = 2R(t_0) = U_R t_0$$

is the necessary choice based on our earlier considerations of proportionality of rupture rate to prestress level, while U_R is a constant rupture rate. In this case the multipole coefficients for the potentials in (34) are given by:

$$\begin{bmatrix} A_{lm}^{(a)}(\omega) \\ B_{lm}^{(a)}(\omega) \end{bmatrix} = \frac{3}{\omega} \sum_{\nu=|l-2|}^{|l+2|} (-1)^{\nu+1} i^{\nu+l} \frac{(2\nu+1)(2l+1)}{5}$$

$$\cdot \sqrt{\frac{(l-m)!\,(2+m)!}{(l+m)!\,(2-m)!}} (l\,\nu\,m\,0 \mid 2m)(l\,\nu\,0\,0 \mid 2\,0)$$

$$\cdot \int_0^{\omega R_0/v_a} \exp\left[-2i\left[v_a/U_R\right]x\right] x j_1(x)\, j_\nu(x)\, dx \begin{bmatrix} a_{lm}^{\prime(a)} \\ b_{lm}^{\prime(a)} \end{bmatrix} \qquad (35)$$

where R_0 is the final radius of the spherical failure zone. It is important to notice that the rupture rate appears in the result through the ratio (v_a/U_R) and so the radiation field is only affected through the *ratios* of the intrinsic elastic velocities to the rupture velocity. This also shows that P and S waves will have differently *shaped* radiation spectra, since this ratio and the integral limit have different values for the two wave types.

The integral in (35) can be evaluated as a Fourier transform, or since the Bessel functions are a finite series of sines and cosines multiplied by polynomials in $(1/x)$, the integrand can be expanded to a finite series and evaluated term by term. The results will be discussed in later sections.

The case of a uniformly expanding spherical failure zone illustrated in Figure 1 is also of considerable interest, not only because the result turns out to be simple and easy to understand, but also because it can be used to model tectonic release effects associated with an explosion. In this case, $d(t_0) = 0$, and the results in (34) reduce to (see also Archambeau, 1972):

$$\tilde{\mathbf{s}}_a^{(1)}(\mathbf{r},\omega) = \sum_{m=0}^{\infty} \left[A_{\ell m}^{(a)}(\omega) \cos m\varphi + B_{\ell m}^{(a)} \sin m\varphi \right] P_\ell^m(\cos\vartheta)\, h_\ell^{(2)}(k_a r) \tag{36a}$$

where:

$$\begin{bmatrix} A_{\ell m}^{(a)}(\omega) \\ B_{\ell m}^{(a)}(\omega) \end{bmatrix} = \frac{k_a^2}{v_a} \int_0^{R_0/U_R} e^{-i\omega t_0} \left[\frac{dR^3(t_0)}{dt_0} \right] \frac{j_1(k_a R(t_0))}{k_a R(t_0)}\, dt_0 \begin{bmatrix} a_{\ell m}^{\prime(a)} \\ b_{\ell m}^{\prime(a)} \end{bmatrix} \tag{36b}$$

with R_0 the final failure zone radius, $R(t_0) = U_R t_0$ and $U_R < v_a$.

If the rupture rate is less than the elastic velocities in the material, then these results apply. If the failure process is driven by a shock wave from an explosion however, then the rupture rate can be greater than the intrinsic elastic velocities and then we must use the "instantaneous source" integral representation, equivalent to equation (6) discussed earlier. In this case we get the somewhat different result:

$$\begin{bmatrix} A_{\ell m}^{(a)}(\omega) \\ B_{\ell m}^{(a)}(\omega) \end{bmatrix} = \frac{k_a^2}{v_a} R_0^3 \left[\frac{j_1(k_a R_0)}{k_a R_0} \right] e^{-i\omega R_0/U_R} \begin{bmatrix} a_{\ell m}^{\prime(a)} \\ b_{\ell m}^{\prime(a)} \end{bmatrix} \tag{36c}$$

where the rupture rate $U_R \geq v_a$ is assumed constant and R_0 is the radius of the final failure zone. (This result follows from (36b) if we insert $R(t_0) = R_0 H(t_0 - R_0/U_R)$, with H denoting a step function.) These results can also be expressed in terms of elementary functions if we use the identify:

$$\frac{j_1(x)}{x} = \frac{1}{x^2} \left[\frac{\sin x}{x} - \cos x \right]$$

In any case, the results in (36) show that the seismic radiation to be expected from the production of a spherical failure zone in a uniformly prestressed medium, with the prestress being a pure shear field, is a pure quadrupole field, having a simple double couple force equivalent. The characteristics of the radiated spectrum are also very simple, and in later sections we shall illustrate the important properties of these spectra using these and similar results.

Results and Predictions from Relaxation Theory Modeling

Figure 2 shows results obtained by Minster (1973) for the displacement spectra, for compression (P) and shear waves (SV and SH), from a simple, uniform prestress, relaxation theory model employing a tangentially expanding spherical failure zone. These results correspond to the initial value field, and do not include the effects of scattering from the failure surface.

The important first order characteristics of the spectra illustrated here are however: (1), *the large difference in P and S wave spectral levels, with the S wave production nearly a order of magnitude larger at all frequencies.* (2), *the difference in "corner frequencies" (that is, the frequency at which the spectral roll-off at high frequencies clearly begins) between the P and S wave spectra, with the S wave spectra having a significantly lower corner frequency.* (The spectral holes, evident in the spectra at one of the azimuths, are primarily due to neglect of the boundary scattering terms in the solution and are essentially removed when scattering is taken into account in the solution.) (3), *the far field spectra, for all wave types, tends to flatten at frequencies lower than the corner frequency for each wave type (P or S), this occurring when the prestress*

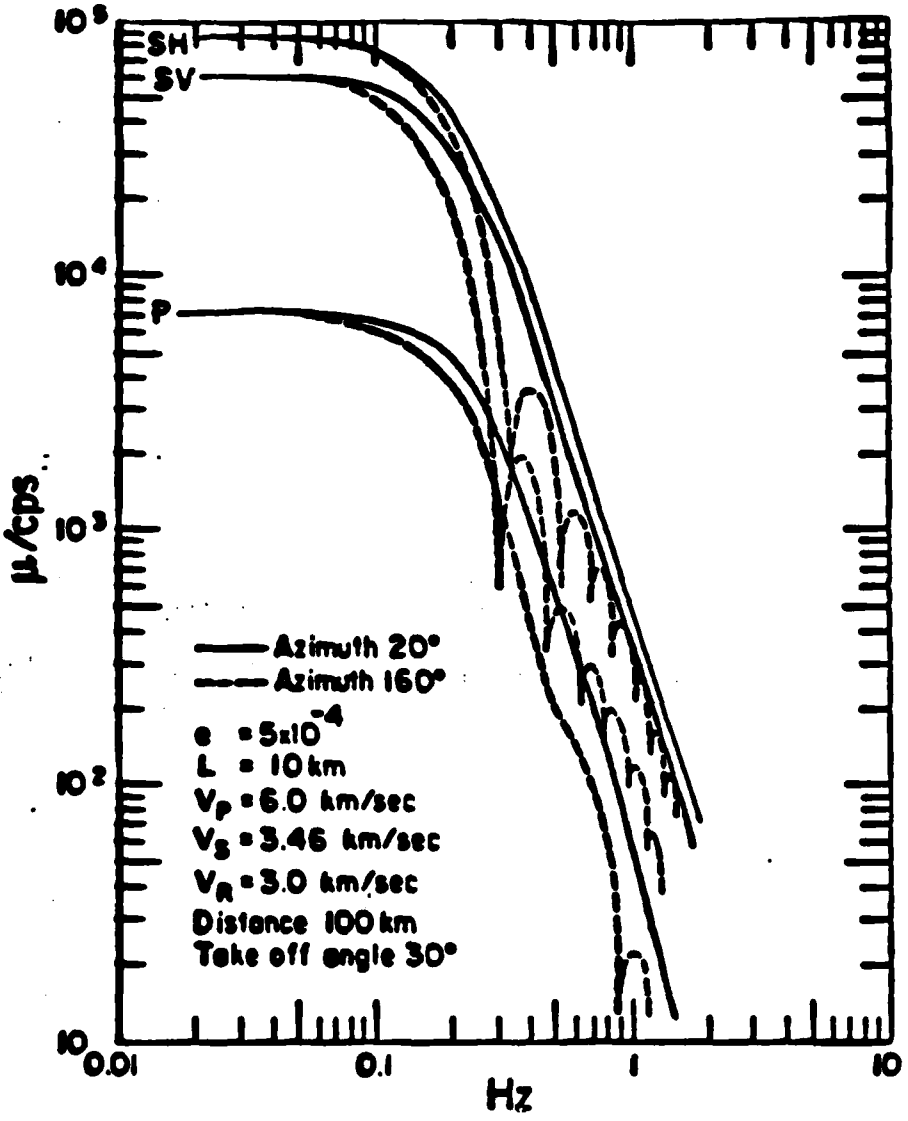

Figure 2. Theoretical displacement spectra from a relaxation source model of a 10 km length earthquake in a homogeneously prestressed medium. The initial strain field, $e = 5 \times 10^{-4}$, corresponds to a prestress of approximately 100 bars (10^8 dynes/cm^2). The rupture rate is taken to be constant and equal to .87 times the shear velocity. Spectra are shown for two azimuths from the source. From Minster (1973).

is uniform (or nearly uniform) to large distances from the failure zone. These three properties of the radiation spectra are important distinctive characteristics of tectonic relaxation sources and are among those most clearly observed for earthquakes.

Figure 3 illustrates the effects of rupture rate on the shape of the compressional (P) and shear (SH) wave spectra from a model similar to that of Figure 1. Here, in addition to the previous three observations concerning the wave spectra, it is clear that the corner frequencies and high frequency spectral slopes, for both P and S waves, are strongly affected by changes in the value of the rupture rate, denoted as V_R in the figure. In particular, this figure illustrates two additional important features, namely: (4) *The corner frequencies for both P and S waves are directly proportional to the rupture rate.* Further, (5): *The high frequency spectrum of the P wave varies asymptotically as ω^{-3} for high rupture velocities near the shear velocity of the medium, while the S wave spectrum falls off as ω^{-2} at high frequencies for such high rupture rates. For lower rupture velocities, both the P and S wave spectra show quite wide frequency bands, immediately above their corner frequencies, where the spectra vary as ω^{-1} to ω^{-2} before assuming steeper slopes at yet higher frequencies.*

Comparisons between spectra with different failure zone dimensions, such as those of Figures (2) and (3), shows that: (6) *The spectral levels all scale as the cube of the failure zone length when the failure zone surface area increases as the square of the length (which is usually the case for small events). The spectral levels increase as the square of the failure zone length when the length is allowed to increase without changes in the other failure zone dimensions (which is most likely for very large earthquakes).* In addition: (7) *The corner frequencies of the P and S wave spectra vary inversely with the (final) length of the failure zone.*

Figure 4 shows compressional and shear wave radiation patterns displayed at three different frequencies. The important radiation field properties illustrated here, which can be added to those previously described, are: (8) *The radiation patterns at low frequencies, that is, below the corner frequencies for each wave type, are dominated by a quadrupole term (having a double couple force equivalent), while at frequencies above the corner frequency, for each wave type, the patterns are strongly distorted by higher order multipole contributions which are associated with rupture propagation. The distortion of the patterns is such that the patterns rotate toward the direction of rupture propagation at frequencies above the "corner frequency" and more of the high frequency energy is radiated inside a cone along the rupture plane in the direction of rupture propagation.*

The properties described constitute the most basic and robust features of the seismic radiation predicted for earthquakes, and they have a reasonably good correlation with observations. In cases where we can't be absolutely confident that the earthquake data is consistent with a predicted feature, it is because other effects, such as anelastic attenuation, scattering, or ordinary wave propagation effects in an uncertain structure, preclude definitive verification due to ambiguity of interpretation, or simply because the observed data is too limited or is too contaminated by noise.

In addition to the characteristics so far described, there are effects that will arise from strong departures from uniform prestress conditions. This will show up, as was already indicated, in variations in the rupture velocity and stress drop during the growth of the failure zone. If these variations are strong enough, then we can simply view the event as a superposition of several nearly constant stress drop events each with a rupture rate scaled appropriately, as

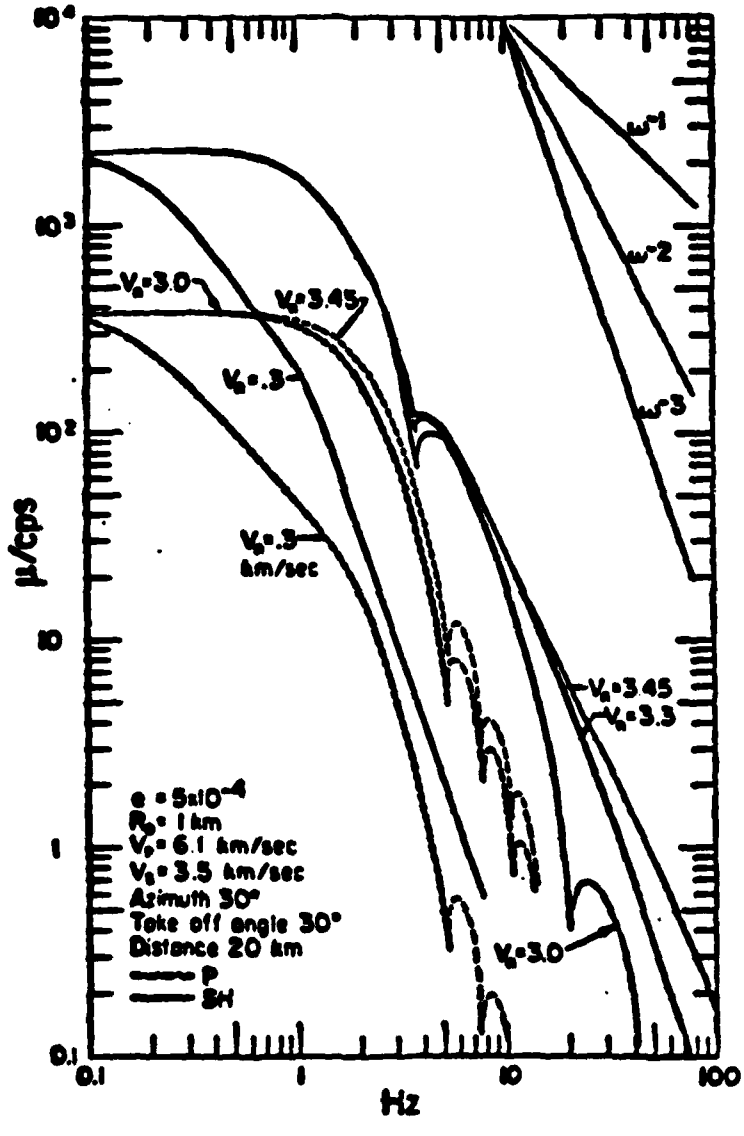

Figure 3. Theoretical displacement spectra from a relaxation source model of a 1 km length earthquake showing effects of variations in the rupture rate on the spectral shapes for P and S waves. From Minster (1973).

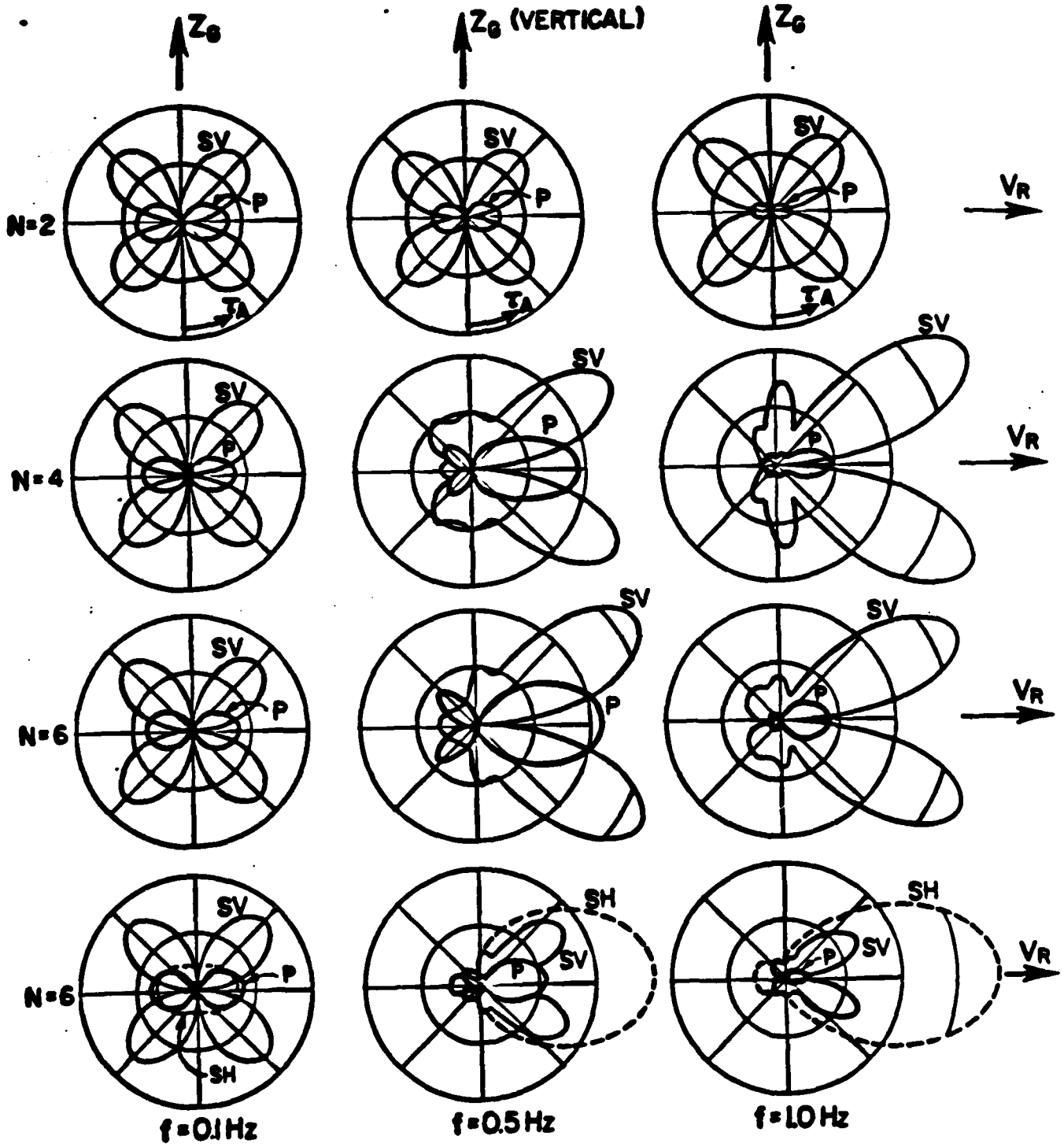

Figure 4. Compressional (P) and shear wave (SV and SH) radiation patterns from a relaxation theory model of an earthquake showing the quadrupole (N = 2) patterns and the sums of quadrupole plus higher order multipole terms (up to N = 4 and N = 6) at three different frequencies. The patterns are vertical sections, with τ_A denoting the "take-off" angle from the source hypocenter and with the rupture velocity vector indicated by V_R. The source model has a "corner frequency" between f = 0.1 and f = .5 Hz. The patterns show the effects of rupture propagation at frequencies above the corner frequency, due to contributions from the higher order multipoles.

indicated by equation (16) for example. Then we would have spectral characteristics, for each one of these "events", which behave as previously described, with the complete seismic field from the variable stress drop event being a linear superposition of all the "component event" spectra, with appropriate time or phase delays added of course.

In this regard, Figure 5 shows a model of the San Fernando earthquake, by Bache and Barker (1977), which employs a multiple-event superposition of relaxation theory sources. In this case two source models with variable stress drop and rupture rate were employed. The near field model predictions for the ground motion at the nearby Pacoima Dam site are shown to be in good first order agreement with the observations at this location. However, in view of the departure of the predictions from the observations after about 6 seconds from the start, it seems evident that a third shallow "event", intersecting the free surface, could be added to the model to give a more complete fit to the entire observed time series. Nevertheless, the first six seconds of the observed ground motion is predicted reasonably well by the model.

We observe that the detailed nature of the departure of the predicted and observed ground velocities shows that the true velocity is more complex than that predicted, with relatively small high frequency variations in the recorded ground velocity that are only fit by the model in an average sense. This indicates that the event actually has fine scale variations in stress drop and rupture rate that involve spatial fluctuations in these variables on a scale length of hundreds or tens of meters, as well as on the scale length of kilometers, as represented in the model.

In spite of the lack of fine scale detail, this simple "double event" model quite accurately predicts the observed teleseismic radiation from this earthquake. Figure 6 shows observed far field seismograms at 10 locations, with the theoretically predicted results superimposed, as the darker lines, on the observations. Comparison of the upper figure results, for the "event 1" of Figure 5 alone, with those in the lower figure where both "events" are included, shows the improvement in the fit to the data when the two event model is used. It is also quite clear that a third "event" at shallow depth is needed to obtain a good fit to the data beyond 10 to 15 seconds after the first energy arrival. In any case the data is considered to be well fit by the average "double event" model for the first 10 to 15 seconds, particularly when we take account of the lack of very detailed information regarding the crustal structure at the various receiver sites, so that some deviations are due to local site structure inaccuracies rather than source model inaccuracies. The lower frequency content and narrower band width of this data, compared to the near field data shown in Figure 5, allows this model, which clearly does not account for fine scale variations in stress drop and rupture rate, to provide a good fit to the far field data.

A somewhat more elaborate model made up of, say, three such "events" and with some of the more major fine scale stress drop-rupture rate fluctuations included could undoubtedly be found that would give a more detailed fit to the entire wave field from the earthquake. However, for the purpose of this discussion, it is sufficient to be able to point out that models based on relaxation source theory give rather detailed fits to observed data when plausible earthquake stress drop and rupture rate variables are used, and secondly that comparisons with well recorded near and far field data show conclusively that both large scale and fine scale spatial variations in the basic event parameters (including the failure zone geometry) occur and are highly significant, particularly for the high frequency radiation fields from these events. The example shown here also demonstrates that approximations using a superposition of

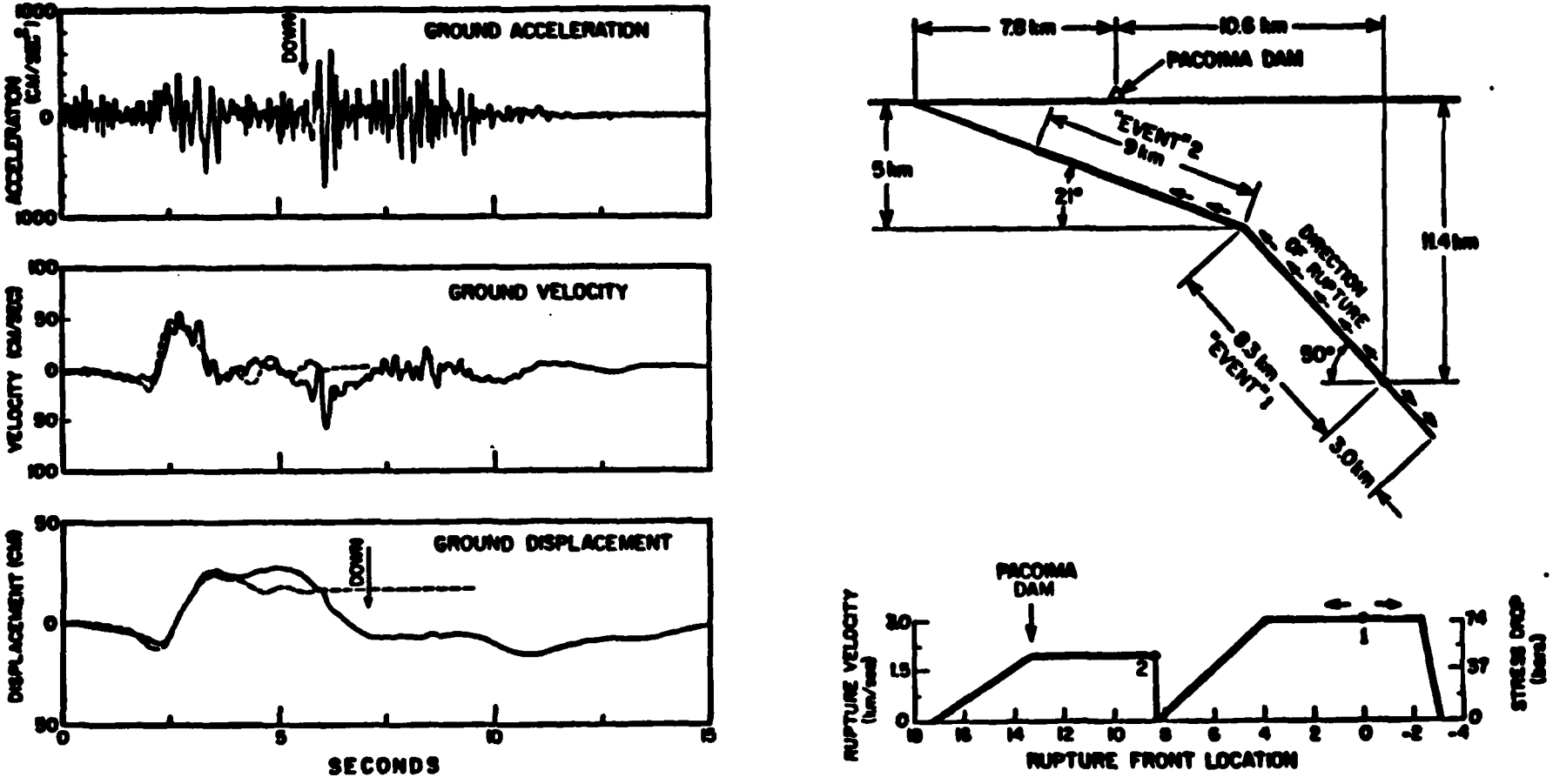

Figure 5. Near field acceleration from the San Fernando earthquake recorded at the Pacoima Dam site, along with the corresponding velocity and displacement obtained by integration. The dotted lines are the near field predictions obtained from the "double event" relaxation theory source model indicated by the schematics on the right. The rupture rate and stress drop at the failure surface were variable, with these two source variables constrained to be proportional to each other. (From Bache and Barker, 1977)

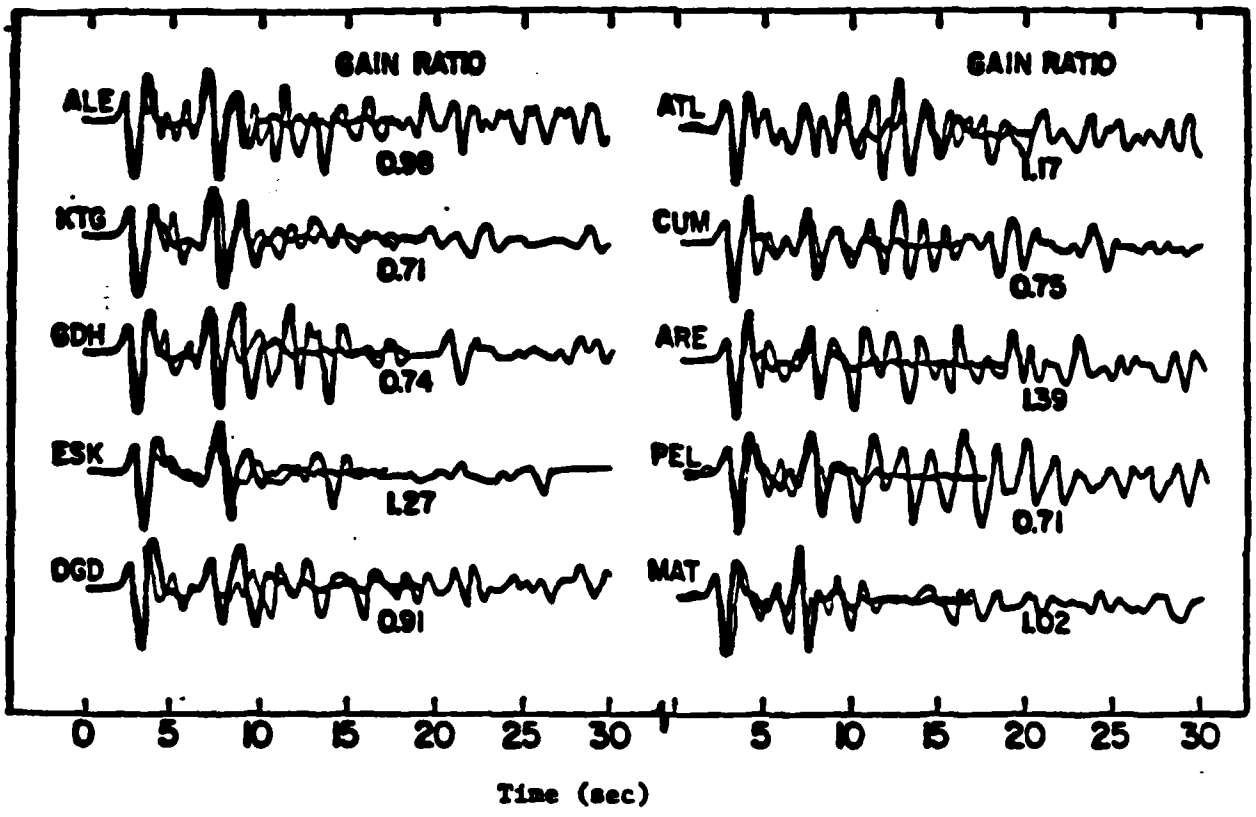

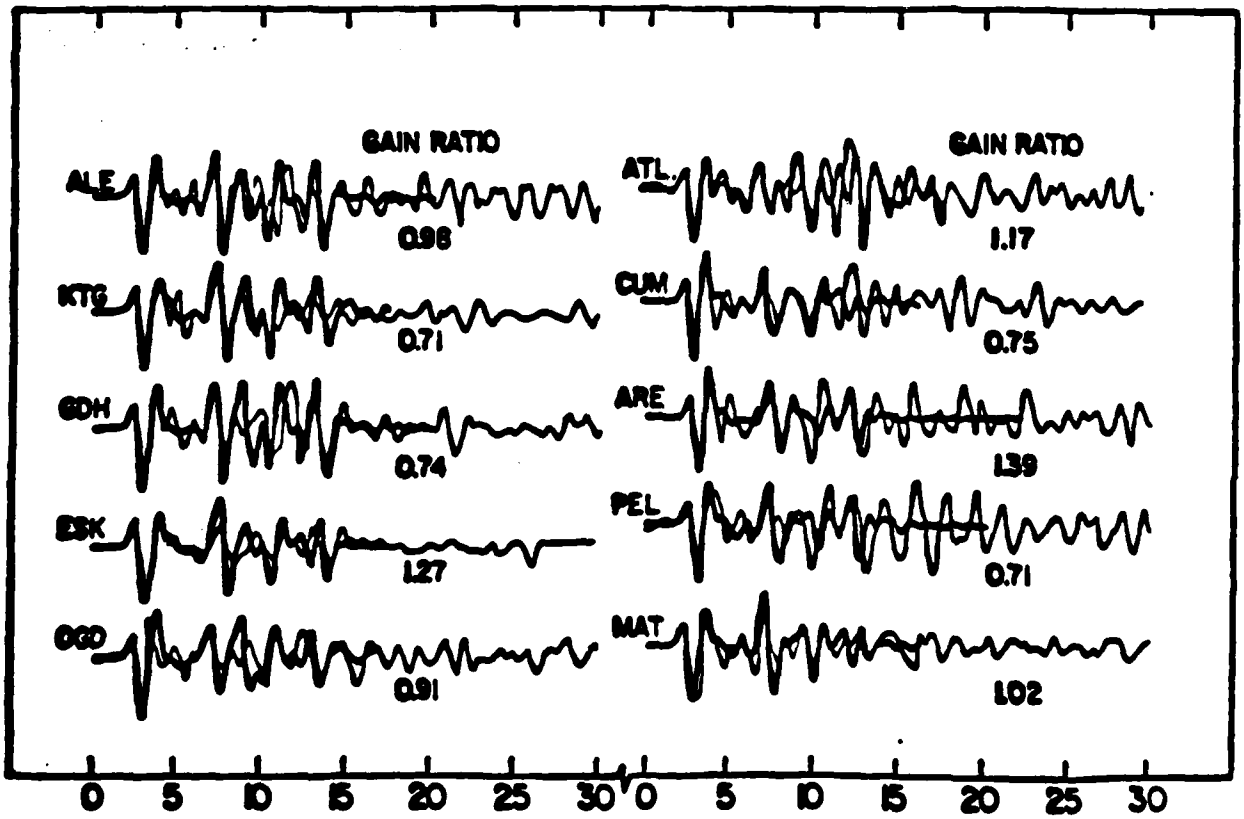

Figure 6. Teleseismic signals from the San Fernando Earthquake (light lines) compared to theoretically predicted signals from (1) the single relaxation source ("Event 1"), near the hypocenter (upper figure) and (2) the multiple (double) relaxation source model of Figure 5. All predicted and observed time series are scaled to unit amplitude for the first cycle of the direct P wave, with the "gain ratio" being the true first cycle amplitude ratio of synthetic to observed. (from Bache and Barker, 1977)

relaxation source models (each with an approximate solution of the formal source representation theory for a simplified geometric failure zone) can be used to make good "first order" predictions. (For details of the source theory approximation, as well as the wave propagation methods used, see Bache and Barker, 1977.)

It is, however, also possible to compute relaxation source theory models with spatially heterogeneous initial stress fields specified. Results from one such computation, by Stevens (1981), are shown in Figure 7. In this case the rupture zone is simply specified to be spherical and to be formed "instantaneously", so that the model actually conforms to an explosion produced failure zone in a heterogeneously prestressed medium. Nevertheless, the features of the predicted seismic radiation from this model, that are solely due to the departure of the prestress from homogeneity, are easily discerned. In particular: (9) *Both the P and S wave spectra have a quadrupole spectral component that is the same as that for a source of the same geometry but with uniform prestress equal to the spatial average of the non-uniform prestress field. Specifically, this quadrupole field component has a flat spectral level at frequencies below the corner frequency and has corner frequencies and high frequency spectral slopes that scale in the same manner as was described for the uniform prestress case. In addition however, the source has higher order multipole components that are entirely due to the heterogeneity of the initial stress field and produce interference effects which are superposed on the quadrupole field in such a way as to produce peaked spectra, which are particularly apparent near nulls in the quadrupole radiation pattern. The relative strength of the higher order multipoles is directly proportional to the deviation of the heterogeneous stress level from the mean stress and the contributions to the radiation field are most significant at and above the quadrupole spectrum corner frequency for a given P or S wave type. The larger the spatial extent of the deviation in the initial stress from the mean, the lower will be the frequency at which there will be a significant non-quadrupole contribution to the radiation field.*

Figure 8 illustrates how a strong prestress heterogeneity can produce an "apparent corner frequency" in the observed spectra from a tectonic source which is more representative of the characteristic dimension of the zone of high stress than it is of the maximum dimension of the failure zone. This example is again from Stevens (1981), and illustrates the radiation induced by the creation of a spherical failure zone (*e.g.*, as might be produced by an explosive shock wave) in a strongly inhomogeneously stressed medium. In this case the prestress is created by insertion of a fixed ("locked") dislocation in the material at a variety of distances from the spherical failure zone, with the dislocation therefore producing the initial stress field and the relaxation of this stress, due to creation of the spherical shatter zone with vanishing rigidity, producing the elastic radiation. As is shown, when the dislocation is at a distance of ten times the shatter zone radius (R_0) from the center of this failure zone, then the prestress in the vicinity of the failure region is fairly uniform and a "normal", predominantly quadrupole spectrum is produced with a corner frequency approximately equal to the rupture rate (here taken as the P wave velocity in the material) divided by the radius of the failure zone. However, when the dislocation is located at a distance of 1.1 R_0, and so very near the failure zone boundary, then the quadrupole spectrum is strongly perturbed by the addition of higher order multipole terms arising from the strong spatial variability of the initial prestress. These higher order multipole terms are seen, at least in this case, to produce high frequency contributions, at and above the quadrupole corner frequency, which result in a much higher apparent corner freuency.

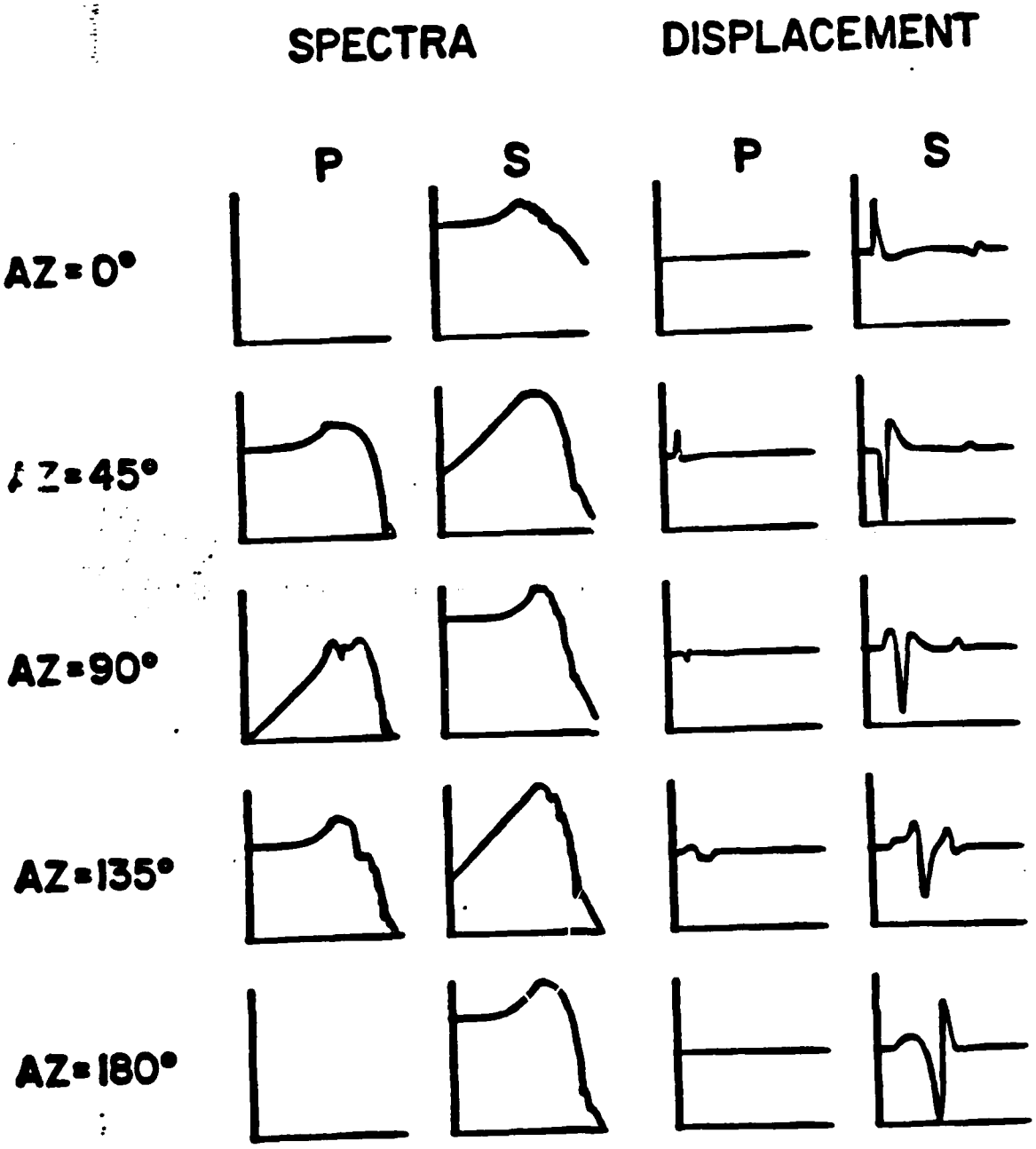

Figure 7. Exact solution spectra and wave forms at various azimuths from a spherical relaxation source in a heterogeneously prestressed medium. From Stevens (1981). The heterogeneous initial stress field was created by a static point dislocation in the medium at a distance of one and a half times the spherical failure zone radius. The spectra are plotted as log amplitude versus log frequency.

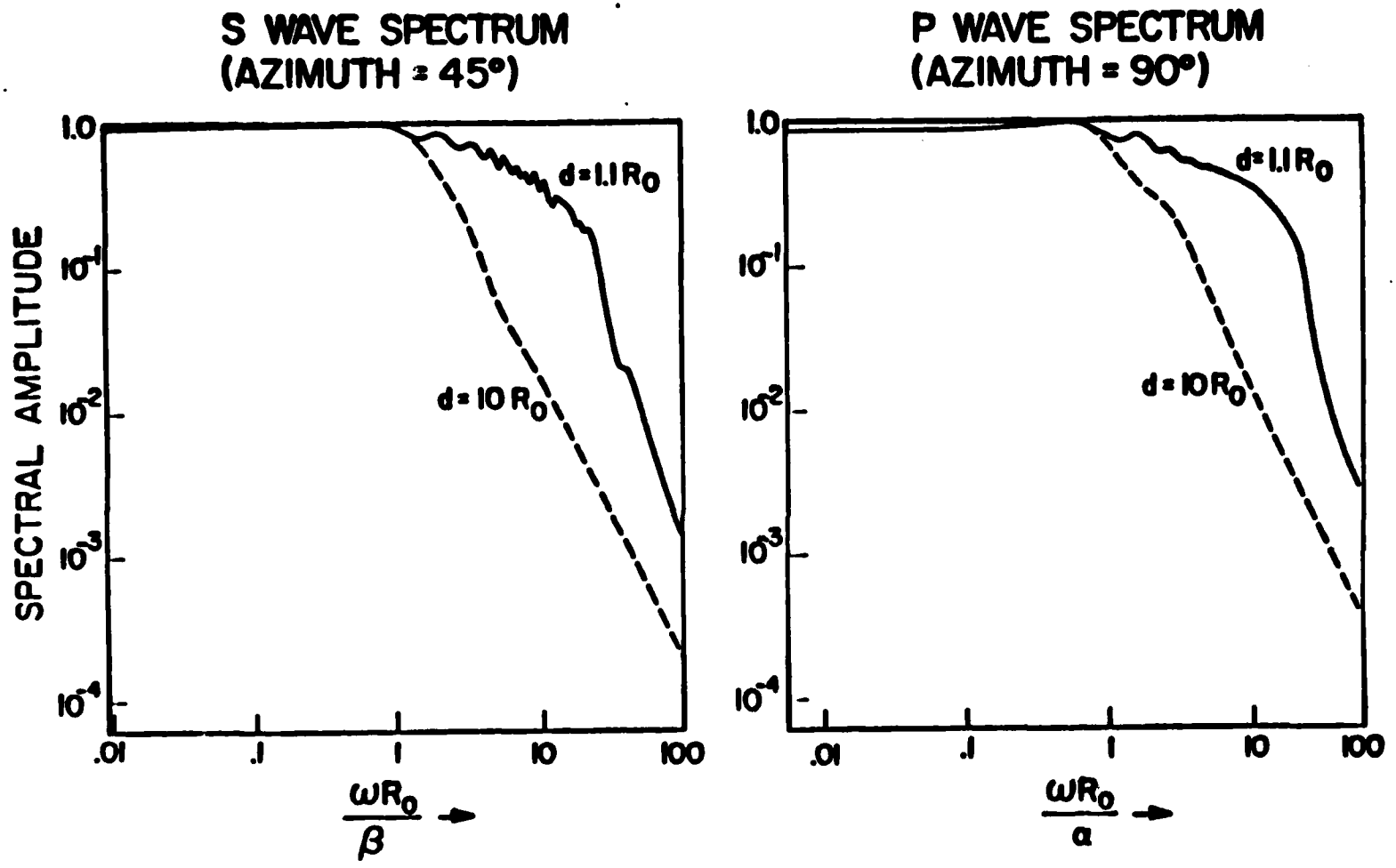

Figure 8. Spectral amplitude of the direct P and S waves, at a maxima in the radiation patterns of each, versus normalized frequency, for an "instantaneous" spherical failure in a heterogeneously prestressed infinite medium. The medium P and S velocities are denoted by α and β, and the spherical failure zone has radius R_0. The symbol "d" denotes the distance from the center of the spherical failure zone to a static point dislocation, which is the origin of the heterogeneous prestress field. Note that high frequency portion of the spectra changes drastically as the dislocation is moved close to the spherical failure zone.

This "apparent" corner frequency implies a characteristic dimension, when interpreted in terms of a length divided by rupture rate, which is of the order of the radius of the high stress zone surrounding the static dislocation rather than the (much larger) radius of the failure zone itself. Furthermore, when both the spectral amplitude and phase are used to obtain the time domain seismograms corresponding to this situation, it is found that a large high frequency pulse appears with a time of arrival, determined by the phase spectrum and associated groups delay, that corresponds to a source of energy in the vicinity of the dislocation. Therefore, even though the dislocation displacement discontinuity is fixed for all time, the energy is clearly found to arrive from the dislocation. This, on reflection, would be expected from a volume relaxation source where the energy is released from the medium itself, and would be most evident when strong heterogeneities in the prestress exist.

From the standpoint of predicted characteristics of the radiation from earthquakes, it is therefore important to keep in mind that: (10) *Both the P and S waves can have spectral properties that reflect the characteristics of strong, nearby, stress concentrations, in particular very high stress levels can produce large energy arrivals within the P and S wave trains which produce apparent corner frequencies of the composite spectra of the train that are more characteristic of the dimension of the stress concentration than of the failure zone dimension. However, the energy arrival(s) producing this "perturbation" in the P or S wave amplitude spectra have travel times appropriate to energy released from the location of the stress concentration, which may not be the same as the location of the point of initiation of failure (the hypocenter), and so such energy may frequently arrive in the P or S wave coda after the first arriving energy, although it could, in fact, constitute the first arriving pulse if the hypocentral zone was initially an intensely stressed zone.*

Scaling Laws for Earthquakes Based on Theoretical Results

The predicted properties of the seismic radiation from these dynamical models can also be obtained analytically if we consider the asymptotic behavior of relaxation source model radiation, such as described by equations (34) through (37). This approach provides quantitative relations which, while approximate, are valid to first order and can be used as scaling laws for the radiated spectrum for earthquakes. That is, we can scale the spectra for one particular tectonic source into the spectra for a different source with a different stress drop, rupture length and rupture velocity using these relations.

Since the theory predicts results that are different for the compressional and shear waves radiated by tectonic sources, we will treat the spectra for these wave types separately. Most of the following results are from Archambeau (1968, 1972) and Minster (1978), and details omitted here can be found in these references, particularly in Minster (1978).

In order to simplify the results, without losing any essential generality, we consider the case in which the prestress field is homogeneous and pure shear, with only the initial stress component $\sigma_{13}^{(0)}$ nonzero. Then, using the expression (34) for the radiation in the limit of low frequencies and in the far field (so $k_p r \gg 1$), we have for the *compressional (P) wave field* (Minster, 1978):

$$\lim_{\omega \ll 1} \tilde{u}_r^{(P)}(r, \omega) \sim \frac{5(1-2\sigma)}{16\mu(7-5\sigma)} \sigma_{13}^{(0)} \left[\frac{L^3}{v_p r}\right] e^{i\omega_p r} \sin 2\vartheta \cos\phi \qquad (37)$$

where the asymptotic result has been expressed in terms of the radial component of the displacement spectrum $\tilde{u}_r^{(P)}$. Here σ is the Poisson's ratio for the

material in the region surrounding the failure zone, μ is the elastic rigidity in this zone, $\sigma_{ij}^{(0)}$ the prestress, v_p the compression wave velocity at the source, $k_p = \omega / v_p$ is the wave number and L is the maximum dimension (or "length") of the failure zone. This limiting form of the low frequency far field radiation shows that the field has a simple quadrupole form which is directly proportional to the prestress and the cube of the rupture length.

Using this low frequency result along with asymptotic results valid at high frequencies, we can define a "P wave corner frequency" $f_c^{(P)}$ (or $\omega_c^{(P)} = 2\pi f_c^{(P)}$) as the point where the two asymptotic spectral results are equal. In addition, we can specify the high frequency behavior of the spectrum from the high frequency asymptotic results. Since the high frequency asymptotic relations are rather complex we simply summarize their consequences when used, along with (37), to define a "corner frequency" and the high frequency behavior of the P-wave spectrum, at frequencies above $f_c^{(P)}$. We have:

$$\omega_c^{(P)} = \frac{2 U_R}{L} \left[\frac{3 v_p^2}{U_R^2} \right]^{1/3} \tag{38}$$

for the angular "corner frequency" relation, and

$$\left.\begin{aligned} \lim_{\omega \gg 1} |\dot{\bar{U}}_i^{(P)}| &\sim O\left[\frac{1}{\omega^3}\right] : \text{when} \quad U_R < v_p \\ \lim_{\omega \gg 1} |\dot{\bar{U}}_i^{(P)}| &\sim O\left[\frac{1}{\omega^2}\right] : \text{when} \quad U_R \geq v_p \end{aligned}\right\} \tag{39}$$

for the very high frequency asymptotic behavior of the far field P wave spectrum as a function of frequency. Here U_R is the rupture rate and the notation $O\left[\frac{1}{\omega^2}\right]$, for example, is to be read as "the order of $1/\omega^2$". The behavior at lower frequencies, but such that $\omega \gtrsim \omega_c^{(P)}$, where the frequency is near but somewhat larger than the corner frequency, is such that:

$$\lim_{\omega > \omega_c^{(P)}} |\dot{\bar{U}}_i^{(P)}| \sim O\left[\frac{1}{\omega^2}\right], \quad \text{for } U_R < v_p \text{ and } U_R \geq v_p \tag{40}$$

Thus, the P wave spectrum decreases with a slope near ω^{-2} at frequencies above $\omega_c^{(P)}$ and, when the rupture rate U_R is less than the compressional velocity, then this slope increases to ω^{-3} at yet higher frequencies. As the rupture rate approaches the compressional velocity in value, the frequency at which the spectrum assumes a ω^{-3} behavior moves to higher frequencies, such that when the rupture velocity actually reaches or surpasses the compressional velocity (*e.g.*, as for failure caused by a shock wave), then the frequency at which ω^{-3} behavior occurs is infinite. Further, the spectral decay beyond the corner frequency $\omega_c^{(P)}$ is strongly influenced by the ratio of U_R to v_p, and is essentially independent of the rupture dimensions. When the rupture rate is much less than the shear velocity, and therefore very much less than the compressional velocity, then the spectral decay ranges from ω^{-1} to ω^{-3} over a broad frequency band and the corner frequency predicted by equation (38) is not very accurate. This behavior is illustrated in Figure 3, and was also noted earlier.

These results are appropriate for a uniform prestress field and, as was illustrated and discussed earlier, prestress inhomogeneities, particularly strong

stress concentrations, can affect the spectrum near and above the corner frequency so as to cause peaking and corner frequency shifts. These effects will nearly always arise from later arriving energy within the P wave train, and so the first arriving P wave pulse will typically have a simpler spectrum, with characteristics most closely matched by the results predicted in (37)-(39). It is only when the spectrum of the entire P wave train is considered that complicated interference of arrivals in the train produces strong perturbations in the total P-wave spectra.

Using these results we can construct approximate scaling laws for the P wave spectra between different sources having different fault length, stress drop and rupture rate parameters. These relations are accurate and useful when the rupture rate is less than, but fairly near, the shear velocity in the medium, which appears to be the usual case for failure in the earth, as was noted earlier. The relation (37) also holds for the "supersonic" failure rate, when $U_R \simeq v_P$. However, the corner frequency estimate is less accurate for a very low rupture rate process, and the usefulness of the relation in (38) for the corner frequency is minimal in this case. Nevertheless, with these provisions, the results given in (37) through (39) provide the following scaling relations for the P wave spectra from relaxation models of earthquakes:

(1) The spectral level of the *far field P wave at low frequencies, below the corner frequency*, is *independent of frequency and rupture rate* and this *flat level* scales with fault dimension according to:

$$\frac{A^{(P)}(\omega)}{A_0^{(P)}(\omega)} = \left[\frac{L}{L_0}\right]^3 : \omega < \omega_c^{(P)} \tag{41}$$

where $A_0^{(P)}(\omega)$ denotes the low frequency spectral amplitude level of a reference event, while $A^{(P)}(\omega)$ is the flat spectral level of an event with a different failure zone dimension, but with *all other source parameters the same as the reference event*. This result is most accurately obeyed when the failure zone has a second dimension, W, comparable in size to L, that is of the same order of magnitude. Further, it is assumed that W changes proportionally with L. If this is not the case, then a somewhat more accurate scaling relation is:

$$\frac{A^{(P)}(\omega)}{A_0^{(P)}(\omega)} = \left[\frac{WL^2}{W_0 L_0^2}\right]$$

In the case of a spherical failure zone, of radius R, then

$$\frac{A^{(P)}(\omega)}{A_0^{(P)}(\omega)} = \left[\frac{R}{R_0}\right]^3$$

(2) The spectral level of the *entire P wave spectrum scales directly with the prestress*, and so:

$$\frac{|\tilde{u}^{(P)}(\omega)|}{|\tilde{u}_0^{(P)}(\omega)|} = \frac{|\sigma^{(0)}|}{|\sigma_0^{(0)}|} \tag{42}$$

where $|\tilde{u}_0^{(P)}|$ denotes the entire P wave amplitude spectrum for a reference event while, $|\tilde{u}^{(P)}|$ is the spectrum for an event having a *different homogeneous (shear) prestress magnitude*, but with *all other source parameters*

the same as those for the reference event. (Here it is assumed that the shear stress drop at the failure boundary is total so that the scaling relation is given in terms of the initial prestress. If the stress drop at the boundary of the failure zone is partial, then the stress quantities in (42) denote shear stress changes across the failure zone boundary.)

(3) The corner frequency, $f_c^{(P)}$, for the compressional wave spectrum from the source *scales directly as the ratio of rupture velocity to failure zone length,* and in particular for rupture rates near shear velocity in the medium (the most common situation) then:

$$f_c^{(P)} = \frac{1}{\pi}\left[\frac{U_R}{L}\right]\left[\frac{3v_P^2}{U_R^2}\right]^{1/2} \cong .662\left[\frac{U_R}{L}\right];\ U_R \lesssim v_S \text{ and } \sigma = \frac{1}{4}$$

Further, event spectrum scaling relative to a reference source, with "corner frequency" denoted by ${}^{(0)}f_c^{(P)}$, is given by

$$\frac{f_c^{(P)}}{{}^{(0)}f_c^{(P)}} = \left[\frac{U_R}{U_R^{(0)}}\right]\left[\frac{L_0}{L}\right] \tag{43}$$

We note that once the scaling laws in (41)-(43) have been appropriately applied to the spectrum of a reference event, then the proper flat spectral level at low frequencies will have been established for the new event, along with its appropriate corner frequency. Then, for P-wave spectra, there will be a rather short frequency band above $f_c^{(P)}$ where the spectrum decays, roughly as ω^{-2}, before achieving the predicted ω^{-3} decay at higher frequencies. However, since the rupture velocities of natural events is such that $U_R \leq v_S < v_P$, so that U_R is significantly less than v_P, then the spectrum achieves a ω^{-3} slope quite rapidly with increasing frequency. (This behavior is illustrated in Figure 3 by the P-wave spectra with rupture velocity U_R = 3.45 km/sec and U_R = 3.0 km/sec.) Thus, assumption of a ratio of the rupture rate to compressional wave velocity establishes the spectral decay for frequencies above the corner frequency and since this ratio is always significantly less than unity for natural earthquake (or spontaneous) failure, then the first equation in (39) applies and the ω^{-3} spectral decay holds over nearly all of the frequency band where $f > f_c^{(P)}$. In this way then, the first order spectrum of the compressional wave field can be established with reasonable accuracy over the entire frequency range.

As noted earlier however, when the rupture rate is controlled by a high speed shock wave, such as is produced by an explosion, then the rupture rate is close to the compressional wave velocity and a ω^{-2} spectral decay rate beyond the corner frequency will occur.

Therefore, the scaling laws, plus knowledge or assumption of the rupture rate, can be used to provide an estimate of the entire P-wave spectrum generated by the relaxation of tectonic stress in the medium surrounding a natural or explosion induced failure zone. Of course, in view of the previously discussed predictions and observations concerning prestress concentration effects, the spectrum produced by scaling will not include the perturbative effects of inhomogeneous prestress. However, the scaled spectrum should be a good average (or smoothed) representation in general, and only in (rare) cases of quite strong prestress concentrations will significant deviations occur. Further, even when strong prestress concentrations do occur, they will most often be manifested in the later arriving energy within the P wave train and will not significantly affect the first arriving energy. Thus, for predictions of the first arrival

energy, the scaled spectra should usually be quite accurate.

The structure and form of the S wave spectrum produced by a tectonic source has some important differences from the P-wave spectrum. In particular, the expression comparable to the far field P wave spectrum at low frequencies, given by equation (37), is:

$$\lim_{\omega \ll 1} \mathcal{U}_{\theta,\varphi}^{(S)}(r,\omega) \sim \frac{5(1-\sigma)}{16\mu(7-5\sigma)} \left[\frac{L^3}{v_S r}\right] e^{i\omega_0 r} \cos 2\theta \sin\phi \tag{44}$$

Here $\mathcal{U}_{\theta,\varphi}^{(S)}$ represents either the θ or φ displacement component and v_S is the shear velocity. This field has a quadrupole form and also has a flat spectral amplitude, as did the P wave. However, the ratio of the *low frequency amplitude* of the S wave, $A^S(\omega)$, to the same amplitude function for the P wave is easily seen, from (37) and (44), to be given by:

$$\frac{A^{(S)}(\omega)}{A^{(P)}(\omega)} = \frac{v_P}{v_S}\left[\frac{1-\sigma}{1-2\sigma}\right] = \left[\frac{v_P}{v_S}\right]^3 \tag{45}$$

Therefore, a particular tectonic source will have a low frequency S wave amplitude spectrum that is larger than the P wave spectrum by a factor equal to the cube of the ratio of the P to S wave velocities in the medium. For a typical solid this factor is about $3\sqrt{3}$ and so represents a very significant difference. (A difference in P and S spectra of about this order of magnitude is clearly observed for earthquakes, so that this prediction is well supported by direct observations.)

In addition, the predicted S-wave spectra can be shown to have a corner frequency given (approximately) by:

$$\omega_c^{(S)} = \frac{2U_R}{L}\left[\frac{3v_S^2}{U_R^2}\right]^{1/3} \tag{46}$$

Thus the corner frequency for the S-wave spectra is different than that for P waves, and is lower because of the dependence on the ratio of v_S to U_R, as compared to the P wave corner frequency, which has the same form but depends on the (larger) ratio of v_P to U_R. In the usual case, when the rupture rate is near the shear velocity value in the material, then

$$f_c^{(S)} \simeq \frac{3\sqrt{3}}{\pi}\left[\frac{U_R}{L}\right] = .459\left[\frac{U_R}{L}\right];\ U_R \lesssim v_S$$

this value is about 30% lower than the P wave corner frequency for the same event.

The high frequency asymptotic behavior of the S wave spectra is given by:

$$\begin{aligned} \lim_{\omega \gg 1} |\mathcal{U}_{\theta,\varphi}^{(S)}| &\sim O\left[\frac{1}{\omega^3}\right];\ when\ U_R < v_S \\ \lim_{\omega \gg 1} |\mathcal{U}_{\theta,\varphi}^{(S)}| &\sim O\left[\frac{1}{\omega^2}\right];\ when\ U_R \gtrsim v_S \end{aligned} \tag{47}$$

Because of the fact that the asymptotic behavior is different for the different ranges of rupture velocity, and since the rupture rate is usually of the order of

the shear wave velocity (i.e., U_R is only slightly less or equal to the shear velocity), then the S wave spectra will have a very broad frequency range within which the spectral decay varies approximately as ω^{-2}. This is in contrast to the P wave spectra, for which the spectral band within which the ω^{-2} decay applies is just above ω_c^P and is quite narrow, while over most of the range, where $\omega > \omega_c^{(P)}$, the decay is ω^{-3}. Thus, when the rupture rate is close to the shear velocity in the medium, then the S wave decay is ω^{-2} out to quite high frequencies, relative to $\omega_c^{(S)}$, before it assumes a ω^{-3} decay. When the rupture rate is larger than the S wave velocity, then the S wave spectral decay is ω^{-2} for all frequencies above $\omega_c^{(S)}$. Observationally, the S wave spectrum should appear to have a ω^{-2} decay, while the P wave spectrum will decay as ω^{-3} in essentially all cases except for very slow rupture rates, or for rupture rates near or at the compressional velocity. The latter situation probably only applying for explosive shock induced failure.

Based on the results in (44)-(47) the following scaling laws generally apply for S wave spectra:

(1) The spectral level of the *far field S wave* at *low frequencies*, below the *corner frequency*, is *independent of the rupture rate and frequency*, and the *flat level scales with fault dimension* according to:

$$\frac{A^{(S)}(\omega)}{A_0^{(S)}(\omega)} = \left[\frac{L}{L_0}\right]^3 ; \omega < \omega_c^{(S)} \tag{48}$$

where $A_0^{(S)}(\omega)$ denotes the low frequency spectral level of a reference event, while $A^{(S)}(\omega)$ is the *low frequency* spectral level of an event with a different failure zone dimension, but with *all other source parameters the same as the reference event*. When the second largest failure zone dimension, W, is not of the same order as L, or does not change proportionally with L for the events, then a more accurate relation is:

$$\frac{A^{(S)}(\omega)}{A_0^{(S)}(\omega)} = \left[\frac{WL^2}{W_0L_0^2}\right]$$

For spherical rupture zones, then (48) holds with L the diameter of the spherical region. Finally, the low frequency S wave spectral level is related to the P wave spectral level by

$$\frac{A^{(S)}(\omega)}{A^{(P)}(\omega)} = \left[\frac{v_P}{v_S}\right]^3$$

where v_P and v_S are the compressional and shear velocities in the medium surrounding the failure zone.

(2) The spectral level of the *entire S wave spectrum scales directly with the prestress*, and so:

$$\frac{|\tilde{u}^{(S)}(\omega)|}{|\tilde{u}_0^{(S)}(\omega)|} = \frac{|\sigma^{(0)}|}{|\sigma_0^{(0)}|} \tag{49}$$

where $\tilde{u}_0^{(S)}$ denotes the entire S wave amplitude spectrum for a reference event, while $\tilde{u}^{(S)}$ is the spectrum for an event having a *different homogeneous (shear) prestress magnitude, or a different homogeneous stress drop, but with all other source parameters the same as those for the reference*

event.

(3) The corner frequency, $f_c^{(S)}$, for the shear wave spectrum from the source *scales directly as the ratio of rupture velocity to failure zone length. For rupture rates near the shear velocity, as is usually the case:*

$$f_c^{(S)} = \frac{1}{\pi}\left[\frac{U_R}{L}\right]\left[\frac{3v_S^5}{U_R^5}\right]^{1/3} \simeq .459\left[\frac{U_R}{L}\right]; U_R \lesssim v_s \text{ and } \sigma = 1/4$$

The ratio of P to S wave corner frequencies for a particular event is:

$$\frac{f_c^{(P)}}{f_c^{(S)}} = \left[\frac{v_P^5}{v_S^5}\right]^{1/3}$$

Further, event spectrum scaling relative to a reference source, with "corner frequency" denoted by ${}^{(0)}f_c^{(S)}$, is given by

$$\frac{f_c^{(S)}}{{}^{(0)}f_c^{(S)}} = \left[\frac{U_R}{U_R^{(0)}}\right]\left[\frac{L_0}{L}\right] \tag{50}$$

Comments concerning the effects of strongly inhomogeneous prestress (or stress drop) on P wave spectra apply with equal force for the S wave spectra as well. However, in both cases the scaling laws and asymptotic relations will ordinarily hold in an average sense, so that the relations given here are quite useful.

Figure 9 provides a graphical summary of the predicted spectral characteristics for the compressional and shear waves from earthquakes. In this figure the prestress (or stress drop), denoted as $|\sigma|$, and the failure length, L, are left arbitrary, so that the absolute amplitude scale is in arbitrary units. However, the rupture rate is assumed to be close to the shear velocity in the medium, which is the most commonly occurring situation in the earth, while the ratio of fault length to rupture velocity is taken to be unity. (Thus, for example, since $U_R \simeq v_S$ and with $v_S \simeq 3.8$ km/sec, then $L \simeq 3.8$ km.) Finally, the Poisson's ratio for the material is taken to be 1/4, which is also typical. The low frequency amplitude asymptote for the far field P wave has been normalized to unity in the plot.

With the choice $v_S = 3.8$ km/sec, then $v_P = 6.4$ km/sec, $U_R = 3.8$ km/sec and $L = 3.8$ km are required, under the assumptions used, to obtain the spectra in the figure. Using the relation shown for $A_P(\omega)$, with a prestress of 130 bars (1.3×10^8 dynes/cm^2) and a rigidity of 3×10^{11} dyne/cm^2, so that $|\sigma|/\mu = 4.3 \times 10^{-4}$ is the strain magnitude, we have:

$$A_P(\omega) \simeq 10^6 \; cm \; sec$$

Since the P wave displacement spectrum at a radial distance $|r|$ is given by

$$|\mathfrak{U}_r^{(P)}(\omega)| = \frac{A_P(\omega)}{r} \sin 2\vartheta \cos\varphi$$

from equation (37), then the low frequency spectral level at a distance of $r = 10$ km from the 3.8 km failure zone is

$$|\mathfrak{U}_r^{(P)}|_{max} = 1 \; cm-sec; r = 10km$$

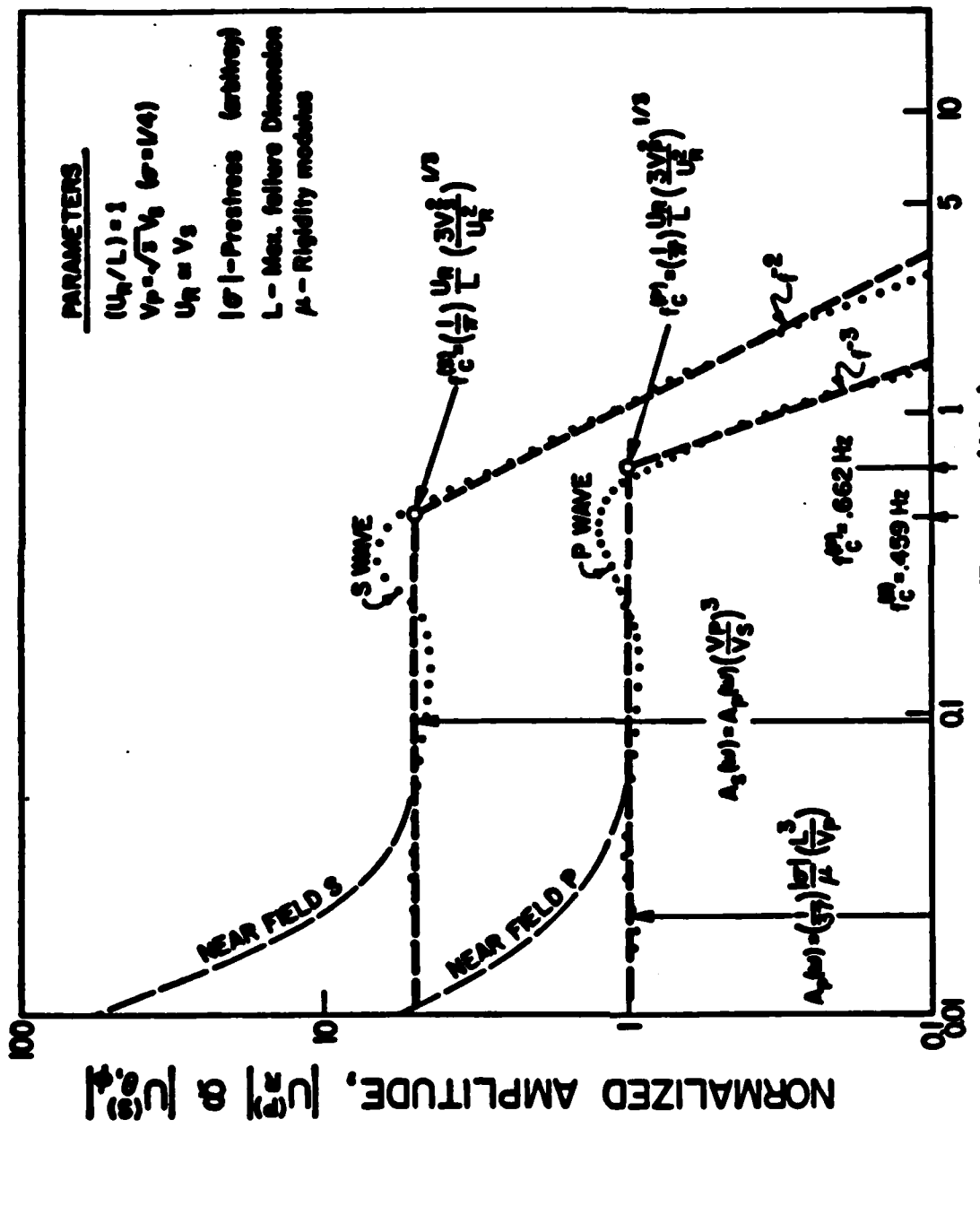

Figure 9. Dependence of far field spectral characteristics of P and S waves from earthquakes on failure parameters. Asymptotic characteristics are indicated by the heavy dashed lines. Here, U_R, is the rupture rate, which is assumed to be constant. Near field spectra are also indicated and only affect the low frequency spectral levels when the wavelengths are of the order of, or greater than, 2π times the receiver distance.

Hence if the amplitude scale in the figure is in cm-sec, then the spectra shown are appropriate at a distance of 10 km from a 3.8 km fault, with failure occurring at a uniform rupture rate of 3.8 km/sec in a medium prestressed to 130 bars. The elastic velocities $v_S = 3.8$ km/sec, $v_P = 6.4$ km/sec and rigidity $\mu = 3 \times 10^{11}$ dynes/cm^2 are appropriate to the middle crust of the earth in most areas (*e.g.*, from 10 to about 25 km depth). Further, with the rupture rate near the shear velocity and the ratio of rupture rate to fault length unity, then the corner frequencies of the spectra will be at .662 Hz for the P wave spectra and at .459 Hz for the S wave spectra. (However, these corner frequency values do not depend on the absolute values of L, U_R and v_S, but only on their ratios.)

Figures 10a. and 10b. illustrate an application of the scaling laws to P and S-wave spectra, for the case in which only the rupture length varies. Only the far field spectra are indicated and only the smoothed form of the spectra are indicated. Also it is assumed that the prestress field is nearly homogeneous, with a relatively small stress concentration near the initial rupture point giving the slightly peaked spectra indicated. (The "peaking" in the spectra will be a function of azimuth in general and only a typical azimuth is indicated here.) In any case, for rather "small" rupture lengths with $L \lesssim 10$ km, then we expect the rupture surface areas to be proportional to L^2 and that the L^3 scaling law for amplitudes can be applied. Since the corner frequency for both P and S waves scales inversely with L, then as a consequence of these two scaling laws, the locus of corner frequency points will lie along a straight line with a f^{-3} slope in these plots. Since the P wave spectrum has a f^{-3} high frequency asymptote for rupture rates near the shear velocity, then the spectra for P waves will also approach and lie along this "scaling line" at frequencies above the corner frequency. Therefore, all the events will have the same P wave spectral levels at high frequency, since they all approach the f^{-3} scaling line. However, S wave spectra have a f^{-2} asymptotic behavior over a wide frequency range above the corner frequency, and so the S-wave spectra will not approach the scaling line except at extremely high frequencies, which are usually outside the range of seismic observation.

Figure 11 illustrates the applicable spectra scaling for variable average stress drops or changes in the average prestress level. Here we assume that the prestress (or stress drop) is quite homogeneous and that the changes in stress are confined to changes in the average value. For such changes, both the entire P and S wave spectra scale directly with the magnitude of the stress and hence the scaling line of the corner frequencies is vertical. Here we show only the far field P wave spectra since the S-wave spectral scaling is identical. In addition, the near field spectral contributions also scale directly with the stress magnitude and so behave exactly like the far field.

The vertical scaling line for prestress or stress drop changes will be modified if the rupture rate is proportional to the stress drop or prestress. This possibility was discussed earlier and is quite likely for failure processes in the earth. If this is the case, then the stress scaling must be combined with the rupture velocity scaling law illustrated in Figure 12. As shown in Figure 12, the scaling line for the corner frequencies for P wave spectra is a horizontal line. Further, the high frequency spectral slope can change from f^{-3}, for $U_R \lesssim v_S$, to f^{-2}, for $U_R \simeq v_P$. Also for very low rupture rates there is a frequency range above the corner frequency within which the spectral slope is low, varying from f^{-1} to f^{-3} in a continuous fashion.

If we were to combine the rupture rate scaling with the stress drop scaling, as would be required for rupture rates proportional to stress drop, then we would expect to see a corner frequency locus defining a scaling line that had a

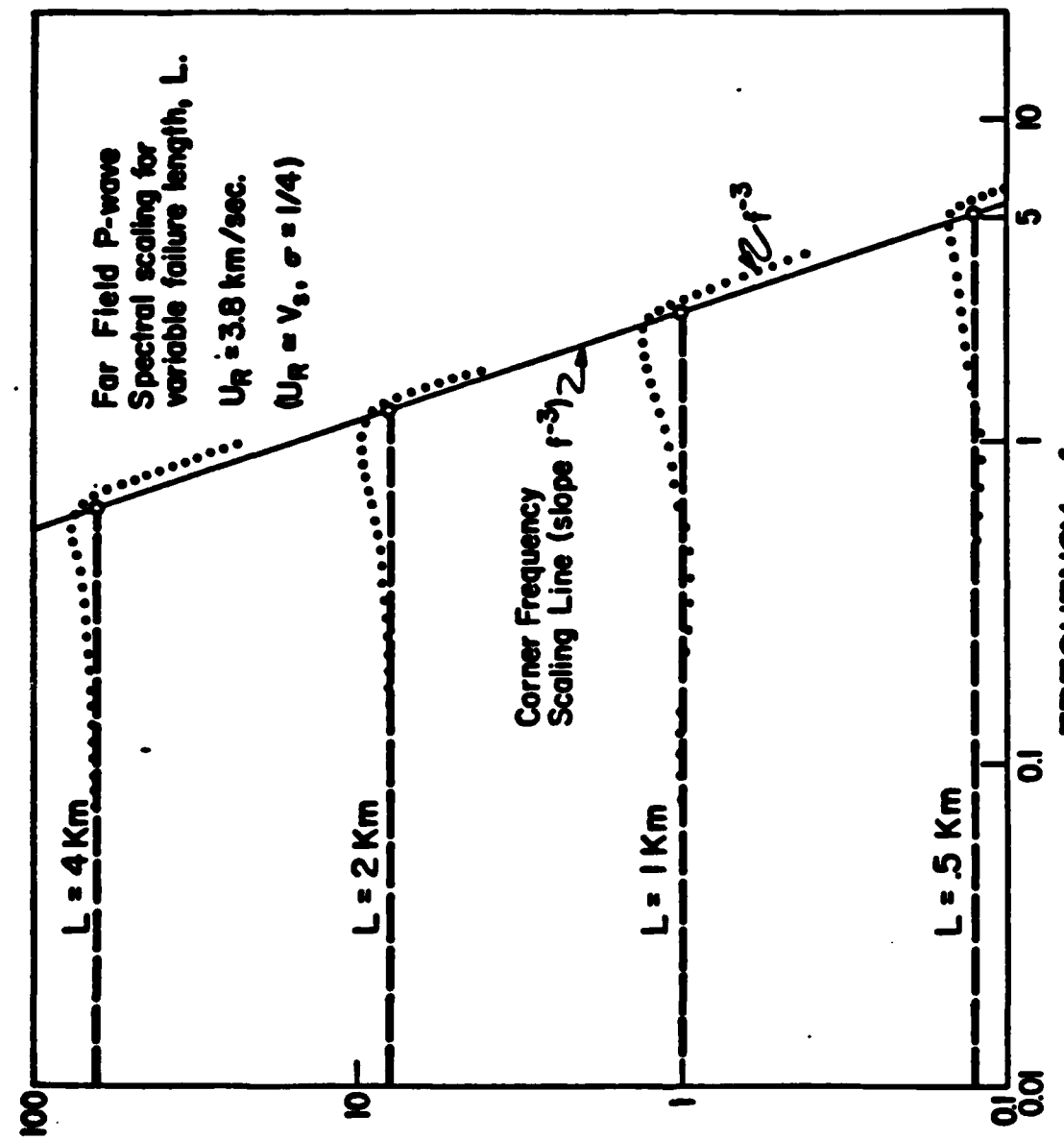

Figure 10a. Illustration of an application of the scaling laws to P wave spectra for variable rupture length (L), with all other source parameters fixed. The corner frequency traces an f^{-3} locus, defining a "Scaling Line". Scaling assumes rupture surface area increases as L^2 ("Small" L case).

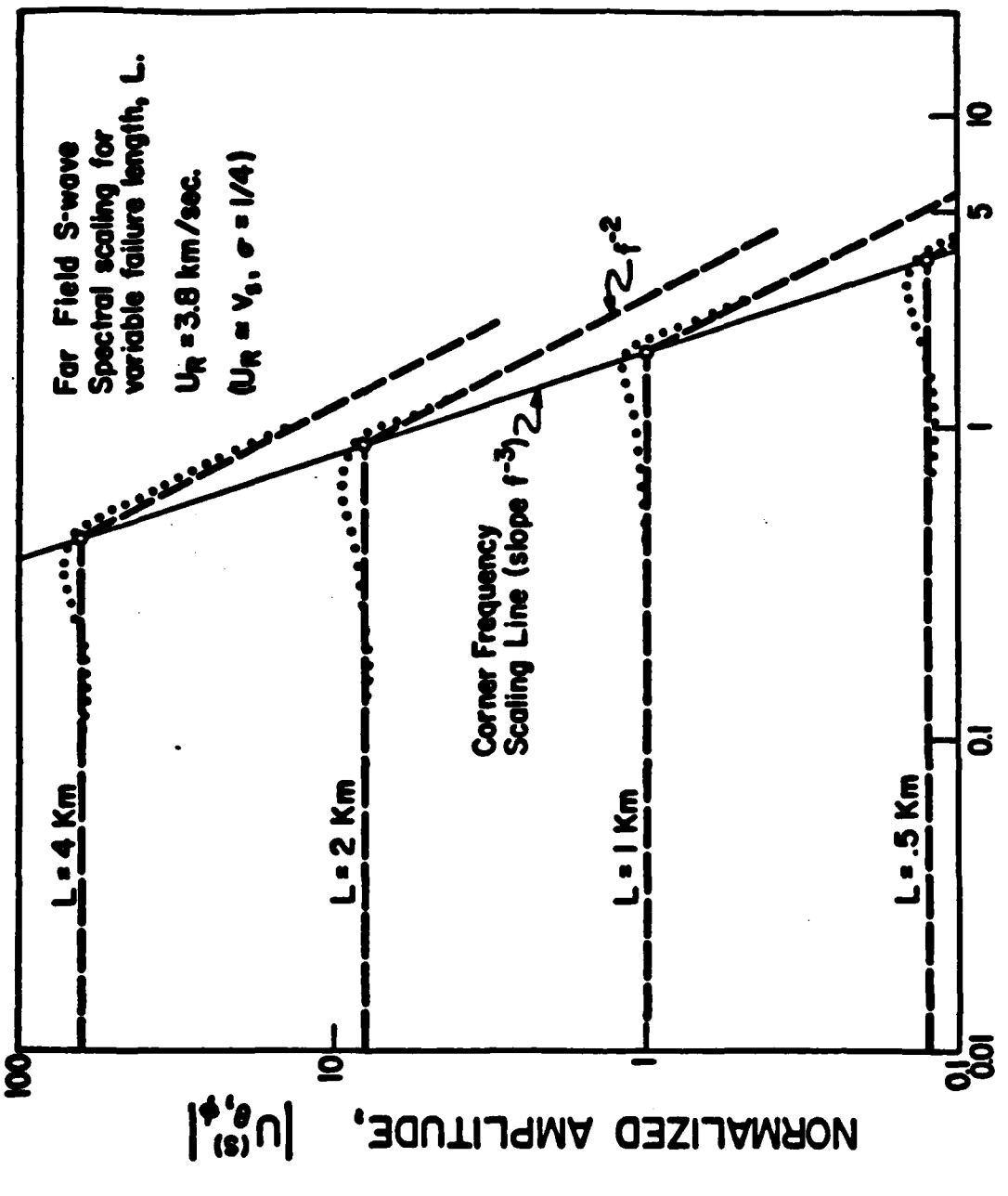

Figure 10b. Illustration of an application of the scaling laws to S-wave spectra for variable rupture length (L), with all other source parameters fixed. The corner frequency traces an f^{-3} locus defining a "Scaling Line". Scaling assumes rupture surface area increases as L^2. ("Small" L case)

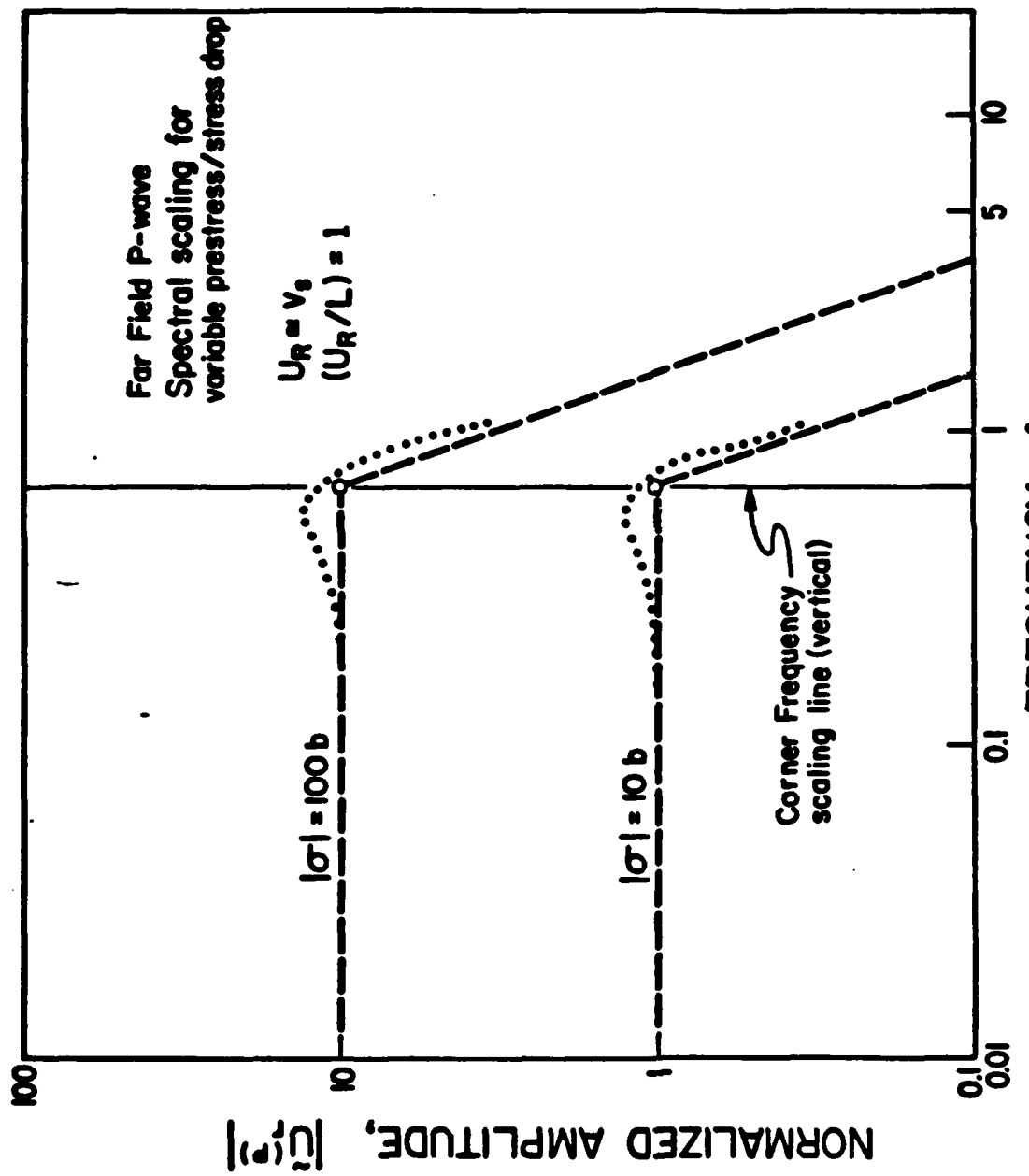

Figure 11. Illustration of an application of the scaling laws to P-wave spectra for variable prestress/stress drop, $|\sigma|$, with all other source parameters fixed. The locus of corner frequency points define a vertical "Scaling Law".

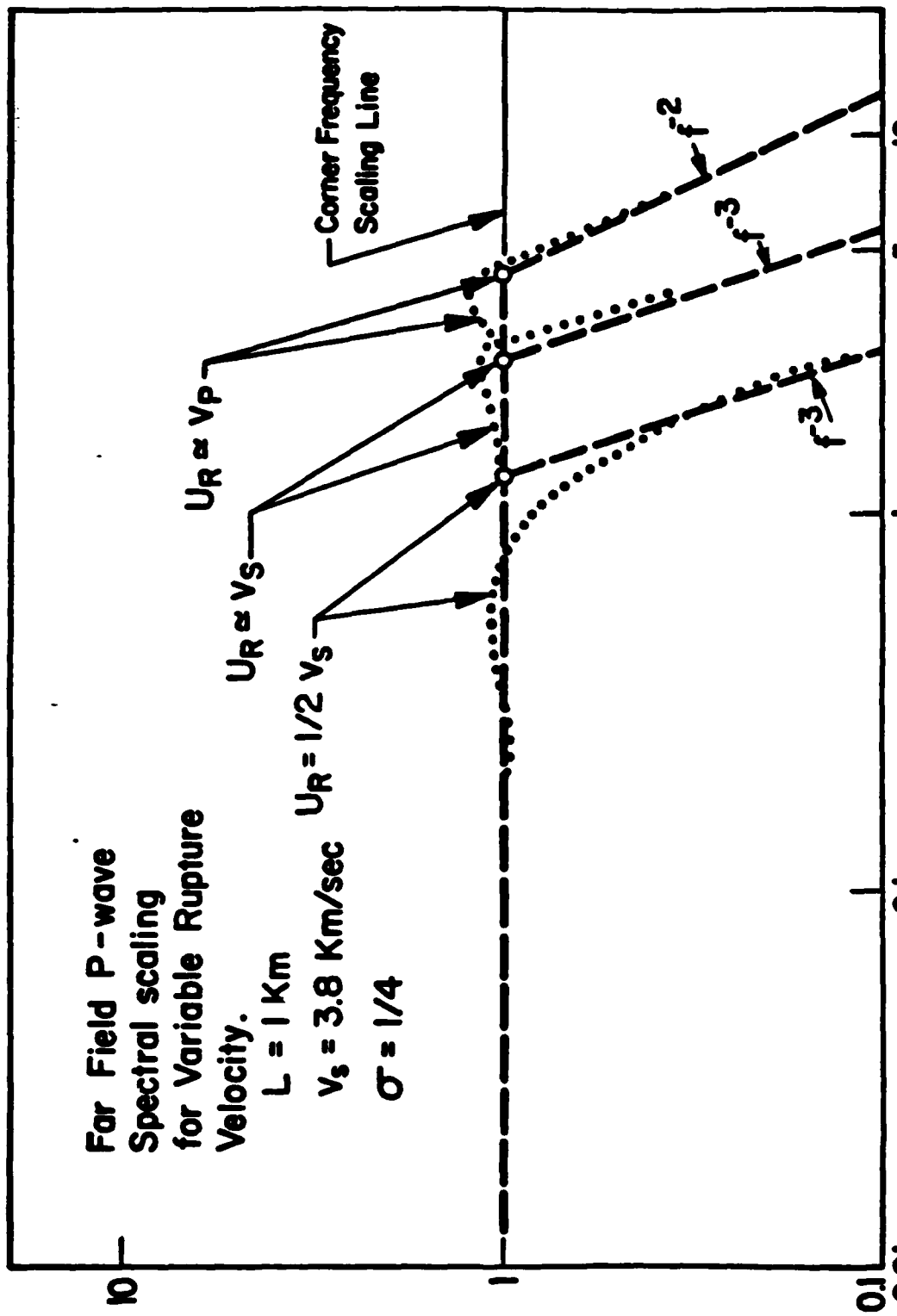

Figure 12. Application of scaling laws to P wave spectra asymptote for variable rupture velocity (U_R), with all other source parameters fixed. The locus of corner frequencies defines a horizontal "Scaling Line". Note that the high frequency asymptote for $U_R \simeq v_p$ is f^{-2}, while for lower U_R values it is f^{-3}.

positive slope (*e.g.*, f^2 or f^3, say) rather than a vertical scaling line, and the spectra for higher stress drop events would have a higher corner frequency than those for lower stress drops. Further, one could expect to observe slight changes in high frequency spectral slopes. As noted, this behavior is more likely than not to occur in the earth, and should certainly be considered when applying the scaling relations.

The scaling relations in Figure 12, as well as in Figure 11, are applied only to far field P wave spectra, however, the situation is nearly identical for the S-wave spectra except for the fact that the high frequency asymptotic behavior is different for the S-wave. This difference does not lead to any fundamental changes in the S-wave spectral scaling results however.

The applications of the scaling laws in Figures 9-12 have been limited to rather "small" tectonic sources, that is to events with failure zone dimensions that are small enough that we can expect that the surface area of the failure zone will scale as L^2. This probably applies to events with $L \lesssim 10$ km. However, for much larger events, we certainly do not expect that the area is proportional to the square of the length or maximum dimension of the failure zone. Thus for large events, with rupture zones of the order of hundreds or thousands of kilometers, the second largest dimension, W, would be expected to be nearly fixed in value and independent of length of these large failure zones. In this case, the surface area of the failure zone would scale as L, rather than as L^2, and the scaling relation for the low frequency amplitude would be proportional to L^2 rather than to L^3. This would have the effect of producing a scaling line, for the corner frequencies of both P and S wave spectra, that varied as f^{-2} with failure zone length for the very large events. Thus, while this line varies as f^{-3} for small events with $L \lesssim 10$ km, it would be expected to vary as f^{-2} for very large events, certainly for events with $L \gtrsim 100$ km. In the intermediate range, where $10 \lesssim L \lesssim 100$ km, the variation of the slope of this scaling line should be between f^{-3} and f^{-2}, with the variation being continuous between the two, reaching these slopes smoothly at the extreme values of L, near 100 km and 10 km, respectively.

A consequence of this scaling of the spectra with failure zone dimension is that the P and S wave spectral levels will cease to increase, at frequencies above the corner freuency, even though the failure dimension L continues to increase. This occurs, as already shown in Figure 10a, for P wave spectra at even the smallest L values. On the other hand, as shown in Figure 10b, the S wave continues to have larger high frequency spectral levels with increasing L, for the lower L value range. However, for L values that are large, the amplitude scaling law varies as L^2, rather than as L^3, and the scaling line has a f^{-2} slope, so that in this large L range the high frequency S wave spectra will cease to increase with increasing L. That is, as in the case for the P wave spectra in the low L range, there is "spectral saturation" in the high frequency range for S wave radiation and the high frequency S wave spectral level will not increase with increasing L.

As will be emphasized later, this high frequency "saturation" for P waves leads to a cut-off in the body wave magnitude (m_b) measured from P waves, where increases in the rupture dimension L do not result in an increase in the body wave magnitude measured at 1 Hz. This, of course, arises from the fact that the body wave magnitude is defined as the logarithm of the one second period P wave amplitude. Thus, when the corner frequency is significantly less than 1 Hz, then the 1 Hz point will be on the f^{-3} asymptote of the P wave spectrum and all events with larger failure zone lengths will still have (very nearly) the same spectral amplitude at 1 Hz. Hence there will be no change in the

magnitude beyond this limiting value and one will observe a body wave magnitude cut-off. Observationally, this clearly occurs for body wave magnitudes somewhat above magnitude 6. (This corresponds, roughly, to a failure zone dimension L of the order of 10 to 15 km.) On the other hand, when the failure zone dimensions become very large, with L of the order of 100 km and more, then both P and S wave high frequency spectra saturate above their corner frequencies. In this case measurements of a surface wave magnitude (M_S) defined in terms of the logarithm of the (vertical component) Rayleigh wave amplitude at .05 Hz, will also cease to increase with increasing failure zone dimension. Thus, there is a surface wave magnitude cut-off which will apply to very large tectonic events. Such a cut-off has not been conclusively verified observationally, but should appear at an M_S value somewhat above $M_S = 8$. For such large events then, neither m_b nor M_S will give a measure of the size of the event, or its energy.